

**Structural and Fluid-Structure Interaction Analysis of Stenotic Aortic
Valves: Application to Percutaneous Aortic Valve Replacement**

Hoda Maleki

A Thesis

in

the Department

of

Mechanical and Industrial Engineering

Presented in Partial Fulfillment of the Requirements
for the Degree of Master of Applied Science (Mechanical Engineering) at
Concordia University
Montréal, Québec, Canada

November 2010

© Hoda Maleki, 2010

CONCORDIA UNIVERSITY
SCHOOL OF GRADUATE STUDIES

This is to certify that the Thesis prepared,

By: **Hoda Maleki**

Entitled: **“Structural and Fluid Structure Interaction Analysis of Stenotic Aortic Valves: Application to Percutaneous Aortic Valve Replacement”**

and submitted in partial fulfillment of the requirements for the Degree of

Master of Applied Science (Mechanical Engineering)

complies with the regulations of this University and meets the accepted standards with respect to originality and quality.

Signed by the Final Examining Committee:

_____	Chair
Dr. H.D. Ng	
_____	Examiner
Dr. R. Wuthrich	
_____	Examiner
Dr. N. Bouguila	CIISE External
_____	Supervisor
Dr. L. Kadem	

Approved by:

Dr. A.K.W. Ahmed, MASc Program Director
Department of Mechanical and Industrial Engineering

Dean Robin Drew
Faculty of Engineering & Computer Science

Date: _____

ABSTRACT

Structural and Fluid-Structure Interaction Analysis of Stenotic Aortic Valve: Application to Percutaneous Aortic Valve Replacement

Hoda Maleki

The main objective of this thesis is to study and investigate the mechanical behavior of the aortic valve with an emphasis on aortic stenosis. Moreover, this thesis aims to characterize the severity of AS in terms of material properties. The development of percutaneous heart valves allows valve replacement without open chest surgery. This is the most desirable option for patients with elevated surgical risks. To avoid the risk of failure in percutaneous valve implantation, determination of material properties of diseased leaflets before surgery is necessary. Therefore in this study, a series of numerical simulations, including both structural and fluid-structure interaction approach, and experimental studies were performed to achieve the objectives of this research. The results of the numerical simulations of the aortic stenosis are compared with in vitro results before testing the method using in vivo data. There is good agreement between the results of the numerical simulation and the in vitro experiments and the literature. An algorithm is suggested to estimate the material properties of the stenotic valve, considering the realistic material of the aortic valve with hyperelastic, nonlinear and anisotropic properties. The simulations using the structural modeling allow determination of the patient's specific material property of a calcified aortic valve, knowing invasively measured aortic and ventricular pressure waveforms and the geometrical orifice area prior to percutaneous valve replacement. Also, fluid-structure interaction modeling helps to estimate a more realistic dynamic behavior of the aortic valve and also obtains the hemodynamic performance.

ACKNOWLEDGEMENTS

First and foremost I would like to thank my parents. The great interests that they had in me to continue my education in graduate field; their love, support and sacrifices are always the best reasons to push me forward.

Secondly, I would like to express my deepest gratitude to my husband and colleague, Shahrokh Shahriari, for his support and understanding during the past years. His advice during my M.A.Sc. helped me to be creative and successful in my project.

I would like to express my sincerest gratitude to my academic supervisor Dr. Lyes Kadem, director of cardiovascular fluid dynamics laboratory (LCFD), for his continuous assistance, guidance and financial support throughout the completion of this thesis.

I would like to thank Dr. Louis-Gilles Durand (Co-supervisor) from Institut de recherches cliniques de Montréal (IRCM), for encouraging me and providing financial support from IRCM.

I am truly grateful for the contribution of Dr. Michel Labrosse from the University of Ottawa; his input was valuable throughout this thesis.

I also would like to thank the people at LCFD for contribution to the healthy competitive atmosphere in the group.

Finally, I acknowledge the financial support that I received from Concordia University, which facilitated my research and life by awarding me the Concordia University Graduate Fellowship, International Tuition Fee Remission Award and Conference Traveling Award to give me the opportunity to attend ESB 2010 conference.

Table of Contents

List of Figures	ix
List of Tables	xiv
Nomenclature	xv
Abbreviation	xvii
Chapter 1: Introduction	1
1.1 Overview	1
1.2 Anatomy of Aortic Valve	2
1.3 Physiology of Aortic Valve	3
1.4 Aortic Valve Diseases	6
1.4.1 Congenital Valve Disease	6
1.4.2 Aortic Regurgitation	6
1.4.3 Aortic Stenosis	7
1.5 Prosthetic, Artificial Heart Valves	10
1.5.1 Mechanical Valves	11
1.5.2 Bioprosthetic Valves	14
1.6 Percutaneous Valves	17

1.7 Objective and Outline of Thesis Study	19
Chapter 2: Literature Review	22
2.1 Introduction.....	22
2.2 Structural Modeling	23
2.3 Fluid Structure Interaction.....	28
Chapter 3: In Vitro Experiments.....	32
3.1 Introduction.....	32
3.2 Experimental Facility.....	32
3.3 The Components of the System	34
3.3.1 Super Pump and Pump Regulator	34
3.3.2 Left Heart Simulation System	35
3.3.3 Pressure Transducers and Control Unit.....	36
3.3.4 Electromagnetic Flow Meter and Transducer	37
3.3.5 Programmed Waveform Generator	37
3.4 Experimental Conditions	38
3.5 Experimental Results	39
3.5.1 Aortic Heart Valve Samples.....	39

3.5.2 How to Measure the Geometrical Orifice Area?.....	44
Chapter 4: Structural Model Analysis of Aortic Stenotic Valve.....	46
4.1 Introduction.....	46
4.2 Numerical Method	47
4.3 Model Description	49
4.4 In Vitro Experiments	56
4.4.1 Case 1: Bioprosthetic Pericardial Valve.....	56
4.4.2 Case 2: Silicone Valve with Moderate Stenosis.....	64
4.4.3 Case 3: Silicone Valve with Severe Stenosis	72
4.5 In Vivo Application (Patients' Specific Aortic Stenosis).....	80
4.5.1 In Vivo Case: Patient No. 1.....	82
4.5.2 In Vivo Case: Patient No. 2.....	87
4.5.3 In Vivo Case: Patient No. 3.....	89
4.6 Summary.....	91
Chapter 5: Fluid Structure Interaction Analysis of Healthy and Stenotic Aortic Valves	93
5.1 Introduction.....	93
5.2 Numerical Method in Fluid Structure Interaction Analysis.....	94

5.3 Model Description	97
5.3.1 Geometry.....	97
5.3.2 Element Formulation.....	98
5.3.3 Material Properties	99
5.3.4 Boundary Conditions.....	100
5.3.5 Coupling Implementation.....	100
5.4 Results and Discussion	102
5.5 Limitations of the Current FSI Model	112
5.6 Summary.....	112
Chapter 6: Conclusion and Future Work	113
References.....	118
Appendix 1.....	126
Appendix 2.....	129

List of Figures

Figure 1.1 Aortic heart valve: (a) front view (b) above view. (Pick, 2007)	2
Figure 1.2 Aortic valve interior view; L: left coronary and R: right coronary. (www.arthursclipart.org).....	3
Figure 1.3 Aortic and left ventricular pressure waveforms during a cardiac cycle.....	4
Figure 1.4 Human circulatory system. (www.teachnet.ie/farmnet/Circulatory.htm)	5
Figure 1.5 Normal and bicuspid aortic valve	6
Figure 1.6 Severe calcification of a three-leaflet aortic valve (Rajamannan et al., 2007).....	7
Figure 1.7 Schematic of the flow thorough an aortic valve.....	9
Figure 1.8 Prosthetic heart valves:	11
Figure 1.9 Caged ball valve. (Stijnen, 2004).....	12
Figure 1.10 Three types of non-tilting disc valves. (Gott et al., 2003).....	13
Figure 1.11 Tilting disc valves. (Stijnen, 2004)	13
Figure 1.12 Front view of a bileaflet valve. (Stijnen, 2004).....	14
Figure 1.13 Switch operation (Ross procedure).(www.medicinenet.com/aortic_stenosis/article.htm) ..	15
Figure 1.14 Allograft valve. (www.clevelandclinic.org).....	16
Figure 1.15 Bovine pericardium prosthesis. (Bloomfield, 2002)	17
Figure 1.16 Percutaneous aortic valve. (Southard and Low, 2006).....	17
Figure 1.17 A view of the catheter. (Hanzel et al., 2006).....	18
Figure 1.18 Trajectory of catheter inside the heart. (Hanzel et al., 2006)	18
Figure 1.19 Percutaneous aortic valve replacement: a) balloon valvuloplasty; b) balloon catheter with the prosthetic valve inside the diseased valve; c) balloon inflation to secure the prosthetic valve; d) prosthetic valve in place. (http://my.clevelandclinic.org/heart/percutaneous/percutaneousvalve.aspx)	19
Figure 3.1 Front view of the left heart simulator.....	33

Figure 3.2 A schematic of left heart simulator circulatory system. (MV: mitral valve and AV: aortic valve)	34
Figure 3.3 Super pump.	35
Figure 3.4 Left heart system.	36
Figure 3.5 Transducer and control unit.	36
Figure 3.6 Flow meter.	37
Figure 3.7 Front panel of the waveform generator unit.	37
Figure 3.8 (a) Biological aortic pericardial valve; (b) home-made stenotic silicone valve.	38
Figure 3.9 Pressure waveforms obtained in vitro on a biological pericardial valve. Red line: ventricle pressure, yellow: aortic pressure, light green: stroke volume, and green line: flow rate.	40
Figure 3.10 Opening and closing of leaflets in the biological pericardial valve during one cycle recorded at 1000 fps; (order: Top left to bottom right).	40
Figure 3.11 Pressure waveforms obtained in vitro on a silicone valve with moderate stenosis. Red line: ventricle pressure, yellow: aortic pressure, light green: Stroke volume and green line: flow rate.	41
Figure 3.12 Opening and closing of leaflets in silicone valve with moderate stenosis during one cycle recorded at 1000 fps; (order: Top left to bottom right).	42
Figure 3.13 Pressure waveforms obtained in vitro on a silicone valve with severe stenosis. Red line: ventricle pressure, yellow: aortic pressure, light green: Stroke volume and green line: flow rate.	43
Figure 3.14 Opening and closing of leaflets in silicone valve with severe stenosis during one cycle recorded at 1000 fps; (order: Top left to bottom right).	43
Figure 3.15 The maximum geometric opening area (GOA) of the valve (at 0.3 s); the red line is the location of leaflet free edges.	44
Figure 4.1 R_c : commissural radius, H: commissural height, h_s : sinus height, H_s : commissural height, X_s : coaptation height, R_b : radius of the base, L_h : leaflet height, L_f : leaflet free edge length (Thubrikar, 1990).	51
Figure 4.2 Different views of the one third aortic valve geometry used for the simulations. In all pictures, pink and green represent the leaflet and aortic root (sinus and base). First picture from the top (right) shows the location of boundary conditions.	53

Figure 4.3 Algorithm for of the estimation of material property of an aortic stenotic valve.....	55
Figure 4.4 Time varying pressure wave forms for in vitro pericardial aortic valve.	57
Figure 4.5 Variation of the GOA as a function of C_1 (in vitro), for pericardial aortic valve.....	57
Figure 4.6 Instantaneous GOA measured experimentally and computed numerically (as percentage of systolic phase).	58
Figure 4.7 Maximum opening area of AV in pericardial aortic valve.....	59
Figure 4.8 Instantaneous pressure gradient including selected points.	59
Figure 4.9 Opening and closing of pericardial aortic valve at different points selected in Fig. 4.8.	60
Figure 4.10 Minimum closing of in vitro pericardial aortic valve.....	61
Figure 4.11 Contours and vectors of maximum principle stress at: (a) maximum opening; (b) valve closure.	63
Figure 4.12 Stress analysis for two critical points during one cycle.	64
Figure 4.13 Time varying pressure wave forms for in vitro moderate AS.....	65
Figure 4.14 Variation of the GOA as a function of C_1 (in vitro), for moderate AS.....	65
Figure 4.15 Maximum opening area of in the model of moderate AS. The yellow area represents the maximum GOA at $t=0.26$ s.	66
Figure 4.16 Contours of maximum and minimum principal stresses at the instant corresponding to the maximal opening of valve leaflets for the model of moderate AS.	67
Figure 4.17 Contours of 2 nd principal stress and Von- Mises stress at the instant of maximum opening of the valve leaflet for the model of moderate AS.....	68
Figure 4.18 Minimum closure area in vitro moderate AS, yellow area is the simulated regurgitation area..	69
Figure 4.19 Contours of maximum and minimum principal stress during the closure phase, for the model of moderate AS.....	70
Figure 4.20 Contours of 2 nd principal stress and Von- Mises stress during the closure phase, for the model of moderate AS.....	71
Figure 4.21 Time varying pressure wave forms for in vitro severe AS.....	73

Figure 4.22 Variation of the GOA as a function of C_1 (in vitro), for severe AS.....	73
Figure 4.23 Maximum opening area of the model of severe AS, the yellow area is simulated GOA.....	74
Figure 4.24 Contours of maximum and minimum principal stress at the instant of maximum opening for a model of severe aortic stenosis.....	75
Figure 4.25 Contours of 2 nd principal stress and Von- Mises stress at the instant of maximum opening for a model of severe aortic stenosis.....	76
Figure 4.26 Minimum closure area in vitro severe AS, yellow area is the simulated regurgitation area.	77
Figure 4.27 Contours of maximum and minimum principal stress at the minimum closing of valve leaflets for the model of severe AS.....	78
Figure 4.28 Contours of 2 nd principal stress and Von- Mises stress at the minimum closing of valve leaflets for the model of severe AS.....	79
Figure 4.29 Definition of the different areas used in clinical studies, No. #1 represent effective orifice area (minimum cross-sectional area of the blood flow jet), No.#2 represent geometrical orifice area , No.#3 cross-sectional area of the ascending aorta at the sinotubular junction.	81
Figure 4.30 Time varying pressure waveforms (in vivo), for patient #1.....	82
Figure 4.31 Variation of the GOA as a function of C_1 (in vivo), for patient #1.....	83
Figure 4.32 Sensitivity analysis with respect to variation in GOA for patient #1.....	85
Figure 4.33 Sensitivity analysis with respect to variation in the leaflet thickness for patient #1.....	86
Figure 4.34 Material property for different value of valve leaflet thickness.....	87
Figure 4.35 Time varying pressure waveforms (in vivo), for patient #2.....	88
Figure 4.36 Variation of the GOA as a function of C_1 (in vivo), for patient #2.....	88
Figure 4.37 Time varying pressure waveforms (in vivo), for patient #3.....	89
Figure 4.38 Variation of the GOA as a function of C_1 (in vivo), for patient #3.....	90
Figure 4.39 Obtained C_1 for all simulated cases.....	92

Figure 5.1 Movement of solid part in the fluid domain based on ALE approach during one time step, “a” is the Lagrangian cycle and “b” is the advection cycle (green represents solid domain and lines represent the fluid meshes).	95
Figure 5.2 Aortic valve geometry and meshes merged in fluid domain.	97
Figure 5.3 Velocity pattern at maximum opening for a healthy valve. Fringe level’s unit is (mm/s).	102
Figure 5.4 Velocity pattern at maximum opening for a stenotic valve. Fringe level’s unit is (mm/s).	103
Figure 5.5 Transversal cross section of the aorta at the section corresponding to the maximum velocity for healthy valve (EOA: area inside pink line), Fringe level’s unit is (mm/s).	105
Figure 5.6 Transversal cross section of the aorta at the section corresponding to the maximum velocity for stenotic valve (EOA: area inside pink line), Fringe level’s unit is (mm/s).	105
Figure 5.7 Velocity profiles for healthy valve (Max. opening), Fringe level’s unit is (mm/s).	106
Figure 5.8 Velocity profiles for a stenotic valve (Max. opening), Fringe level’s unit is (mm/s).	107
Figure 5.9 Velocity profile at mid-valve closure.	108
Figure 5.10 Comparison of maximal velocity upstream from the aortic valve, the vena contracta and downstream of the valve for healthy and stenotic valve at Max. opening.	109
Figure 5.11 Comparison of ET, RVOP and RVCT using the dry model; FSI model and comparison with experimental model (for healthy valve).	110
Figure 5.12 Opening and closure of a healthy pericardial aortic valve at different points selected in Fig. 4.8.	111
Figure 6.1 Curvilinear relationship between the EOA and material properties, each point represents one case study (this thesis).	116
Figure 6.2 Curvilinear relationships between the EOA and EBCT score (Messika-Zeitoun et al., 2004). .	116
Figure A1.1 A 2D Geometry of aortic valve.	126
Figure A1.2 (Left) aortic and left ventricular pressure wave forms applied as the boundary condition; (right) the boundary of the domain.	127
Figure A1.3 Velocity vector map at different instants and planes: (a) Healthy valve; (b) valve with AS.	128

List of Tables

Table 1.1 Aortic stenosis severity classification based on EOA	9
Table 3.1 Measured GOA for three different valves (in vitro study)	45
Table 4.1 Specific dimensions of the model.....	52
Table 4.2 Opening and closing characteristics of the in vitro pericardial aortic valve.....	61
Table 4.3 Stress analysis for two critical points.	62
Table 4.4 Opening and closing characteristics of the valve in vitro moderate AS.	72
Table 4.5 Opening and closing characteristics of the valve in vitro severe AS.....	80
Table 4.6 Calculated GOA based on the energy loss coefficient (in vivo study).	82
Table 4.7 Opening and closing characteristics of the valve for patient #1.	83
Table 4.8 Opening and closing characteristics of the valve for patient #2.	89
Table 4.9 Opening and closing characteristics of the valve for patient #3.	90
Table A1.1 Dimensions for human aortic valve.....	127
Table A2.1 Commercially available software and methods used. (Lio and Quek, 2003)	129

Nomenclature

$A, A_{1,2}$	Area (m^2)
A_e	Area of element (m^2)
C	Speed of sound (m/s)
C_{1-4}	Material property constants
$[C]$	Damping matrix (Ns/m)
γ	Poisson's ratio
E	Young's modulus (Pa)
F	Force vector (N)
k	Bulk modulus (kg/ms^2)
$[K]$	Matrix of stiffness (N/m)
L_e	Characteristic length (m)
$[M]$	Matrix of mass (kg)
μ	Dynamic viscosity (kg/ms)
Δp	Pressure gradient (Pa)
p	Pressure (Pa)
Q	Flow rate (m^3/s)
ρ	Density (kg/m^3)

S	Stress tensor for structure (Pa)
σ	Stress tensor for fluid (Pa)
t_e	Time step (s)
$\{u\}$	Matrix of displacement (m)
$\{\dot{u}\}$	Matrix of velocity (m/s)
$\{\ddot{u}\}$	Matrix of acceleration (m/s ²)
V_e	Volume of element (m ³)
V, V_{1-2}	Velocity (m/s)
W	Energy function (kJ)
$[M]$	Matrix of mass (kg)

Abbreviation

ALE	Arbitrary Lagrangian Eulerian
AP	Aortic pressure
AR	Aortic regurgitation
AS	Aortic stenosis
AV	Aortic valve
AVR	Aortic valve replacement
BV	Biological valve
CFD	Computational fluid dynamics
CSD	Computational solid dynamics
CW	Continues wave
EBCT	Electron-beam computed tomography
ECG	Electrocardiogram
EOA	Effective orifice area
FSI	Fluid structure interaction
ET	Ejection time

GOA	Geometric orifice area
LV	Left ventricle
LVOT	Left ventricle out tract
MV	Mechanical valve
PW	Pulse wave
RVCT	Rapid valve closing time
RVOT	Rapid valve opening time
TPG	Transvalvular pressure gradient
VIA	Visco-elastic impedance adapter
VP	Ventricular pressure

Chapter 1: Introduction

1.1 Overview

Heart is a complex pump circulating the blood into the body. All human cells need blood to live. At each beat, heart sends oxygenated blood with all necessities into the body organs and removes waste materials from deoxygenated blood. The aorta is the artery that transports the fresh blood from heart to the body. Aortic valve is placed at the beginning of the aorta and lets blood be pumped into aorta, but prevents blood from flowing back to the heart. This valve has a very important role on the health and long life of the heart. Because of that, it plays a strategic role comparing with other heart valves.

Several diseases can influence the nature and performance of the aortic valve. Aortic regurgitation (i.e., valve does not close properly) and aortic stenosis (i.e., valve dose not open properly) are the two important ones. In North America and Europe, aortic stenosis is the most frequent valvular heart disease and it is more common among men (Otto et al., 1999). Treatment for symptomatic patients with aortic stenosis is surgical replacement of the diseased valve.

Engineers have worked on artificial valves in order to maximize their performance and durability since the first implantation sixty years ago (Gott et al., 2003). In all types of artificial heart valve implantation, open heart surgery has been needed, until recently after the development of percutaneous heart valves, which allowed valve replacement without open chest surgery (Feldman, 2006). This is now the optimal solution in patients with elevated surgical risks.

In this chapter, first of all, the aortic valve anatomy and physiology are presented followed by a discussion on the most common aortic valve diseases and their effects on the valve structure and performance, in order to understand the necessity of valve replacement. Then,

different types of the artificial aortic valves are presented. Finally, the objective of this thesis and proposed studies and methodologies are described.

1.2 Anatomy of Aortic Valve

The aortic valve separates the left heart ventricle from the aorta (Fig. 1.1(a)). It consists of three half-moon-shaped pocket-like flaps of leaflets and three sinuses. For illustration, Fig. 1.1(b) shows a view of the aortic valve from above the heart in open and closed situations. The contact area of neighboring leaflets in closed position is called coaptation surface (Thubrikar, 1990). The leaflets are the most moveable parts in the valve and the sinuses are cavities behind the leaflets. The sinuses are attached to the aorta from the upper part and to the left ventricle from the lower part. The sinuses are consequently named left coronary sinus, right coronary sinus and noncoronary sinus. The coronary arteries supply blood in order to feed the heart itself (see Fig. 1.2).

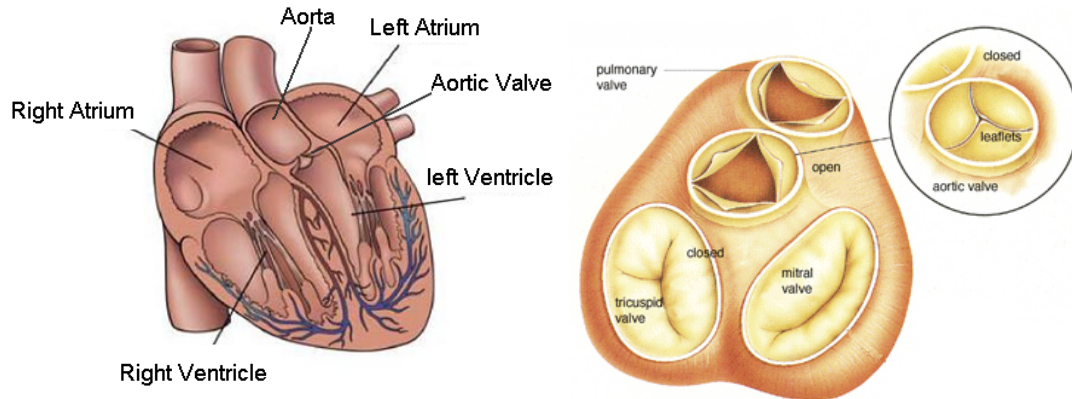


Figure 1.1 Aortic heart valve: (a) front view (b) above view. (Pick, 2007)

The aortic root creates a bridge between the left heart ventricle and the ascending aorta. It is the pathway for blood flow out of the left ventricle. Also, it provides the structure to serve as support for aortic valve leaflets. The aortic valve is composed entirely of connective tissues.

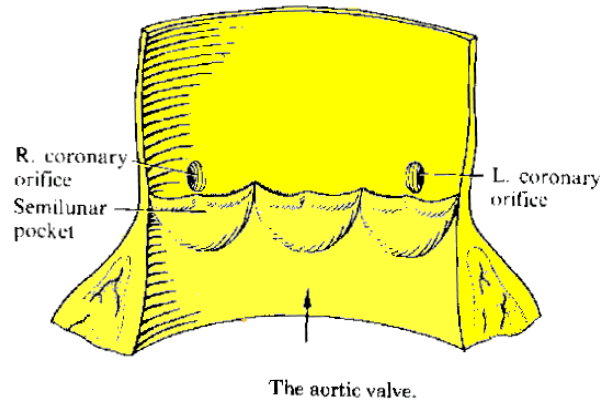


Figure 1.2 Aortic valve interior view; L: left coronary and R: right coronary. (www.arthursclipart.org)

1.3 Physiology of Aortic Valve

The heart pumps blood from the left heart ventricle into the aorta, through the aortic valve, and then throughout the body. The aortic valve is a one-way valve. During systolic phase (contraction), the aortic valve leaflets open to allow oxygenated blood flows forward from left ventricle to aorta, and close to prevent backward flow from aorta to left ventricle during diastolic phase (relaxation). In general, the main functions of aortic valve are:

- To providing a route for leaving blood from the heart.
- To prevention of blood backflow into the heart after blood leaves it.

A cardiac cycle has two main periods: systolic and diastolic (see Fig. 1.3). During systole, contraction of the left ventricle causes blood ejection into the aorta while the aortic valve remains open during this interval. During diastole, a relaxation leads to filling of the left ventricle with blood from the atrium.

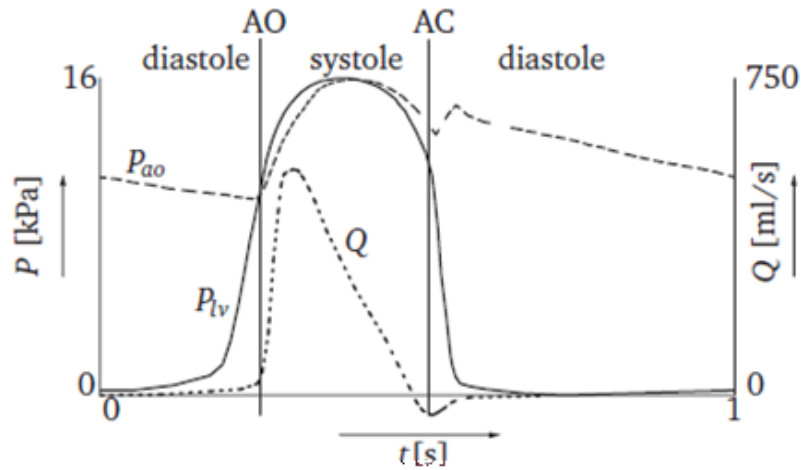


Figure 1.3 Aortic and left ventricular pressure waveforms during a cardiac cycle. Q: the flow curve, AO: valve opening and AC: valve closure. (De Hart, 2002)

The performance of the aortic valve can be affected in different ways. If calcium deposition builds up on the aortic valve leaflets, the valve structure becomes hard (calcified) over time. When this problem happens, the leaflets do not open normally and the volume of ejected blood from the left ventricle decreases, and as a consequence, heart performance is reduced. Age increasing and high blood pressure are the most important risk factors of calcified leaflets. In Fig. 1.4, the entire circulatory system and the flow directions of blood in the body are shown. The red color is associated with the oxygenated blood and the blue color shows the deoxygenated blood.

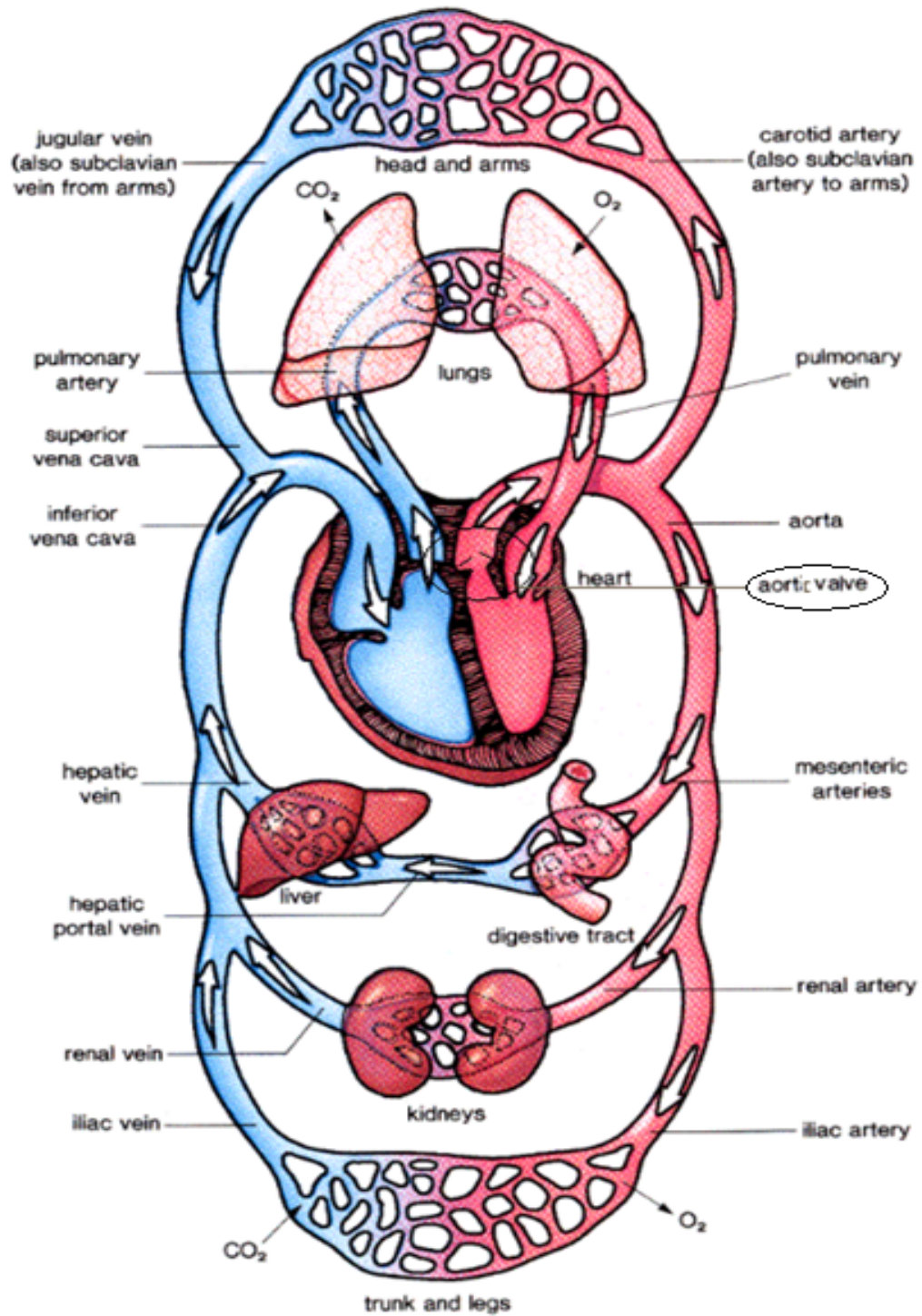


Figure 1.4 Human circulatory system. (www.teachnet.ie/farmnet/Circulatory.htm)

1.4 Aortic Valve Diseases

Valvular heart diseases mean disorders in structure or function of the heart valves. A valvular disease can be congenital (present at birth) or acquired later in the life. Infection and structural changes which happen over time are the common causes of acquired valve diseases. Treatment for symptomatic patients with severe aortic valve disease is surgical replacement of the valve.

In the followings, the common aortic valve diseases: congenital valve diseases, aortic regurgitation and aortic stenosis are described. As the aortic stenosis is the most common valvular disease, it is the subject of this research.

1.4.1 Congenital Valve Disease

Congenital valve disease is a kind of deformity in valve structure developed before birth. Bicuspid aortic valve disease is a type of congenital valve disease that affects the aortic valve leaflet shapes and connections and lead to aortic flow obstruction (Fig. 1.5).

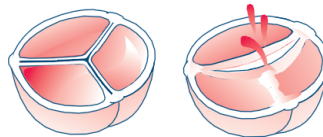


Figure1.5 Normal and bicuspid aortic valve

(Bicuspid valve has only two leaflets instead of three). (www.clevelandclinic.org/heart)

1.4.2 Aortic Regurgitation

Aortic regurgitation (AR) occurs when the valve does not close properly, and blood can leak backward into the left ventricle during diastolic phase. As a result, the left ventricle has to pump blood more than in a healthy case and this extra work causes enlargement of ventricle and its muscles will become thicker. The serious AR cases may require surgical treatment. This

involves replacing the diseased valve with an artificial one. Patients with AR are at increasing risk for developing heart valve infection.

1.4.3 Aortic Stenosis

The narrowing of flow passing through the aortic valve during systole is called aortic stenosis (AS). The leaflets do not open wide enough and the left ventricular work load increases significantly to maintain a physiological flow rate. AS can be caused by calcium deposition on the aortic side of the leaflets or caused by congenital abnormality of the valve. Nowadays, the most common cause of AS is buildup of calcium and cusps fusion that occurs with age.

Patients with AS may not have any symptom and the diagnosis is based on examination by hearing the heart murmur. When the AS becomes severe, many symptoms may develop: shortness of breath (dyspnea), chest pain (angina) and dizziness (Nishimura, 2002).



Figure 1.6 Severe calcification of a three-leaflet aortic valve (Rajamannan et al., 2007).

AS can be diagnosed using different techniques, below are the most common ways to examine and identify occurrence of AS are:

Clinical examination: includes of examining the neck and hearing a murmur.

Electrocardiogram (ECG): It is a recording of the heart's electrical activity.

Chest X-ray: In people with AS, the aorta above the aortic valve is often enlarged which can be seen with chest X-ray. Also X-ray can reveal the calcification of the aortic valve.

Echocardiography: In echocardiography, ultrasound waves are used to obtain images of the heart chambers, valves and surrounding structures. It is a non-invasive test, which helps physicians to diagnose aortic valve diseases. An echocardiogram can show a thickened, calcified aortic valve. It can also show the size and functioning of the heart chambers.

Doppler echocardiography: this technique can be used to determine the blood pressure difference through the aortic valve and to estimate the aortic valve area (Kisslo et al., 2000). It can be performed by using two techniques, pulse wave (PW) or continuous wave (CW). PW Doppler generates and transmits a periodic pulse wave through a transducer (sensor) at a certain frequency (signal). The frequency of reflected signal from the blood is shifted by an amount proportional to the velocity of the blood flow (the "Doppler effect"). Using this method, measuring very high blood flow velocities is not possible due to the Nyquist-Shannon theorem (Ching and Wu, 1998). CW Doppler involves a constant and continuous wave signal that sends and receives from two different sensors. It is used to measure the highest velocity through the valve (peak systolic flow velocity across the orifice area) making possible the measurement of the effective aortic valve area (EOA) by the continuity equation to provide better assessment for severity of aortic stenosis (Alan et al., 1991). EOA is the minimum cross-sectional area of the blood flow jet.

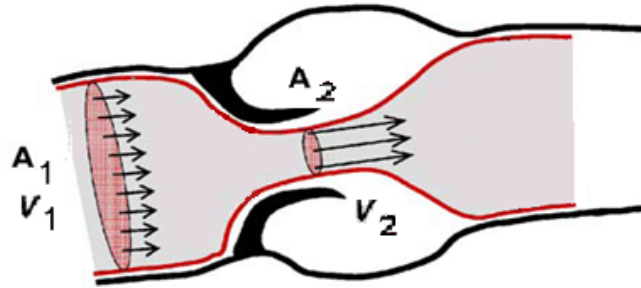


Figure 1.7 Schematic of the flow through an aortic valve.

The area of the outflow tract (A_1) can be measured by two-dimensional echocardiography. In Fig. 1.7 the areas and velocities associated with aortic valve domain are shown. We are able to determine A_2 (EOA) by, (Kisslo et al., 2000)

$$A_2 = (A_1 \times V_1) / V_2 \quad 1-1$$

where V_1 is the left ventricular outflow tract velocity measured using PW Doppler and V_2 is the highest velocity through the narrowed area of the stenotic orifice using CW Doppler. Also, the pressure difference through the valve can be determined by $\Delta P = 4V_2^2$. A_2 is called the effective orifice area (EOA) of the valve.

Table 1.1 shows the criteria to assess the aortic valve condition regarding stenosis based on the effective orifice area calculation. (Fuster et al., 2004)

Table 1.1 Aortic stenosis severity classification based on EOA

Aortic Valve Condition	EOA
Valve with mild stenosis	valve area exceeds 1.5 cm ²
Valve with moderate stenosis	valve area in the range of 1.0 to 1.5 cm ²
Valve with severe stenosis	valve area is less than 1.0 cm ²

Cardiac catheterization: Cardiac catheterization is one of the methods to evaluate AS. A small plastic tube (catheter) is inserted from a vein or artery and pushed through the aorta under X-ray guidance up to the aortic valve and into the left ventricle. Real-time pressures are measured on both sides of the aortic valve.

Magnetic resonance imaging (MRI): MRI is a safe and non-invasive medical test that helps physicians to see the detailed pictures of the organs and soft tissues and then diagnose AS. Patients are placed in a magnetic field. So, the magnetic moment of protons in organs align with the magnetic field. When the field turned off, the protons in different tissues go back to their equilibrium state at different rates that can be detected in images. A computer receives information and constructs the images.

Patients who have AS with symptoms of chest pain or shortness of breath need replacement surgery. Patients with symptoms usually undergo cardiac catheterization. In case of severe AS, aortic valve replacement (AVR) is usually recommended. Patients with the maximum and mean pressure gradient greater than 64 mmHg and 40 mmHg, respectively (Bonow et al., 2006), and an effective orifice area less than 1 cm² are recognized as having a severe AS. The overall mortality risk for AVR surgery is about 5%. Advanced age should not be a reason for not recommending AVR for AS. Patients in their 80s with strong heart muscles often benefit dramatically from AVR due to critical AS. (Dumesnil et al., 2008)

1.5 Prosthetic, Artificial Heart Valves

There are two types of prosthetic valves for replacement of aortic valves: mechanical valves (MV) and bioprosthetic valves (BV). A typical schematic of mechanical and a porcine type bioprosthetic valves are shown in Fig. 1.8. A biological prosthesis is usually made of porcine

aortic valve tissue or bovine pericardial tissue. Mechanical valves are made of pyrolytic carbon or combination of pyrolytic carbon and metal. Each type has its own advantages and disadvantages. Each year, more than 170,000 prostheses are implanted in patients in the world. Approximately 60% of those are mechanical and 40% are biological valves (Schoen and Levy, 1999). The average lifetime of a biological valve is between 10 and 15 years (Sauren, 1981). Mechanical valves comparing with biological valves have more durability. As a result, to decrease the risk of another valve replacement, in younger patients it is often recommended using mechanical valves.

Biological valves are more biocompatible than mechanical ones; most patients who receive a biological valve replacement do not need life-long anticoagulant therapy after surgery. In fact, the final decision on which a valve type is more appropriate for a specific patient depends on several factors such as age, gender and health condition of the patient and the preferences of the surgical team. After a brief review of the different types of prosthetic valves, a specific type of biological valves (Percutaneous valves) and its advantages and implantation technique will be described (see Sec. 1.6), as they are the main subject of this research.

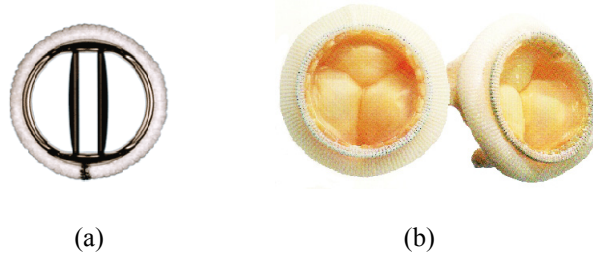


Figure 1.8 Prosthetic heart valves:

(a) a St. Jude Medical bileaflet prosthesis; (b) a Hancock porcine bioprosthesis. (Sauren, 1981)

1.5.1 Mechanical Valves

Mechanical valves have progressed in different designs from the ball and cage to bileaflet valves. Because of their high durability, they are implanted in young patients. However, increasing the risk of blood clotting is the main disadvantages of these valves and can cause a

thrombosis formation and stroke. To prevent this problem, patients must take anti-coagulant drugs persistently, which creates hemophilia. Also, patients with mechanical heart valves usually complain about hearing the sound of their artificial valve.

1.5.1.1 Caged Ball Valve

The first implanted mechanical valve prosthesis was a caged ball model in 1952 by Dr. C. Hufnagel (Hufnagel et al., 1954). In this model, a small ball is held in place by a welded metal cage (Fig. 1.9). In caged ball valves blood flow has high shear stresses and pressure gradient even in fully open position. Another effect of the ball on blood is damage of blood cells leading to release blood clotting ingredients. In addition, the patients need to take lifelong prescriptions of anticoagulants. Also, implantation of this valve takes a large space in the aorta, and because of that, it cannot be implanted in all patients (Stijnen, 2004).

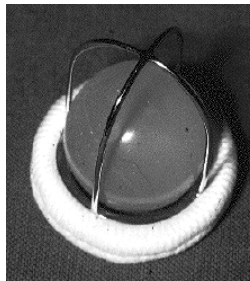


Figure 1.9 Caged ball valve. (Stijnen, 2004)

1.5.1.2 Non-Tilting Disc Valve

As it is seen in Fig. 1.10, these types of valves are very similar to the ball caged valves. All the disadvantages mentioned for the ball caged valve exist also for this type, but these valves have smaller size and take less space in the aorta.

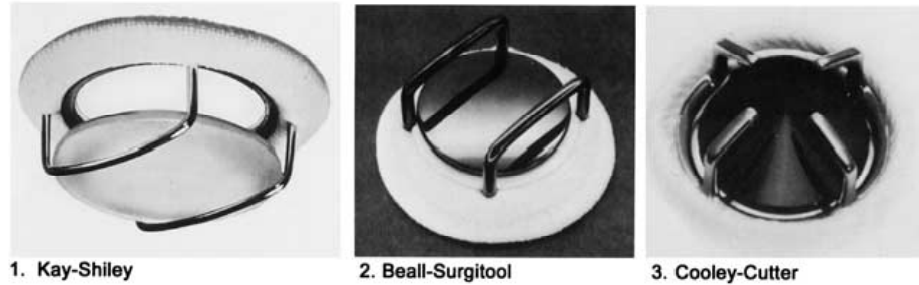


Figure 1.10 Three types of non-tilting disc valves. (Gott et al., 2003)

1.5.1.3 Tilting Disc Valve

For fifteen years, the caged ball valve was the best design. In the mid 1960s, a new type of mechanical valves was designed using a tilting disc to mimic the natural blood flow patterns. The disc floats between the struts, when the backward flow begins it closed and reopened when forward flow begins (Grixti et al. 2004) (Figure 1.11).



Figure 1.11 Tilting disc valves. (Stijnen, 2004)

The tilting disc valve improves the central flow while prevents backflow. Also for this valve type, blood cell damage is reduced comparing with caged ball valves.

1.5.1.4 Bileaflet Valve

The first design of bileaflet valves was performed in 1963. It consists of two semicircular leaflets that pivot on hinges. The carbon leaflets show high strength and excellent

biocompatibility. The leaflets stand parallel to the direction of the flow in completely open position (see Fig. 1.12).



Figure 1.12 Front view of a bileaflet valve. (Stijnen, 2004)

In around 2000 in UK, 91.8% of the implanted mechanical valves were bi-leaflet valves, 6.5% were single leaflet valves and 1.7% were caged ball valves from a total of 4049 implants (Nair, 2003).

1.5.2 Bioprosthetic Valves

The implantation of all mechanical heart valves needs anticoagulant medication. However, replacement of a natural valve with a prosthetic biological valve which would not need a long term anticoagulant cure provides the advantage of avoiding the risks of taking anticoagulants, especially for young women planning pregnancy and patients with hemophilic problems. Different types of biological valves have so far been developed.

An autograft valve is referred to the one translocated from one to other position of a same patient. As shown in Fig. 1.13, the patient's pulmonary valve is used to replace the diseased aortic valve. An allograft valve is a valve removed from another person and implanted to the patient.

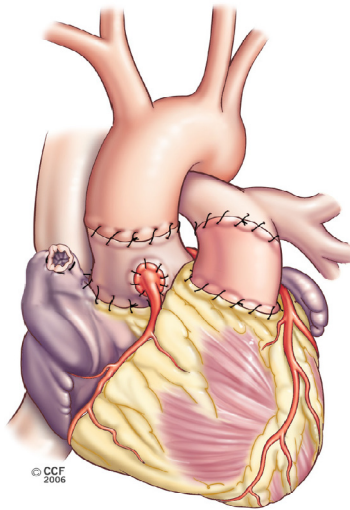


Figure 1.13 Switch operation (Ross procedure). (www.medicinenet.com/aortic_stenosis/article.htm)

A xenograft valve is one transplanted from animals such as pig, or manufactured from their tissue such as bovine pericardium (Bloomfield, 2002). The xenograft valves are less durable than mechanical prostheses; however, they have the advantage of not requiring a life-long blood medication (to prevent blood clots from forming on the valve surfaces).

A bioprosthesis can degenerate and calcify rapidly (cause to stenosis or a narrow opening in young patients). Therefore, bioprostheses are primarily used in patients over 65 years old or in patients who cannot take anticoagulant medication.

Biomedical engineers in the fields of material and structure have worked on the design of these valves in order to maximize their performance and durability. Recently, the development of a new type of bioprosthetic valves, the percutaneous valves, allowed valve replacement without open chest surgery. This is an optimal solution for patients whose surgical risks are elevated.

1.5.2.1 Autograft Valves

Donald Ross in 1967 introduced the Ross procedure that involves replacing the patients' diseased aortic valve with their own pulmonary valve (Fig. 1.13 and Fig. 1.14). This procedure requires a double valve replacement during one operation, thus increasing the surgical risk (Stelzer et al. 1997).

1.5.2.2 Allograft Valves

Allograft valve is a human heart valve that is obtained from a donor after death. The valve is frozen and then transplanted in the recipient. A homograft may be used to replace a diseased aortic valve or to replace the pulmonic valve during the Ross procedure. The patients' heart well accepts allograft valves as they are like their native valves (see Fig. 1.14).

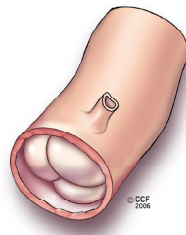


Figure 1.14 Allograft valve. (www.clevelandclinic.org)

1.5.2.3 Xenograft Valves

a) Porcine Valves: Most bioprosthetic valves are mounted on stents attached to a sewing ring. The stentless valves are more difficult to implant but they have a greater effective orifice area than the stented valves (Bloomfield, 2002). Hancock II Porcine (Medtronic) and the Biocor Porcine (St Jude Medical) prostheses are the most widely used types of this valve.

b) Bovine Pericardial Valves: These valves are made from bovine pericardium mounted on a stented frame (Fig. 1.15).



Figure 1.15 Bovine pericardium prosthesis. (Bloomfield, 2002)

1.6 Percutaneous Valves

In this section, a new type of bioprosthetic valves, the percutaneous valves, is introduced. A percutaneous valve does not need an open heart surgery. Its durability is in an acceptable range. For both groups of young and aged people, those who did not have a valve replacement previously and for whom their biological valve has to be replaced, it is a practical choice and the patients do not have to undergo the risks of open heart surgery.

The first human percutaneous aortic valve implantation was performed by Cribier in April 2002 as a treatment for a severe AS (Feldman, 2006). The percutaneous aortic valve is a three leaflets bovine pericardial valve mounted inside a stainless steel stent (Hanzel et al., 2006). A schematic of this valve is shown in Fig. 1.16. Percutaneous aortic valve replacement is a novel alternative and under investigation treatment for patients with severe symptomatic AS.



Figure 1.16 Percutaneous aortic valve. (Southard and Low, 2006)

A catheter is inserted into the body through the femoral artery and guided into the left heart. In Figs. 1.17 and 1.18, the catheter and its trajectory inside the heart are shown. When catheter reaches the heart, a balloon is inflated and pushed the calcified valve toward the aortic root and makes enough space for the new valve implantation (see Fig. 1.19 A). Then, a compressed percutaneous valve placed over the balloon-mounted catheter is located inside the diseased aortic valve (Fig. 1.19 B). The balloon is inflated and placed the valve in its final position (Fig. 1.19 C). In Fig. 1.19 D the implanted valve is shown.

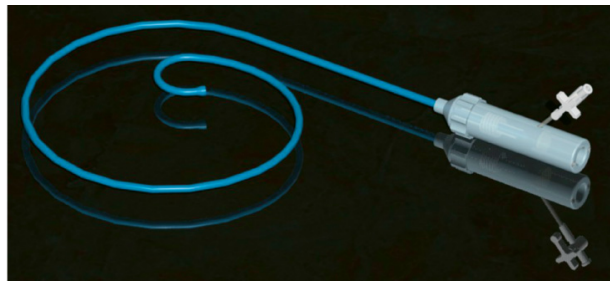


Figure 1.17 A view of the catheter. (Hanzel et al., 2006)

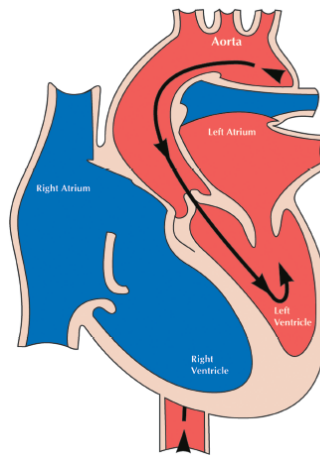


Figure 1.18 Trajectory of catheter inside the heart. (Hanzel et al., 2006)

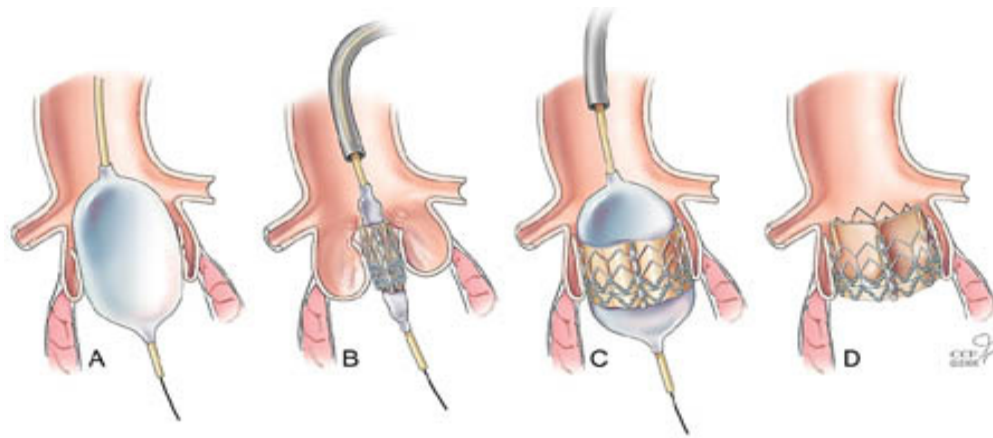


Figure 1.19 Percutaneous aortic valve replacement:
 a) balloon valvuloplasty; b) balloon catheter with the prosthetic valve inside the diseased valve; c) balloon inflation to secure the prosthetic valve; d) prosthetic valve in place.
<http://my.clevelandclinic.org/heart/percutaneous/percutaneousvalve.aspx>

1.7 Objective and Outline of Thesis Study

Thousands of people experience aortic valve diseases in North America every year. Among aortic valve diseases, Aortic stenosis (AS) is the most frequent cardiovascular disease after hypertension and coronary artery diseases. Patients with severe AS need surgery to replace their diseased valve with a prosthetic one. Open heart surgery to implant mechanical and traditional biological heart valves is difficult and painful for the patients and also is considerably costly for the government. Moreover, implantation of mechanical heart valves always increases the risk of thrombosis events and stroke, due to blood clotting. Also, biological valves implanted in the patients need to be re-implanted in ten to fifteen years. As it was discussed earlier, the development of percutaneous valves allowed valve replacement without open chest surgery. This is the optimal solution in patients whose the surgical risks are elevated. However, in a significant number of cases, the valve replacement with percutaneous valves failed due to the stiff leaflet material of the patient's stenotic valves due to thick calcium deposition.

Physicians can only rely on their personal experience to choose the treatment procedure for patients, which is a significant limitation in the management of cardiovascular disease. Also, it is important for surgeons to have an estimation of the material property of the valve leaflets in patients with severe stenosis to choose the most suitable surgery procedure to improve the patients' outcome.

The investigation of material property of the stenotic valve in vivo needs insertion of instruments into the body while in vitro, it is expensive and difficult in terms of reproducing the patients' own physiological conditions. Thus, it is of great interest to develop a virtual computer simulation to give surgeons a good estimation of the material properties of aortic valve leaflets based on easily achievable clinical patients' information. This may help to select the appropriate model of percutaneous valve or to change the surgery procedure (not to implant a percutaneous valve but replacement with a mechanical or bioprosthetic substitute).

The main objective of this research is to develop numerical modeling based on in vitro data in order to simulate and understand the dynamic behavior of the aortic valve mainly in presence of stenosis. The importance of this study is to develop a method for the noninvasively estimation of the patient's aortic valve material property. Also, the results can be useful to design of the tissue engineered valves.

Based on the defined objective, two separate numerical simulations are performed in this research: First, a structural model (dry model) of the aortic valve that is able to estimate the material properties of the aortic leaflets without considering a fully coupling interaction with the blood flow is developed. The review of the literature reveals that there is no previous works dedicated to the structural analysis of a stenotic aortic valve. Second, a numerical fluid structure interaction (FSI) simulation is performed in order to investigate the interaction between the flow and the structure of the aortic valve in a two way coupling modeling. A limited number of

research groups have studied FSI modeling of aortic stenotic valves and the existing models need improvements in terms of the FSI implantation technique and applied material property.

In particular the following chapters of this thesis are organized as follow:

Chapter 2 presents a review of the literature of the subject of this research. The literature review is divided in two parts: first a review on structural models (dry model) dealing with aortic valves will be presented and second a review on FSI modeling (wet modeling) of the aortic valve will be discussed.

The in vitro experimental study is presented in Chapter 3. The experimental facility, components of the system, experimental procedure and results are explained in this chapter.

Chapter 4 contains details of structural model (dry model). The numerical simulation results of three dimensional dry modeling of a healthy and five stenotic aortic valves are presented. Then, the proposed methodology to find the material properties of these valves based on the numerical simulations is introduced.

In Chapter 5, the three dimensional FSI modeling of realistic healthy and stenotic valves are presented. FSI modeling can also address the flow characteristics through the valve besides the structural information.

The last chapter, Chapter 6, forms the conclusion and discussion on the results of this research. The possibility of future studies and directions are suggested.

Chapter 2: Literature Review

2.1 Introduction

The cardiovascular system has been targeted by many researchers investigating its dynamic behavior function and hemodynamic physics. Among all studies in cardiology, modeling of the heart valves still has the opportunity for more improvement and study. The importance of the study on aortic valves can be understood when referring to statistics. Approximately each year 26,000 people die in the United States because of aortic valve disorder and also it is predicted that by the year 2020, 800,000 people worldwide will require heart valve replacements every year (Croft and Kaazempur Mofrad, 2010). Different strategies have been used to study the heart valves: in vivo studies using magnetic resonance imaging, echocardiography and other cardiac imaging modalities; in vitro experiments and numerical simulations. In numerical simulations, different simplifications and assumptions must be defined to analyze the behavior of aortic valves, but numerical simulations of the aortic valve can greatly contribute to a better understanding of the mechanics and hemodynamics of the valve. Moreover, it can help to explore the cause of diseased natural valves and also predict the durability and efficiency of artificial valves.

Numerical simulation can be used as an exceptional tool to study the mechanics of the aortic valves. There are two points of view: structural modeling (dry model) and fluid structure interaction modeling (wet model). In the dry model, pressure is applied to the surface elements of the structure as a boundary condition or applied load. There are two kinds of analysis; steady analysis (constant pressure applied) and dynamic analysis (time dependent pressure applied). It is the same also for fluid structure interaction (FSI) modeling, the steady case in which constant

pressure or velocity are applied as an inlet boundary condition and dynamic analysis which uses the time varying pressure or velocity.

The aim of using a dry model is to simulate the motion of the leaflets and find the stress and strain rates and other physical properties in the valve structure. In this modeling, there is no access to the hemodynamics. To have better understanding of blood flow characteristics such as velocity components, flow shear stress and vortices that play the major role in blood hemolysis and thrombosis, FSI modeling should be considered. In FSI modeling, there is a coupling between structure which is aortic root and fluid domain which is blood. In this method, fluid flow velocities are computed by solving Navier–Stokes equation through a computational fluid dynamics (CFD) algorithm while the structural elements remain fixed in place, then the structural elements are influenced by the flow velocities and pressure. In fully coupling algorithms, flow is also affected by the movement of the structure.

The present chapter consists of a comprehensive review on numerical modeling of the natural and prosthetic aortic valves.

2.2 Structural Modeling

In the field of cardiovascular research, increasing the power of computers led to a fast growth of numerical simulations in computational solid dynamics from the pioneer studies of the 70s up to present. Models were changed from two-dimensional to three-dimensional, dynamic analysis was employed instead of steady one and a huge progress happened in terms of applying more complex material properties to mimics the realistic behavior of biological tissues. In this section, a review of the works performed in numerical modeling of aortic valves using the dry model analysis is presented from the early 90s.

Huang et al. (1990) presented a two-dimensional (2D) finite element model of a Sheffield bicuspid valve (pericardial valve). They considered two models of a leaflet modeling (a radial and a circumferential slice) using an updated Lagrangian scheme in order to capture the dynamical behaviour in a semi-static loading. The model was based on a nonlinear hyperelastic material for tissue. The computed stress distribution in the deformable leaflets was presented.

Black et al. (1991) developed a three-dimensional (3D) geometry of the Sheffield bioprosthesis bicuspid heart valve using a steady analysis. They used a nonlinear elastic material. They found that using shell elements (4 node elements) was not enough to achieve accurate results. The results were however validated for the calculation of peak stress.

Thornton et al. (1997) simulated a 3D model of the Sheffield bicuspid valve using finite element method. They concentrated on the leaflets and considered them as shell elements with linear material properties and different leaflet thicknesses. Unexpectedly, they found that maximum stress happens in the belly of leaflets and is decreased with reducing thickness.

In 1999, Burriesci et al. provided additional details to the model of Black et al. (1991) on the Sheffield bioprosthesis bicuspid valve. They used LS-DYNA software to simulate a dynamical model with nonlinear orthotropic material properties. They showed that orthotropy causes a significant effect on the dynamic behavior and stress distribution in the valve.

De Hart et al. in 2000 used finite element method to simulate a three leaflet valve. They created a model based on one-half of a single leaflet. Two different fiber orientations (a sinusoidal and a unidirectional circumferential) were used to model the tissue material. The circumferential fiber reinforcements reduced stresses in the rubber layers by up to 60. The maximum stress happened at the commissures and the belly regions of the layers. In a separate study, they presented two more leaflet models (one with stent and one without stent) using a

linear elastic material for sinuses and a non-linear elastic material for leaflets. They described the Mooney-Rivlin material as a good candidate being similar to a realistic valve; however, because of difficulty in finding the material parameters they did not employ that model to their simulation. The results revealed a 47% reduction of the maximum principal stress in stented models compared to stentless models. The stentless sinusoidal model had much lower maximum principal stresses than the stented model. In both studies, applied maximum pressure was lower than the realistic physiological range, but they justified this by limitations due to the numerical instability.

Grande et al., 1998 and 2001, created a realistic geometric model of the aortic valve based on the MRI images using ANSYS software. They used an implicit, quasi-static scheme in their finite-element analysis. The results showed that by increasing the aortic root diameter and stiffening the surrounding structures, the leaflet stresses increased. In terms of material properties, they found that using graft material results in a more realistic valve behavior and stress distribution than using polyurethane.

In 2001, Li et al. simulated a model of porcine aortic valve using a nonlinear anisotropic material. Their study was based on steady condition using LS-DYNA software. They found even small amount of orthotropy can significantly affect the stress distribution on the valve leaflets. They concluded that anisotropic property is necessary to describe the realistic in vivo mechanism of the failure of porcine valves. They also compared the effect of linear and nonlinear material properties. However, as their simulation was based on applying a steady load, the effect of material nonlinearity was not noticeable.

Another study using LS-DYNA software was done by Arcidiacono et al. (2004) on pericardial valves. Their dynamic analysis consists of a linear elastic orthotropic material. They

found that even a small change in orthotropy can influence the leaflet performance in terms of stress distribution and dynamical behavior.

Some publications did not present experimental studies to validate their dynamical simulation such as those of Li et al. (2001), Grande et al. (1999), and Huang et al. (1990). But in 2005, Sun et al. simulated a pericardial valve under the quasi-static loading and showed that the experimental study is necessary for improving simulation and the design of the bioprosthetic valve. They validated their model using an experimental setup. The study found a small discrepancy between the finite element model and the experiment in terms of overall strain.

One of the advantages of using computational modeling is the ability to determine the ideal dimensions of the aortic valve in order to figure out the appropriate behavior of the normal valve. This work was done by Labrosse et al. (2006) in the context of clinical applications. The goal of the study was to determine a range of valve dimensions allowing a proper functioning of the leaflets (means normal opening and normal closing without regurgitation). This study consisted of numerical analysis and analytical and graphical works based on in vitro experiments. The results led to a list of geometric parameters ensuring normal valve function.

Ranga et al. (2004) developed a static model of the healthy aortic valve using the ANSYS software. They applied systolic phase pressure on the open configuration and diastolic phase pressure in the closed position. A longitudinal stretch was applied to the entire aortic root. The valve had an isotropic non-linear, five parameter Mooney-Rivlin, material. The material parameters were obtained based on the experimental data for stress and strain. They also compared the linear and nonlinear models and found that the non-linear model gives better results. The study also concluded that increasing Young's modulus results in an increase in stress and decrease in strain.

In 2008, Haj-Ali et al. did a structural simulation of a prosthetic heart valve by using the ABAQUS software with an implicit scheme. A nonlinear shell-based structural model was employed. A quasi static load was generated and the input data was obtained from in vitro experiments. The results were validated in terms of stress analysis by the experimental results of Alferiev et al. (2003). The objective of the study was to measure the six distance parameters of leaflet displacement by image processing. They evaluated the distance characteristics numerically and experimentally.

Koch et al. (2009) used the nonlinear, anisotropic and hyperelastic material for the leaflets. The hyperelastic parameters were obtained from curve fits to results of orthogonal uniaxial tensile tests on porcine aortic valve leaflets. They used steady analysis to model a complete aortic valve.

One of the best ways to simulate a realistic geometry is to obtain the geometry from MRI images. Conti et al. (2010) obtained the MRI data for ten people with healthy valves and used it as an input to their numerical simulation. They tested nonlinear and anisotropic materials. The results showed that the anatomical differences cause differences in stress and strain patterns. To validate the study, they used the experimental results reported in the literature.

One of the recent studies in finite element modeling of pericardial aortic valves was done by Xiong et al. (2010) using ABAQUS software. They compared the numerical simulations in three different implementation models: single point attached commissure (SPAC) tubular model, SPAC molded and conventional model. The main objective of this work was to compare the leaflet designs in order to achieve a clinical application. The molded leaflet design showed more improvement in performance compared to the tubular design and affected the durability of the valve. It represented better dynamic behavior with increase in effective orifice area and decrease in the magnitude of comprehensive stress.

One of the comprehensive models of aortic valve geometry was developed by Labrosse et al. (2010) using LS-DYNA software. The model is 1/6 of a complete geometry of the healthy, native aortic valve with anisotropic and hyperelastic material properties. The material parameters were obtained based on the experimental data. The dynamic pressure was applied to the surface of the valve. The results were validated by in vitro experiment. In terms of stress analysis they found that the maximum stress on the leaflet occurs on the attach line near the commissure during the diastolic phase.

In conclusion, the review of all structural modeling studies reveals that the numerical simulation of aortic stenotic valve, which is the subject of this thesis, has not been investigated before.

2.3 Fluid Structure Interaction

Development in numerical algorithms and computer facilities paved the way for simulation of blood flow in coupling with internal body structures using fluid structure interaction (FSI) modeling.

One of the pioneer works on FSI modeling of aortic valves was done by Chew et al. in 1999. Their model consisted of a 3D bioprosthetic porcine valve with a non-linear elastic behavior of the tissue and the reinforcement of the leaflets by collagen fibre bundles. Results were validated in comparison with pulse duplicator images. Their objective was to simulate tissue damage in porcine prosthetic valves.

De Hart et al. in 2000 developed a 2D FSI model, and later, extended it to 3D in 2003. For the 2D model, linear material properties were considered. The model consisted of two walls with the leaflets. The sinus, aorta and left ventricle were assumed to be completely rigid. A no-slip condition was applied on the wall boundaries and a time varying flow rate was applied at the

inlet. To validate the numerical simulations, they built an experimental set up. The results showed a good agreement between the numerical and experimental works. A small delay for the numerical model in terms of opening of the valve happened but the velocity profiles were in the acceptable range. Their new FSI methodology was based on their code and was validated, although the number of elements in fluid domain seems inadequate. For the 3D and isotropic model, they simulated during the systolic phase, one-sixth of the geometry with a fixed aortic root using SEPRAN software. They used a low elastic modulus and also an unrealistic inlet condition (Reynolds number five times less than the physiological one) in order to avoid numerical instabilities. This affected the results of maximum principal stress. But generally, the model showed a good dynamic behavior.

Another study by Nicosia et al. (2003) was done on the FSI modeling of an asymmetric aortic valve using LS-DYNA software. The geometry was developed based on MRI images of human aortic valves and coronary ostia. The material for aortic root had a linear elastic modulus and the leaflets were modeled using a nonlinear material. This is the only group who applied the pressure gradient as the inlet condition, but as they used an elastic module they had to scale down the pressure in order to avoid element distortion. The variation in instantaneous orifice area was shown; however, the trend for a healthy valve was not physiological.

Ranga et al. in 2006 studied the dynamical behavior of aortic valves employing FSI modeling. The geometrical data of fifteen volunteers was extracted using MRI. They considered three different geometries for normal, reimplanted and remodeled aortic valves. Ventricular and aortic pressures were applied as inlet and outlet boundary conditions. Dynamic behavior of the valve in terms of ejection time and rapid opening and closing time for each case was compared to the MRI results. Their results were not satisfactory since the computed maximum velocities were far from the MRI results.

Carmody et al. (2006) employed LS-DYNA software to study a three dimensional integrated left heart ventricle and aortic valve model using FSI approach. First, the blood flow in and out of the left ventricle was modeled. After that, they used the results of the ventricular outflow as an inlet velocity for the aortic valve. The advantage of this approach is to avoid assumption of flat or simplified parabolic inlet velocity condition as it is common in most of the numerical simulations. They concluded that the pressure difference across the valve leaflets is uniform. It means the pressure gradient which should be applied on the surface of valve leaflets in dry models can be uniform but has to be time varying.

Weinberg et al. (2007) developed a FSI modeling of one-sixth of a natural aortic valve. They investigated the dynamic and static behavior of the valve at cell, tissue and organ levels. They used nonlinear, anisotropic material (single term Mooney-Revlin) using LS-DYNA software. The instantaneous ventricle and aortic pressure were applied at inlet and outlet boundary conditions. For both static and dynamic analysis, they found that the radial stretch is higher than the circumferential one. The other work of this group was on the comparison between bicuspid and tricuspid valves which was published in 2008 (Weinberg et al., 2008). They concluded that the bicuspid valve does not open smoothly; the maximum velocity of bicuspid is lower than the tricuspid and besides the blood velocity pattern is completely different. In 2009 (Weinberg et al., 2009), the same authors studied the effect of ageing and calcium deposition on the aortic valve leaflets. They used the same geometry and boundary conditions as in their former works. The calcified zones were modeled with stiff shell elements and the thickness and material property of the leaflets in their simulation varied based on the age. They showed the relationship between the age of patients and the thickness of leaflets in order to investigate the influence of age on the dynamic and hemodynamic behavior the valve.

In 2008, Katayama et al. performed the FSI modeling of an aortic valve with and without sinuses (sinuses are dilations of the ascending aorta just after the aortic valve) for different semi physiological ventricular pressures. The results showed that a valve with sinuses has a rapid and longer opening. Also, the stress and bending deformation in longitudinal direction are higher. This work did not include in vivo or in vitro validation.

Van loon in 2009 investigated different shapes and stiffness for leaflets in a FSI analysis. This work has been done using SEPRAN package. Three models for valve leaflets were considered in an aortic root similar to the geometrical model of de Hart et al. in 2003. The flow velocity was applied as inlet condition, but the peak velocity was not physiologically correct and it was less than half of the physiological one. Also the flow domain was discretized by a very low number of elements, less than 1000. They considered the Neo-Hookean material for leaflets. The results as they explained were not satisfactory in terms of effective orifice area (EOA). In existing AS, the EOA should be less than 1 cm^2 but in their simulation the computed EOAs were greater than 1 cm^2 , even when using low inlet velocity magnitude. Also, the effect of thickening in the leaflets in appearance of AS was not considered.

As it was explained, there are only two groups who studied numerically the effect of AS on the dynamics of the valve with FSI modeling. These works have some limitations and need more improvements.

In this thesis, besides the results of structural simulation (dry modeling) of healthy and stenotic aortic valves, the results of FSI simulation (wet modeling) are presented and discussed. Also, the improvements made in the present study compared with the literature will be addressed.

Chapter 3: In Vitro Experiments

3.1 Introduction

To study the behavior of aortic valves in healthy and unhealthy conditions, a series of in vitro experiments were performed. The acquired information will be used in the next chapters to demonstrate the applicability of the numerical algorithm for the estimation of stenotic valve properties under the same conditions as with the in vitro experiments.

In vivo, having all the information about a native valve, mostly to have the behavior and dynamics of the valve, is difficult; but, in vitro all those information are accessible. The advantage of such experiments is that the variation of the geometrical orifice area can easily be recorded and that the severity of the stenotic valve is known. For this purpose, three different models of aortic valves (biological pericardial valve, moderate and severe silicone hand-made valves) were placed into a left-heart simulator. The pressure curves upstream and downstream of these valves were stored and the motion of the leaflets (to extract the geometrical orifice area) was recorded. This information will be used as an input for the numerical algorithm.

3.2 Experimental Facility

A left heart simulator (Vivitro Systems; see Fig. 3.1) was used in order to perform the experimental tests [Vivitro Systems Inc., www.vivitro.bc.ca]. This simulator is capable of reproducing the flow and pressure conditions existing in the human heart. Another important application of this simulator is to facilitate examining the effect of different prosthetic and synthetic valves on the flow characteristics.

Figure 3.2 sketches mechanical components of the left heart simulator setup. It consists of a left ventricle including inlet mitral valve and outlet aortic valve, a compliance chamber and a resistive element. Also, the figure shows the close-loop circulation circuit. The compliance

chamber simulates the elasticity of the arteries and the resistive element simulates the peripheral resistance induced by the large arteries and small capillaries.

This chapter also includes a brief explanation of the different components of the left heart simulator, a description of the stenotic valves tested, the experimental conditions and an example of typical pressure waveform obtained using this simulator.



Figure 3.1 Front view of the left heart simulator.

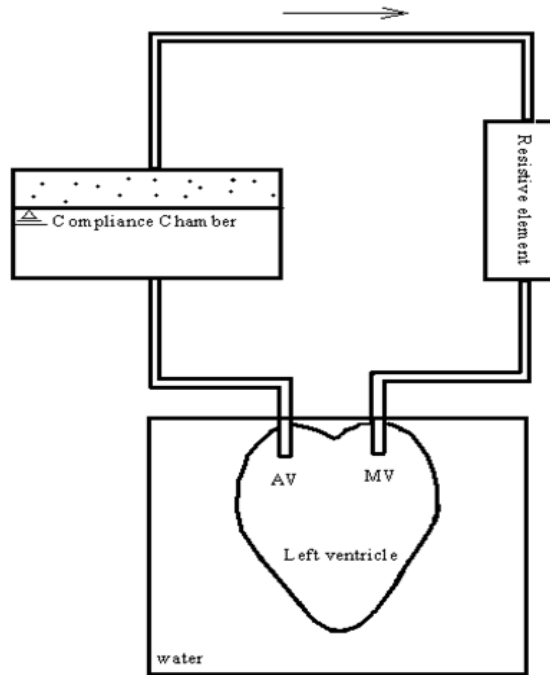


Figure 3.2 A schematic of left heart simulator circulatory system. (MV: mitral valve and AV: aortic valve)

3.3 The Components of the System

The system includes a model of left heart ventricle, a pump, instrumentations to measure flow and pressure, and a data acquisition system. The figures presented in this section (Figs. 3.3 to 3.7) are extracted from the Vivitro operating manual, 2006.

3.3.1 Super Pump and Pump Regulator

In the super pump system, a low inertia electric motor drives a piston cylinder pump. It is used to drive the flow in the left heart circulation. A linear actuator converts the rotary motion of the motor to a linear displacement of the piston using a ball-screw. The input waveform generated by the power amplifier can be controlled by position or velocity switches.

This system consists of different parts: amplifier, linear actuator, motor, pump head, motor cooling fan, and interconnecting cables. A visco-elastic impedance adapter (VIA) is placed

between the pump and the left-heart model. Its task is to damp the pressure and flow waveforms generated by the pump to produce physiological waveforms. The VIA includes a fixed resistive element and two adjustable compliance chambers (Fig. 3.3).



Figure 3.3 Super pump.

3.3.2 Left Heart Simulation System

The left heart system is designed to test heart valves under realistic conditions (Fig. 3.4). Before and after the valves there are pressure transducers. In order to have a good optical access, like for particle image velocimetry measurements, all the parts are made of transparent Plexiglas. The transparent elastic left ventricular model is placed in a hydraulic chamber and surrounded by water. A peripheral resistance knob controls the increase / decrease in the obstruction to the flow.

The compliance of the cardiovascular system is simulated by two compliance chambers. One is connected to the left heart system (right above the aortic valve) and another is connected to the aortic chamber.

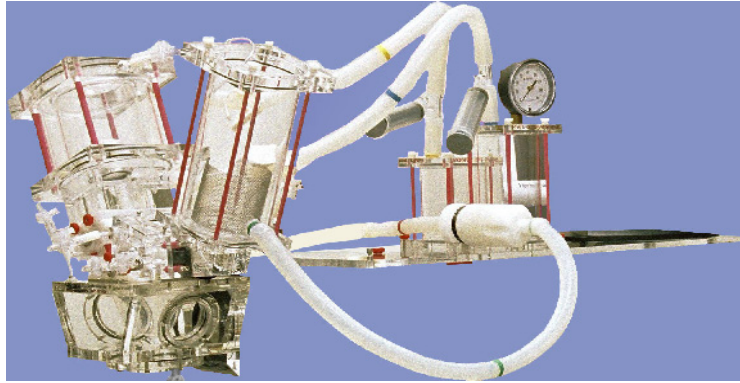


Figure 3.4 Left heart system.

3.3.3 Pressure Transducers and Control Unit

The amplifier is the main part of the pressure control system. Up to three pressure transducers can be plugged in using syringes. Before measuring, each transducer should be filled with fluid and de-bubbled. The transducers used in this study are Millar catheter MPC-500, with an accuracy of $\pm 0.025\%$ on the full scale. (Fig. 3.5)

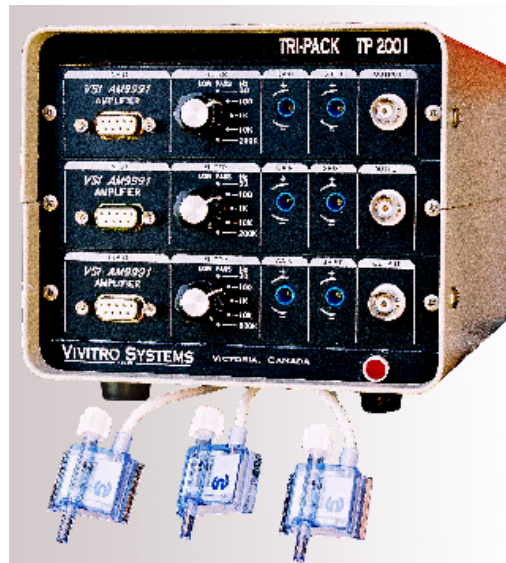


Figure 3.5 Transducer and control unit.

3.3.4 Electromagnetic Flow Meter and Transducer

A flow measuring system is used to measure the cardiac output (Fig. 3.6). The system consists of a wave flow meter (FM501) and an electromagnetic flow probe made by Carolina Medical Electronics Incorporated. The electromagnetic flow probe is inserted just downstream of the aortic valve. The probe has a diameter of 28 mm and matches the internal diameters of the aortic and mitral valve flow channels in the model.



Figure 3.6 Flow meter.

3.3.5 Programmed Waveform Generator

A programmed waveform generator (WG5891 type) is able to generate complex waveforms at different frequencies (ranging from 30 to 200 cycles per minute) for the left heart simulator system (see Fig. 3.7). The unit is designed to provide physiological waveforms as input to the super pump. It is able to store up to seven waveforms.



Figure 3.7 Front panel of the waveform generator unit.

3.4 Experimental Conditions

In this research, three different trileaflet aortic heart valve samples have been tested experimentally: a) a biological prosthetic pericardial heart valve (mimicking a healthy native valve) (Fig. 3.8(a)) and two previously validated home-made models of aortic stenotic heart valves (Blais et al. 2006) (Fig. 3.8b). These valves are made of several layers of silicone determining the rigidity (stenosis severity) of the stenotic valve. The two different examined severities are moderate stenosis with (EOA= 1.4 cm²) and severe stenosis with (EOA= 0.94 cm²).



Figure 3.8 (a) Biological aortic pericardial valve; (b) home-made stenotic silicone valve.

A saline solution with a concentration of 9 grams of salt in 1 liter of distilled water is used to fill the left ventricle model, since the flow sensor measures the voltage of a conductive solution flowing through a magnetic field. This solution has a viscosity of 1.002×10^{-3} Pa.s at 25 °C.

In all the experiments, the heart rate was kept at 70 beats /min, cardiac output was fixed at 5 lit/s and the systolic/diastolic aortic pressure for all three cases was between 80-120 mmHg (physiological condition).

For all cases, a high-speed camera captures the motion of the aortic valve leaflets at each instant. The camera has a frame rate of 1000 frames per seconds and it was installed on the top side of the valve near to sinotubular junction. For a closer view, an endoscope, equipped with a light source, was extended from the camera towards the aorta. These images were used as a reference for the numerical simulation (Chapters 4 and 5). An image processing is needed to extract the required information from theses raw images. This was done in this research by writing a MATLAB code.

3.5 Experimental Results

3.5.1 Aortic Heart Valve Samples

a) A Healthy Biological Prosthetic Heart Valve

The pressure and flow rate waveforms obtained in vitro for the biological prosthetic heart valve are shown in Fig. 3.9. These curves are comparable to what is obtained in a healthy patient. Fig. 3.10 shows the opening and closing of the healthy biological pericardial valve during one cycle captured by the high speed camera.

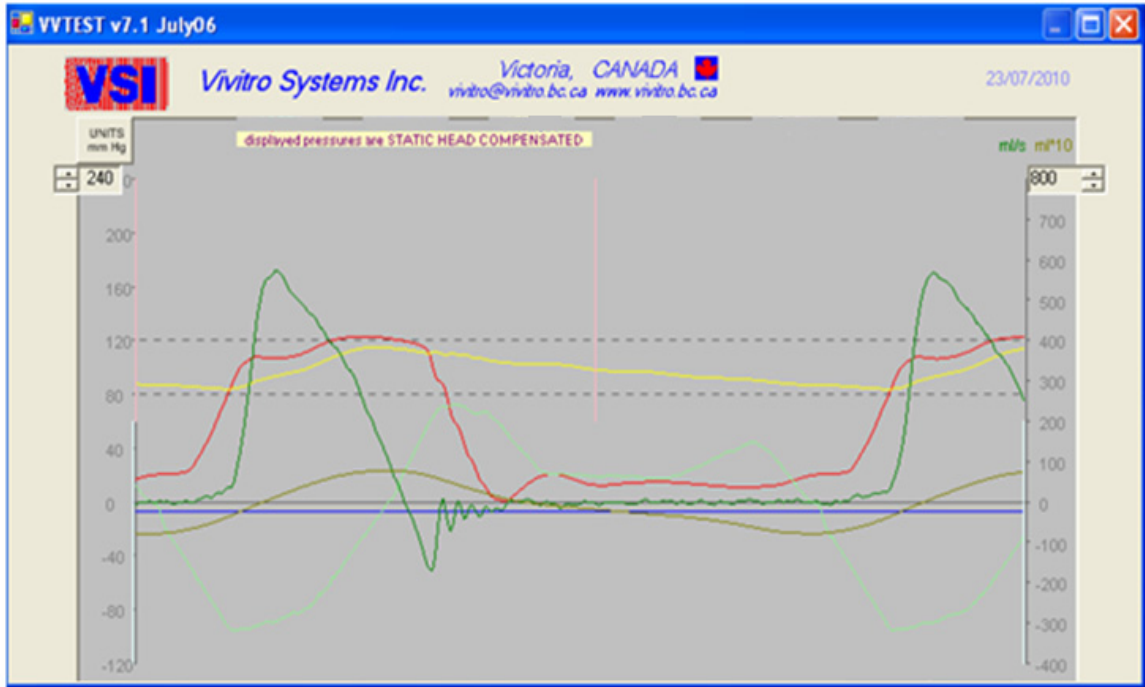


Figure 3.9 Pressure waveforms obtained in vitro on a biological pericardial valve. Red line: ventricle pressure, yellow: aortic pressure, light green: stroke volume, and green line: flow rate.

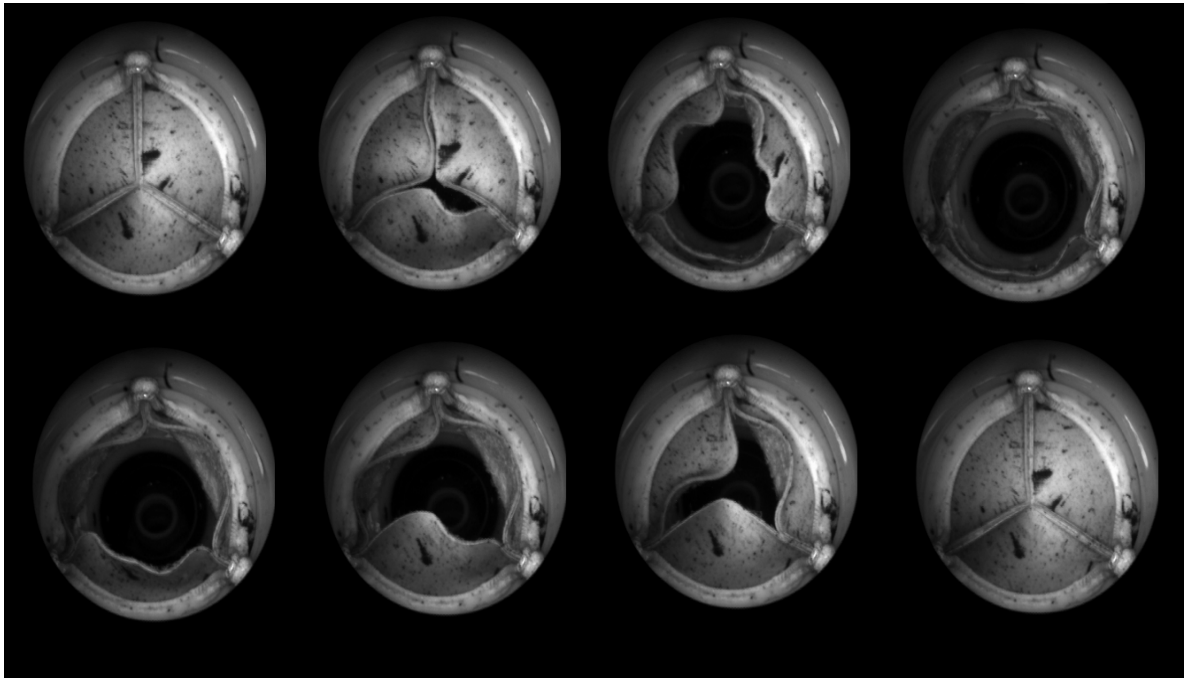


Figure 3.10 Opening and closing of leaflets in the biological pericardial valve during one cycle recorded at 1000 fps; (order: Top left to bottom right).

b) A Silicone Valve with Moderate Stenosis

The results on the moderate stenotic silicone valve are shown in Fig. 3.11. A significant increase in the maximum left ventricular pressure compared to the healthy biological prosthetic heart valve (previous case) is considerable (the maximum value of 150 mmHg vs. 120 mmHg). This is due to the pressure loss induced by the stenotic valve. This pressure loss has to be compensated by the left ventricle to ensure a constant flow rate through the valve.

Figure 3.12 shows the opening and closing of this valve with moderate stenosis during one cycle captured by the high speed camera.

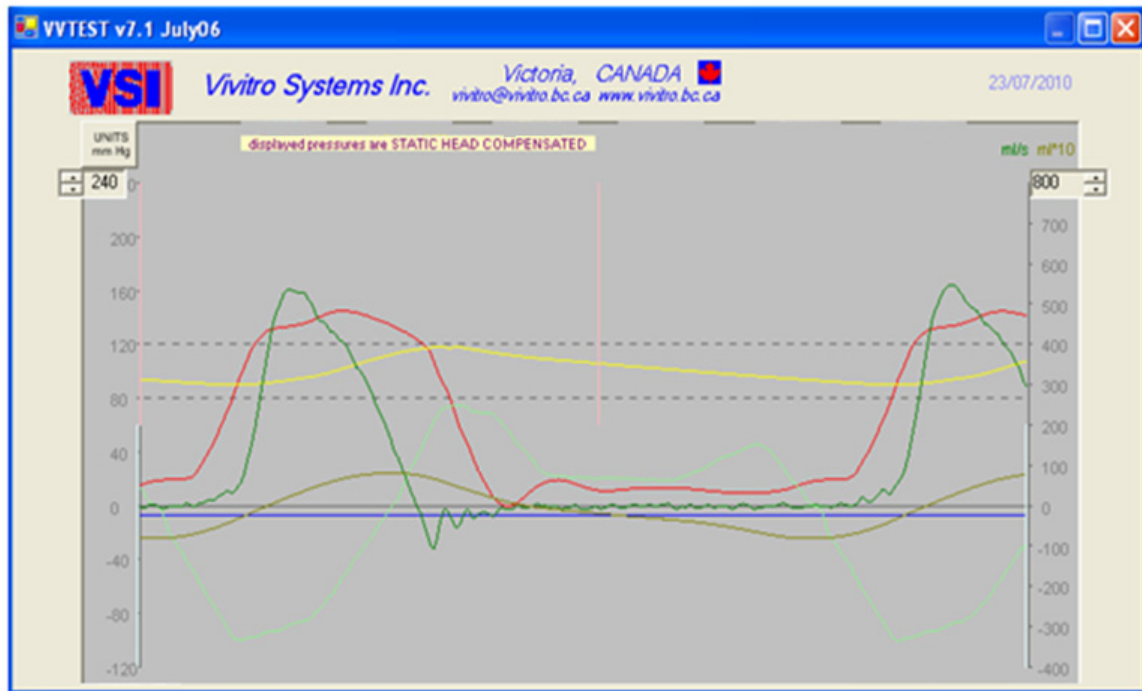


Figure 3.11 Pressure waveforms obtained in vitro on a silicone valve with moderate stenosis. Red line: ventricle pressure, yellow: aortic pressure, light green: Stroke volume and green line: flow rate.

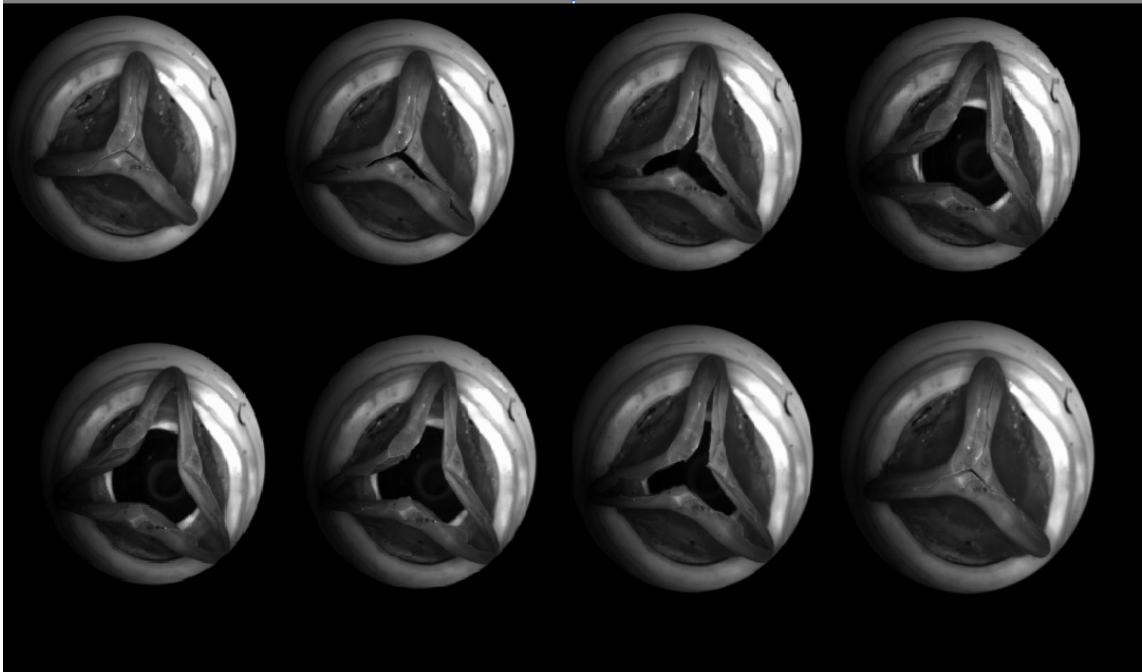


Figure 3.12 Opening and closing of leaflets in silicone valve with moderate stenosis during one cycle recorded at 1000 fps; (order: Top left to bottom right).

c) A Silicon Valve with Severe Stenosis

Figure 3.13 shows the results obtained for the severe stenotic silicon valve. In this case, the maximal left ventricular pressure have a value of 170 mmHg. Physiologically such pressure will increase left ventricle load significantly and result left ventricular hypertrophy. Figure 3.14 shows the opening and closing for this valve with a severe stenosis in a cardiac cycle.

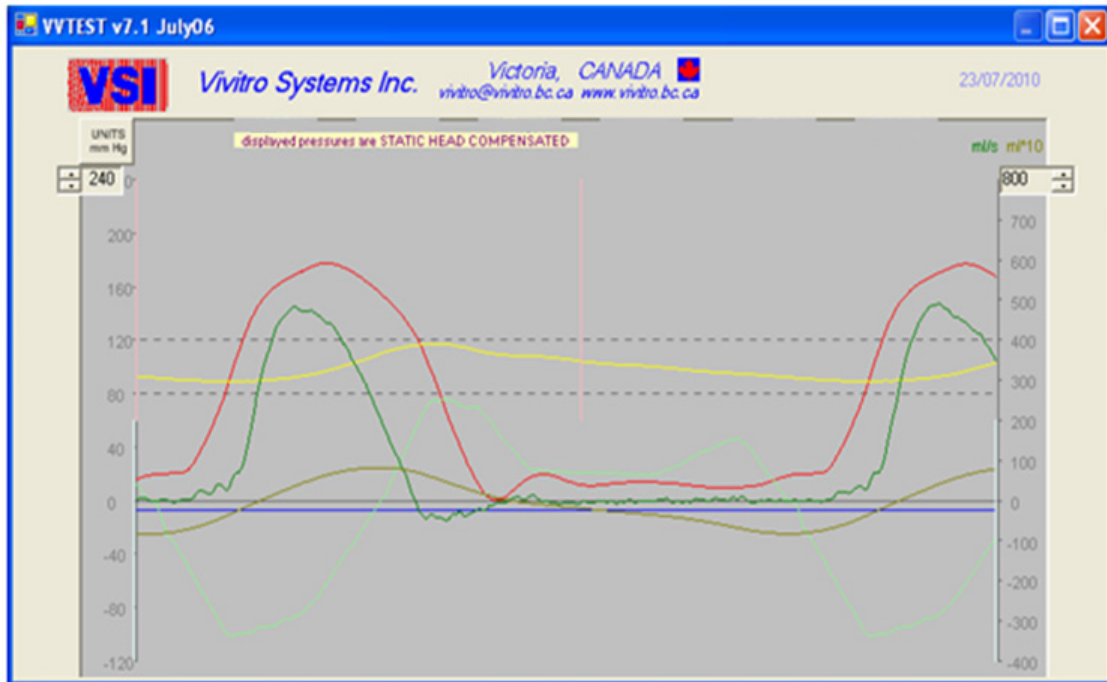


Figure 3.13 Pressure waveforms obtained in vitro on a silicone valve with severe stenosis. Red line: ventricle pressure, yellow: aortic pressure, light green: Stroke volume and green line: flow rate.

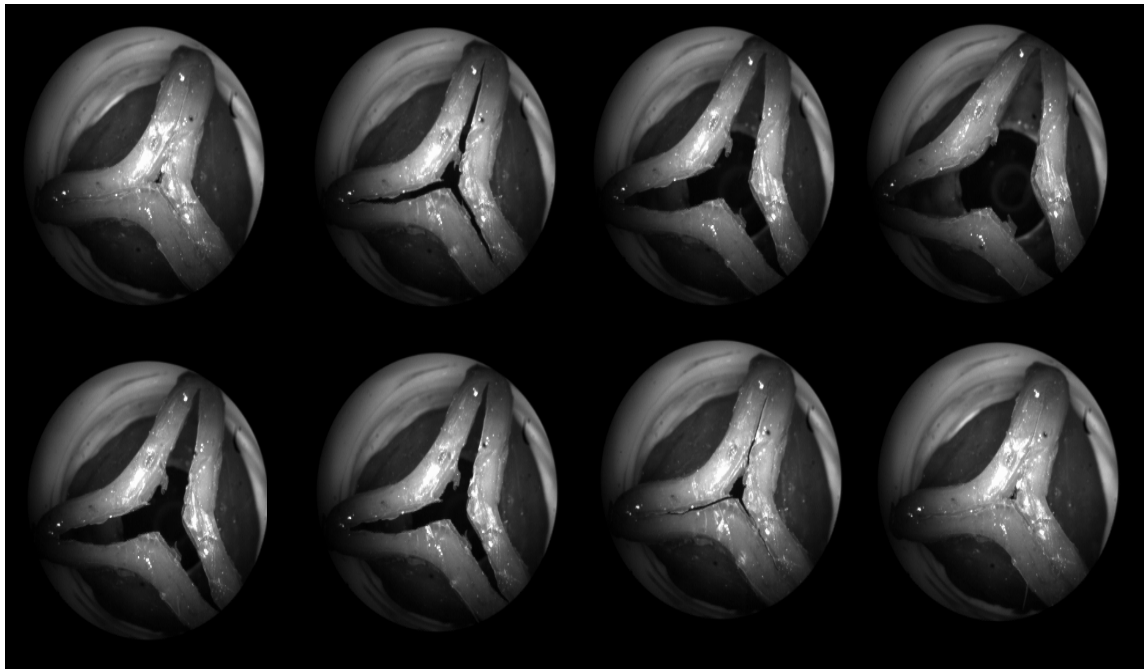


Figure 3.14 Opening and closing of leaflets in silicone valve with severe stenosis during one cycle recorded at 1000 fps; (order: Top left to bottom right).

3.5.2 How to Measure the Geometrical Orifice Area?

Geometrical orifice area (GOA) is defined as the maximum area that a valve can reach during the systolic (ejection) phase. The captured images of opening and closing leaflets (at a high frame rate of 1000 frames per seconds) then can be used to measure the GOA. Different image processing codes and software can be used to allow measuring the geometrical area accurately. In this research, a MATLAB code was used to post process the images to measure the GOA. Figure 3.15 shows the maximum opening state of the valve, GOA is recognized as the area inside the red contours.

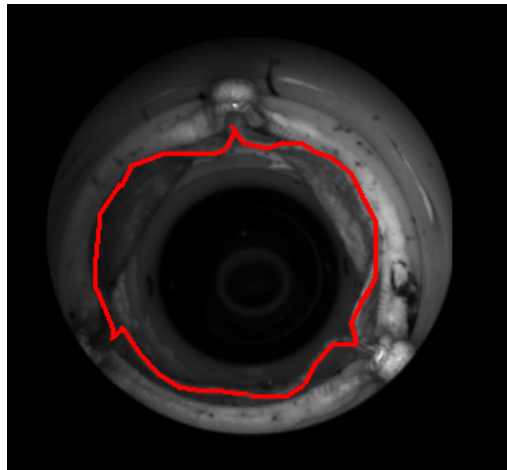


Figure 3.15 The maximum geometric opening area (GOA) of the valve (at 0.3 s); the red line is the location of leaflet free edges.

Using this post processing technique, the GOA for three tested aortic heart valves were obtained and listed in table 3.1. This information along with the recorded pressure waveforms are used in numerical simulation (structural modeling) to find the material properties for each valve. This is more elaborated in chapter 4.

Table 3.1 Measured GOA for three different valves (in vitro study)

Case study	GOA (cm ²)
Biologic pericardial valve	6.03
Moderate silicone valve	1.4
Severe silicone valve	0.94

It should be mentioned that in clinical practice, the effective orifice area (EOA) is measured, instead of the GOA, which can be determined by Doppler echocardiography. However, the determination of the EOA requires the knowledge of the velocity field upstream and downstream of the stenotic valve. This can be achieved numerically using FSI modeling. This is more discussed in chapter 5.

Chapter 4: Structural Model Analysis of Aortic Stenotic Valve

4.1 Introduction

As previously described in the first chapter, treatment for symptomatic patient with AS is open-chest surgical replacement of the diseased valve. The development of percutaneous aortic valves is currently allowing valve replacement without open chest surgery. This is then the optimal solution for patients with elevated surgical risks. However, this new technique is not mature yet and a significant number of cases of valve replacements have failed.

The main goal of this study is to provide clinicians with engineering tools that will guide them in making the best decision when the implantation of a percutaneous aortic valve is required. In fact, percutaneous valve implantation failure is mainly due to the interaction between the new implanted valve (with its stent) and the native stiff calcified aortic valve (Cribier et al. 2002). It is then important to determine the mechanical properties of the calcified aortic valve prior to percutaneous aortic valve implantation. However, this is not feasible since it will require stenotic valve explantation (and then no need for percutaneous valve replacement). To overcome this limitation, in this chapter, a method is suggested allowing the development of an index of valve stiffness. The originality of this model is that it considers aortic valve leaflets as anisotropic hyperelastic material under dynamic loading. Most of the previous studies on the aortic valve used simplified models by assuming isotropic material properties or static loading (mentioned in literature review).

This chapter organized as followed; first the numerical method used for the simulations is described including the structural analysis and material property formulations. Next, the geometry of the aortic root and aortic valve leaflets are described. Finally, the results of simulations on three in vitro and three in vivo cases are presented and discussed.

4.2 Numerical Method

Two types of model can be employed to simulate the aortic valve in structural modeling: static and dynamic.

For static models, the fundamental equation in finite element method is

$$[K] \{u\} = \{F\} \quad 4-1$$

where $[K]$ is the material stiffness matrix, $\{u\}$ is a displacement vector and $\{F\}$ is the vector of forces. By multiplying both sides by the inverted stiffness matrix, the displacement can be solved.

In dynamic models, however, the fundamental equation is

$$[M]\{\ddot{u}\} + [C] \{\dot{u}\} + [K] \{u\} = \{F\} \quad 4-2$$

where $[M]$ represents the mass matrix, $\{\ddot{u}\}$ is the acceleration vector, $[C]$ is damping matrix and $\{\dot{u}\}$ represents the velocity vector (Rao, 1999). To solve this problem, time can be discretized with two possible schemes: implicit or explicit.

For an implicit approach, the displacement vector $\{u\}$ at time $t+\Delta t$ is not simply expressed as a function of properties known at time t , but it also depends on the properties at time $t+\Delta t$. Then,

$$\{u\}_{n+1} = f(\{\ddot{u}\}_{n+1}, \{\dot{u}\}_{n+1}, \{\ddot{u}\}_n, \{\dot{u}\}_n, \{u\}_n, \dots) \quad 4-3$$

As an advantage of this scheme, the numerical stability is independent from the time step; however it requires significant memory storage resources.

In the explicit approach, the solution is based on a central difference scheme for time. As shown in Eq. 4-4, the displacement vector $\{u\}$ at time $t+\Delta t$ can simply be expressed as a function

of quantities known at previous time steps (t and $t-\Delta t$), and it does not involve any complex matrix inversion.

$$\{u\}_{n+1} = f(\{\ddot{u}\}_n, \{\dot{u}\}_n, \{u\}_n, \{\ddot{u}\}_{n-1}, \{\dot{u}\}_{n-1}, \{u\}_{n-1}, \dots) \quad 4-4$$

One of the important things to consider when using an explicit approach is an appropriate choice for the time step, since this highly influences the numerical stability and the computational cost. The time step should be small enough to reduce problems of numerical instability; however it is associated with a high computational cost. The time step depends on the speed of sound through the smallest element of the mesh and also depends on the stiffness of the material. Therefore, the element size and the material properties significantly affect the computational time (Burriesci et al., 1999). As an advantage, explicit solvers are more efficient, compared to implicit ones when a large number of nodes have to be considered in the domain.

The specific characteristics of the problem of interest in this thesis (such as large deformation in a short period of time), place LS-DYNA software as a desirable candidate to model the structural dynamics. LS-DYNA uses explicit scheme for time integration of the governing equations and, as mentioned previously, the time step in explicit solvers plays an important role. In LS-DYNA, for structural modeling, time step is governed by the speed of sound in the tissue material. The critical time step size is computed as (LS-DYNA keyword user manual. 2007),

$$\Delta T_e = \frac{L_e}{\{[Q + \sqrt{Q^2 + c^2}]\}} \quad 4-5$$

$$Q = \begin{cases} q_1 + q_2 L_e |\dot{\epsilon}_{kk}| & \dot{\epsilon}_{kk} < 0 \\ 0 & \dot{\epsilon}_{kk} \geq 0 \end{cases} \quad 4-6$$

The sound speed is set for all simulation as

$$c = \sqrt{\frac{E(1-\gamma)}{(1+\gamma)(1-2\gamma)\rho}} \quad 4-7$$

where, L_e is characteristic length ($L_e=V_e/A_{e\max}$), V_e is volume of the element, $A_{e\max}$ is the maximum area of element, $q_1=1.5$ and $q_2=0.06$ are constant dimensionless parameters of bulk viscosity, C is sound speed, γ is Poisson's ratio and E is Young's module of material.

As the first step, in a finite element analysis, the structure of interest is discretized into elements (mesh generation) with consideration of specific material properties, then loads are applied following the boundary conditions of the problem.

The equation of motion for each node is solved at each time step. Then, the resulting acceleration is integrated in order to find the velocities and displacements. Therefore, the nodes are moved to the new position. At each time step, the forces acting on the nodes are derived from the elemental stresses calculated from the strain along the constitutive equation of material properties.

4.3 Model Description

The model was discretized with brick elements with eight nodes element and loaded with physiological and realistic time-varying pressures. The physical governing equations of the structure are discretized with second order spatial accuracy. The initial aortic valve model is the same as the one used by Labrosse et al. (2010). However, in this thesis some modifications have been added to this model and a one third model of the aortic valve is considered (instead of 1/6).

Figure 4.1 shows aortic valve geometry and Fig. 4.2 shows the geometry used in this study. A total number of 5934 elements and around 8000 nodes are used for one third of the aortic valve.

Boundary conditions:

- 1) A prescribed boundary condition is used at the top surface of the ascending aorta (the purple color in Fig. 4.2). The motion of elemental nodes in this surface is set and constrained in the longitudinal (z) direction and just the 20% stretch of the entire model is applied on the nodes.
- 2) All the nodes on the bottom of the model, which are shown in yellow, are considered fixed to their position.
- 3) Because only one-third of the complete valve is modeled here, all the nodes on the aortic wall (shown in red in fig 4.2) are specified as contact nodes, and are restricted from penetrating the surface of the rigid wall (2 imaginary wall attached to these nodes) and the left ventricle outflow tract (LVOT). These nodes can change their position but they should remain in contact with the rigid wall without penetrating it.

Loads:

- 1) Pressure waveforms are applied as external loads to the model. The first load is the aortic pressure waveform applied on the aortic wall (see Fig. 4.2; blue area). The second load is the left ventricle (LV) pressure waveform applied on the LV wall at the level of the LVOT.
- 2) Transvalvular pressure gradient (TPG) is directly applied on the surface of the valve leaflet.

The specific dimensions of the model used for the simulations are taken from Labrosse et al, 2010 and listed in Table 4.1.

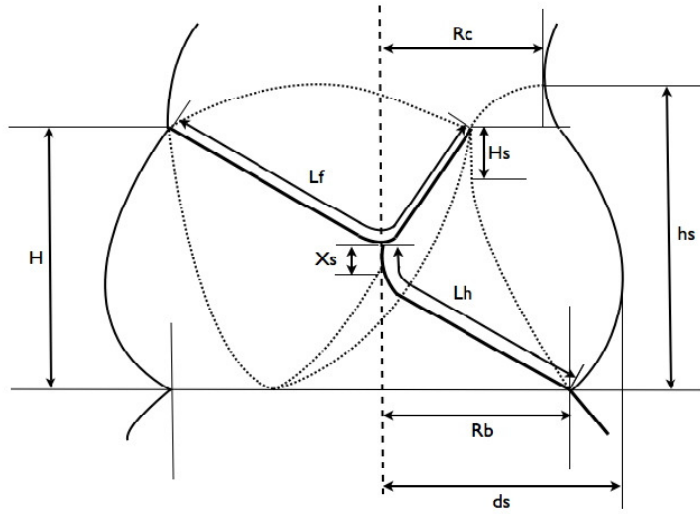


Figure 4.1 R_c : commissural radius, H : commissural height, h_s : sinus height, H_s : commissural height, X_s : coaptation height, R_b : radius of the base, L_h : leaflet height, L_f : leaflet free edge length (Thubrikar, 1990).

Table 4.1 Specific dimensions of the model.

Parameter	Value
Inner diameter of the base	23 mm
Inner diameter at the commissure	18.2 mm
Valve height (H)	17.8 mm
Sinus height (h_s)	21.0 mm
Leaflet height (L_h)	13.1 mm
Leaflet free edge length (L_f)	28.0 mm
Sinus maximum inner radius	17.2 mm
Sinus max .radius height	4.0 mm
Aortic thickness	3.4 mm
Leaflet thickness	0.5 – 2.5 mm
Tissues mass density (ρ)	Healthy 1000 kg/m ³

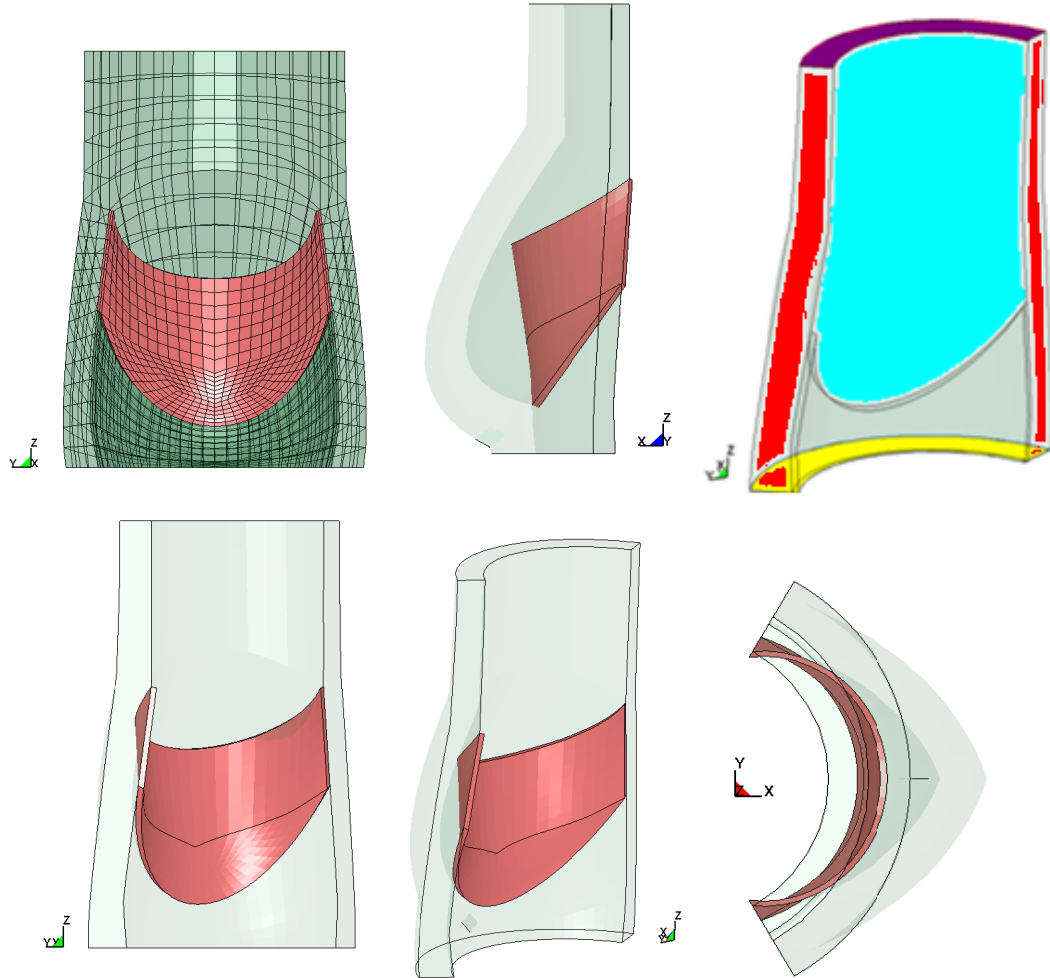


Figure 4.2 Different views of the one third aortic valve geometry used for the simulations. In all pictures, pink and green represent the leaflet and aortic root (sinus and base). First picture from the top (right) shows the location of boundary conditions.

In current study, the material entitled “MAT_Heart_Tissue” is selected in LS-DYNA for material of aortic root (including the ascending aorta, leaflets and the sinuses). This material has nonlinear anisotropic and hyperelastic properties. However, different material constants are applied in order to take into account physiological regional differences in material properties in the aorta. This material were tested and characterized by Guccione et al. (1991) and also were used by Sun et al. (2009), May- Newman et al. (1998), Omens et al. (2002) and Guccione et al. (1995).

In order to apply these material properties, a strain energy function (W) must be chosen. Over the years, many strain energy functions have been developed for different types of biological tissues, for example by Takamizawa and Hayashi (1987), or Fung et al. (1979). A strain energy function introduced by Guccione et al. (1991) has been implemented in LS-DYNA. For large deformations, the stress tensor S (second order Piola-Kirchoff stress tensor) can be calculated as,

$$S = \frac{\partial W}{\partial E} \quad 4-8$$

where E is the Green-Lagrange deformation tensor. The energy function is given as

$$W = \frac{C_1}{2}(e^Q - 1) + \frac{P}{2}(J - 1) \quad 4-9$$

$$Q = b_1 E_{11}^2 + b_2(E_{22}^2 + E_{33}^2 + E_{23}^2 + E_{32}^2) + b_3(E_{12}^2 + E_{21}^2 + E_{13}^2 + E_{31}^2) \quad 4-10$$

where C_1 , b_1 , b_2 and b_3 are material constants, P is a Lagrange multiplier (it is used to implement numerically a semi-incompressibility for material), J is third invariant stress tensor and E_{ij} is the Green-Lagrange strain components. The constants b_1 , b_2 and b_3 represent the circumferential, the radial and the longitudinal directions, respectively. The values of material constants for the healthy leaflet are considered as $b_1 = 10.446$, $b_2 = 1.925$ and $b_3 = 1.925$ (Labrosse et al., 2010). In this study, for modeling an aortic stenotic valve, the constants b_1 , b_2 and b_3 are kept at the same values as those for the healthy valve and the stiffness of the valve is modified by adjusting C_1 . Then, the value of C_1 will represent an index for stiffness valve.

Figure 4.3 shows the algorithm developed in order to estimate the material properties for a stenotic aortic valve. First, as inputs, the pressure waveforms (aortic and LV) must be recorded (using catheterization) and the geometrical orifice area (GOA) of the stenotic valve must be measured (using Doppler echo-cardiography or any other imaging technique) for each patient.

The pressure waveforms are applied as loading and an initial guess for C_1 is chosen for the material property. Then, a value for GOA of the stenotic valve is predicted. This predicted GOA is compared to the real measured GOA. When the predicted one is lower than the measured one, the computation are stopped and a linear interpolation is performed. Then C_1 corresponding to the GOA is obtained.

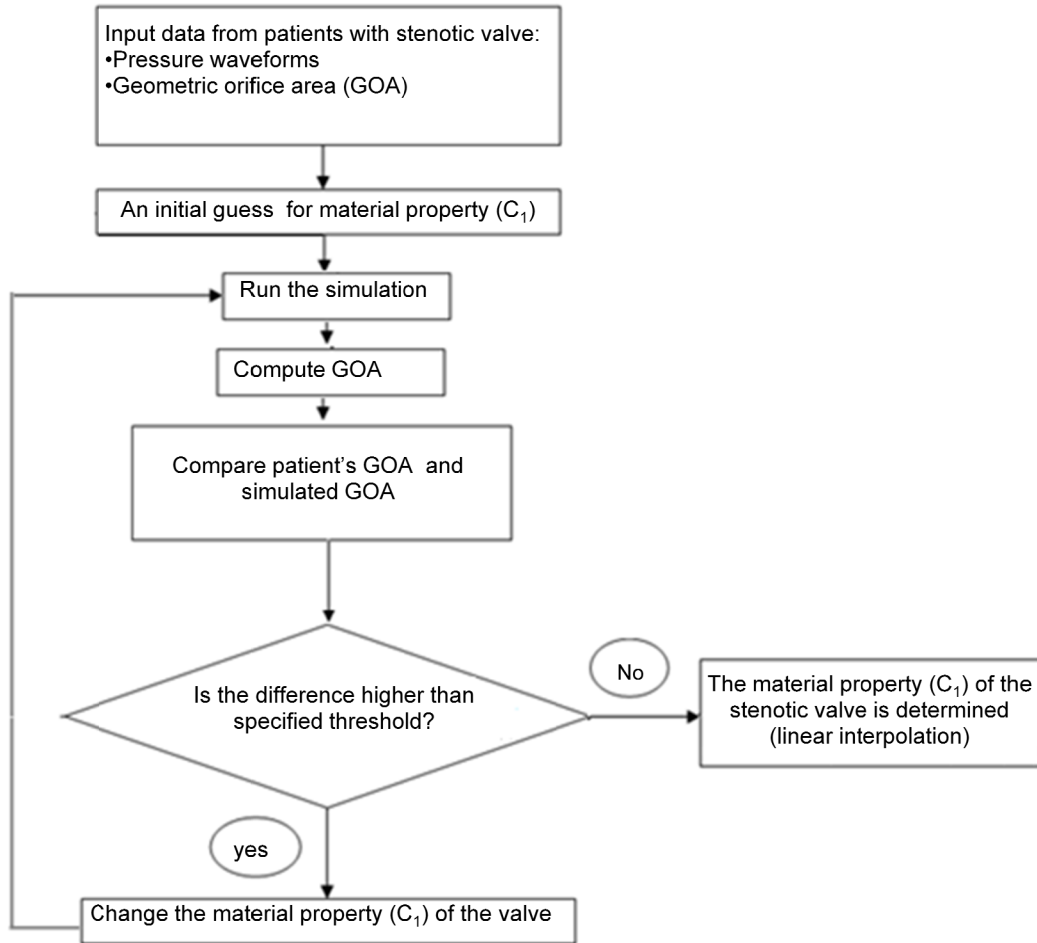


Figure 4.3 Algorithm for of the estimation of material property of an aortic stenotic valve.

In the simulations, the material density of the valve is chosen as 1250 kg/m^3 . This represents an intermediate material density between the density of healthy valve tissue (1000

kg/m³) and the density of calcium (1500 kg/m³). The impact of choosing this specific value for the density is further discussed in the section dedicated to sensitivity analysis.

4.4 In Vitro Experiments

The in vitro part of this study has been described in Chapter 3. A left heart simulator system was used to test the algorithm on healthy, moderate AS and severe AS cases. The pressure waveforms obtained experimentally are used directly in the numerical model as input loading. Also, for each valve, the maximum GOA was captured using the high speed camera and the computed using a Matlab code.

4.4.1 Case 1: Bioprosthetic Pericardial Valve

The real measured geometrical orifice area for the pericardial bioprosthetic valve is 6.03 cm². Also, the pressure curves from in vitro test are shown in Fig. 4.4. For the healthy condition (with the systolic/diastolic aortic pressure between 80-120 mmHg and thickness of 0.5 mm) the value for C_1 obtained using the algorithm is 0.048 MPa (an interpolation method is used to find the exact value for C_1). Figure 4.5 shows how the GOA numerically obtained varies as a function of C_1 . In Fig. 4.6, the instantaneous numerical GOA during one cycle is shown and compared to the real instantaneous GOA obtained experimentally. There is a good agreement between numerical and experimental results, except for the closing phase. This can be explained by the fact that contribution of the fluid to valve closure is not taken into account in structural modeling (dry model).

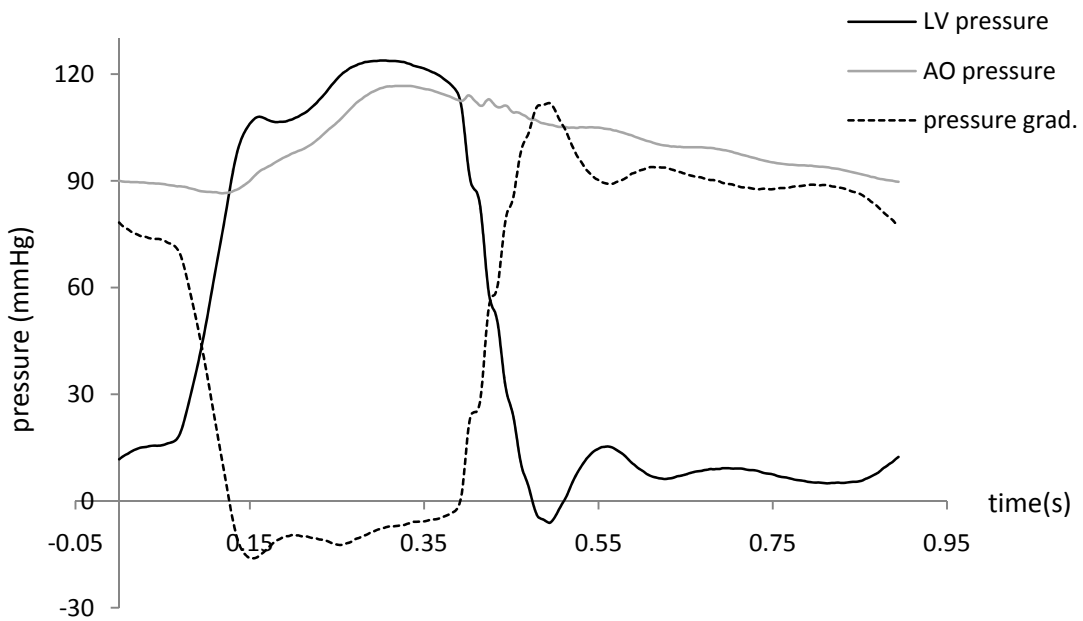


Figure 4.4 Time varying pressure wave forms for in vitro pericardial aortic valve.

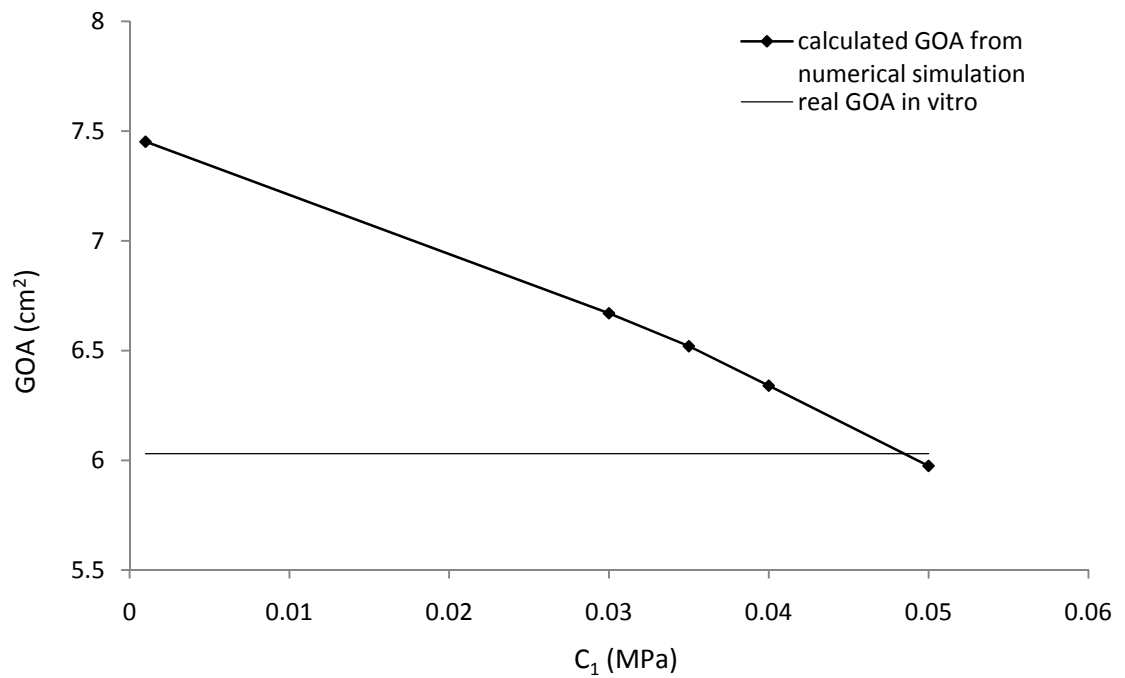


Figure 4.5 Variation of the GOA as a function of C_1 (in vitro), for pericardial aortic valve.

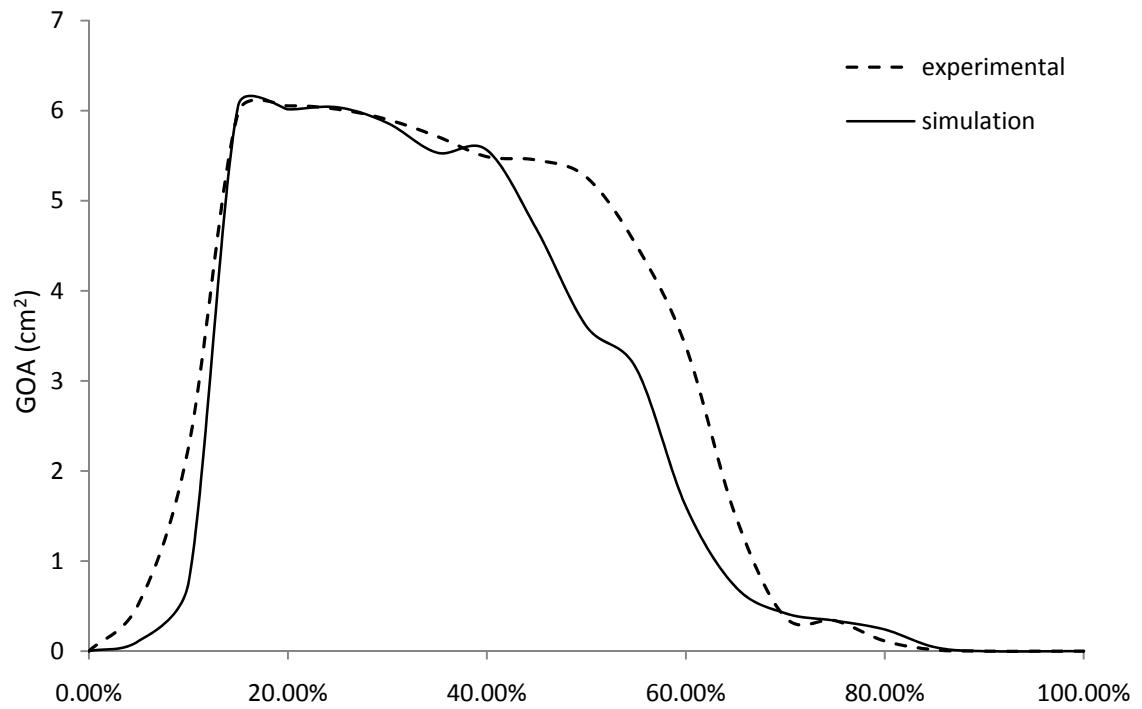


Figure 4.6 Instantaneous GOA measured experimentally and computed numerically (as percentage of systolic phase).

In Fig. 4.7, the maximum opening of the bioprosthetic valve is shown from an upper view (in yellow). The maximum opening of the valve occurs at $t=0.167$ s. Figure 4.8 shows some selected points at different instants during one cardiac cycle. Figure 4.9 shows the instantaneous computed opening and closing of the pericardial valve at different instants of the cycle.

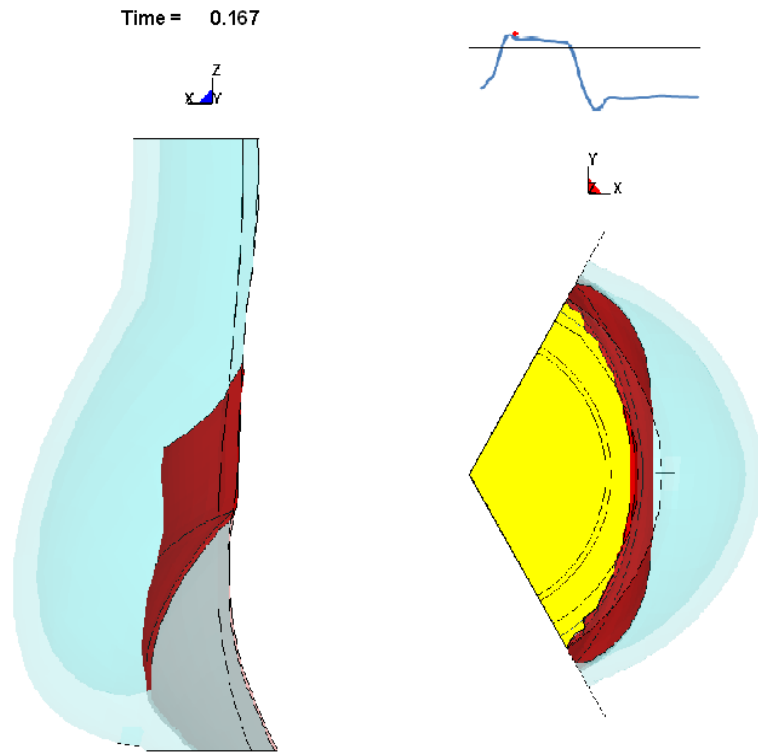


Figure 4.7 Maximum opening area of AV in pericardial aortic valve.

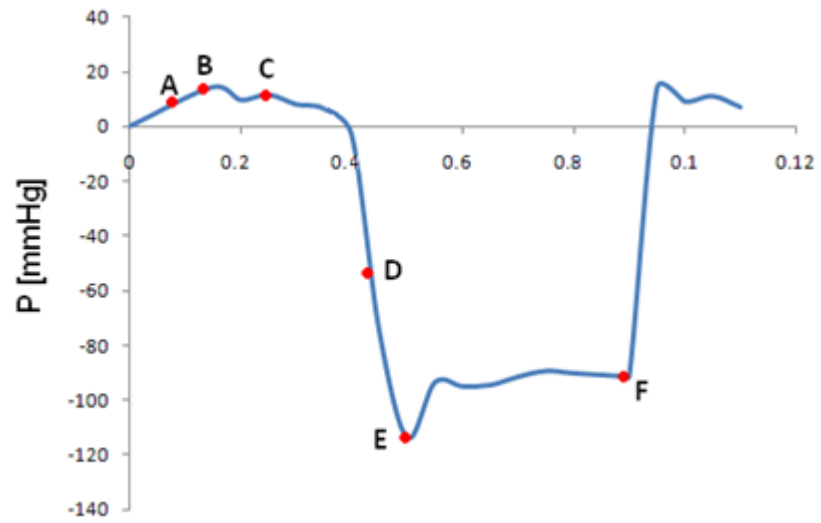


Figure 4.8 Instantaneous pressure gradient including selected points.

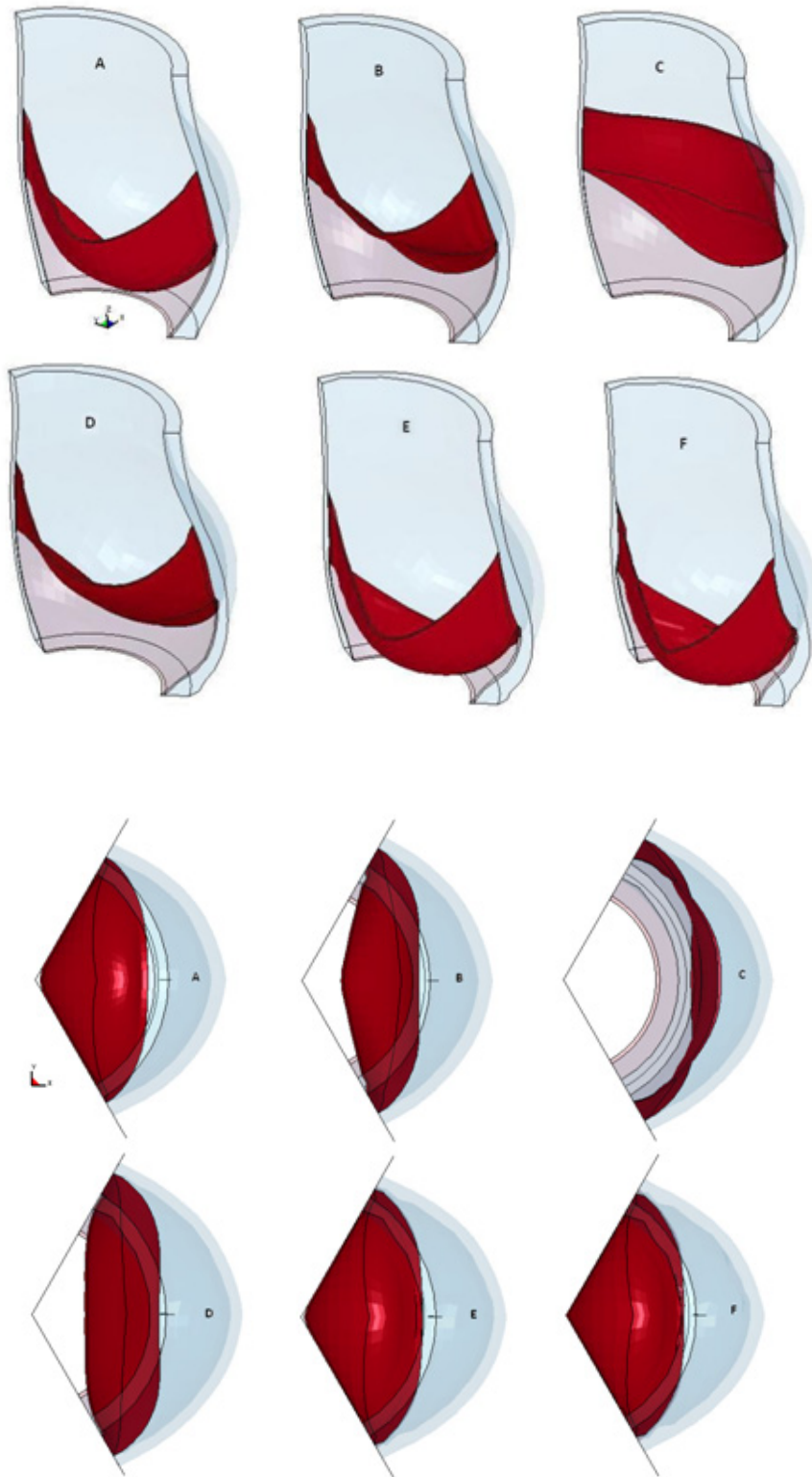


Figure 4.9 Opening and closing of pericardial aortic valve at different points selected in Fig. 4.8.

The complete closing of the valve happens at $t=0.44$ s (see Fig. 4.10). The kinematic characteristics of opening and closing of the valve obtained numerically are compared with the experimental measurements in Table 4.2. Here, ET is the time of ejection of blood from the LV beginning with aortic valve opening and ending with aortic valve closure, RVOT is the time interval between the initiation of leaflet opening and full valve opening, and RVCT is the time interval between initiation of valve closure and full valve closure.

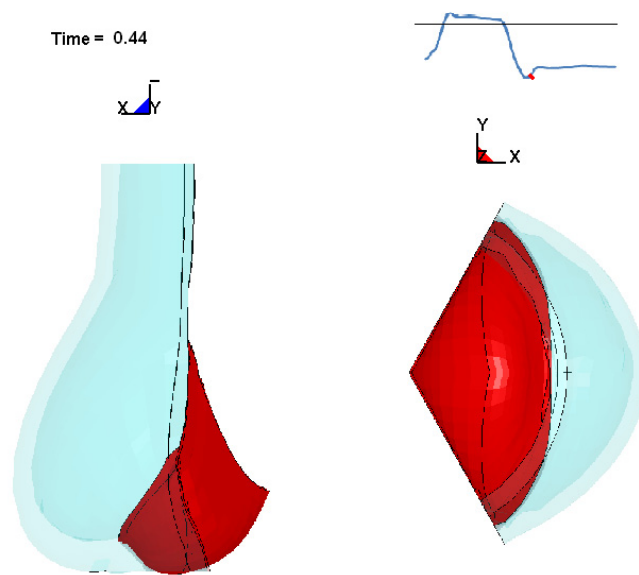


Figure 4.10 Minimum closing of in vitro pericardial aortic valve.

Table 4.2 Opening and closing characteristics of the in vitro pericardial aortic valve.

	Numerical simulation	In vitro data	% error
ET (ejection time)	325 ms	285 ms	14.03 %
RVOT (rapid valve opening time)	50 ms	60 ms	16.67 %
RVCT (rapid valve closing time)	60 ms	72 ms	16.66 %

The contours and vectors plots for maximum principal stress at the $t=0.167$ s (maximal valve opening) and $t= 0.44$ s (valve closure) are shown in Figures 4.11. Figure 4.12 shows the maximum principle stress and Von-Mises stress for the two critical points: 1) the attachment of leaflet to the sinus, and 2) the middle of belly leaflet. Table 4.3 shows the stress analysis results at the maximum opening and closing.

Table 4.3 Stress analysis for two critical points.

Location	Stress	At maximum opening (0.167 s)	At valve closure (0.440 s)
Middle of the leaflet belly	Von-Mises stress	1.01 MPa	0.98 MPa
	Max. Princ. Stress	1.06 MPa	1.05 MPa
Leaflet attached to the sinus	Von-Mises stress	0.45 MPa	1.94 MPa
	Max. Princ. Stress	0.47 MPa	1.90 MPa

At maximum opening of the valve ($t=0.167$ s), the maximum principle stress is 1.06 MPa and Von-Mises stress is 1.01 MPa (happen at the middle of the leaflet belly). The maximum principle and Von-Mises stresses at the valve closure ($t=0.440$ s) happen in the region of leaflet attachment to the sinotubular junction which is 1.9 MPa and 1.94 MPa respectively. The maximum principle stress found by Burriesci et al. (1999) was 0.87 MPa, by Conti et al. (2010) was 0.5 MPa and by Labrosse et al. (2010) was 0.75 MPa. These values were reported for healthy native or the porcine valves. Because of that, the reported values are smaller than what is computed in the current study. For a pericardial valve, Xiong et al. (2010) reported the maximum Von-Mises stress of 3.4 MPa which happened after maximum opening; in the present study, it is

found as 2.5 MPa (see Fig. 4.12 at $t=0.46$ s). The stress analysis shows agreement with other works.

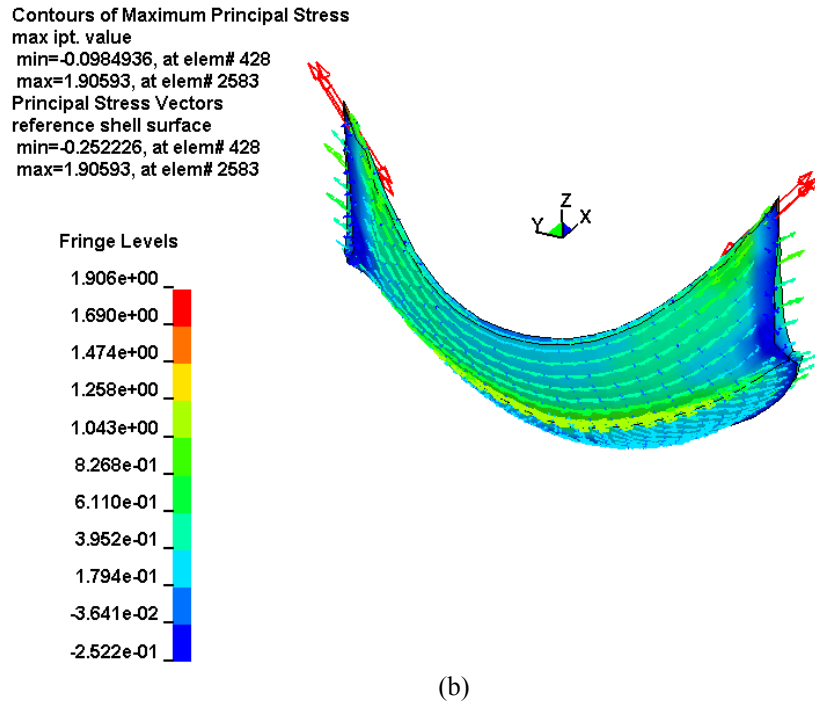
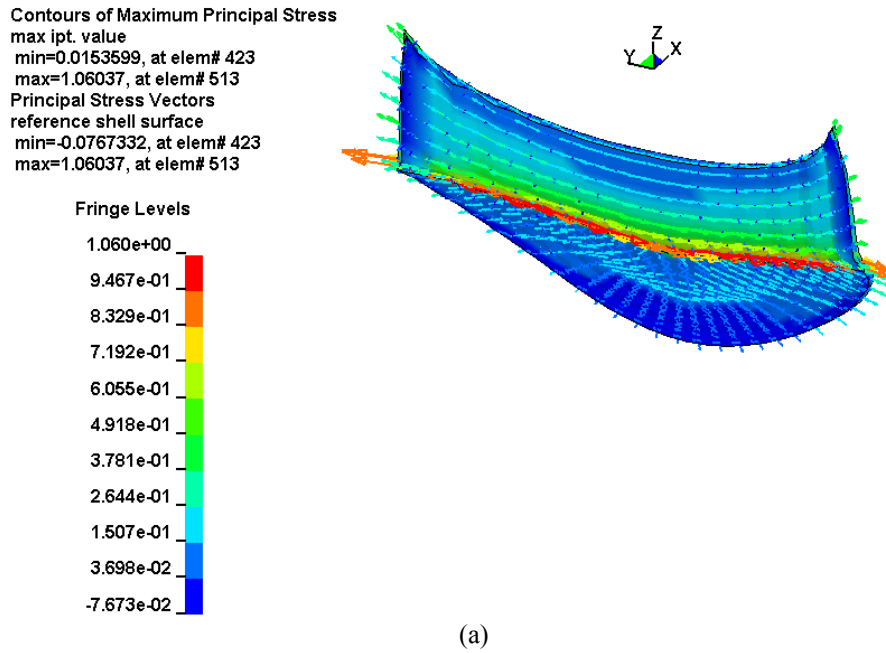


Figure 4.11 Contours and vectors of maximum principle stress at: (a) maximum opening; (b) valve closure.

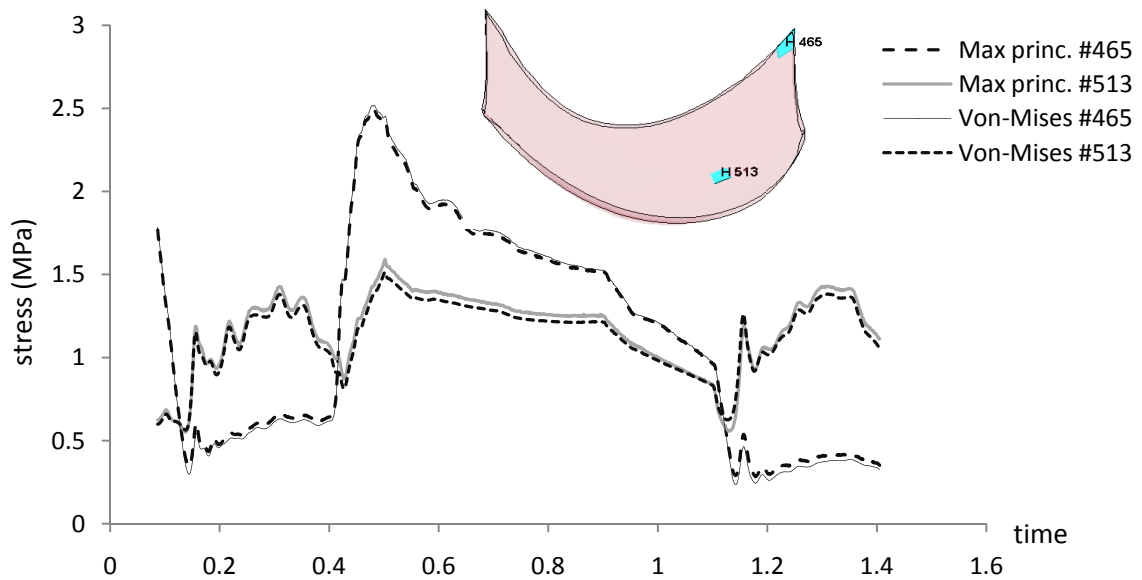


Figure 4.12 Stress analysis for two critical points during one cycle.

In stress analysis, an interesting finding is the location of maximum principal stress. This maximum occurs at the point of leaflet attachment to the sinus, close to the sinotubular junction. The other critical region is at the middle of the leaflet. Interestingly, this region has been reported as a critical region for valve tissue rupture by Carpentier et al. (1976).

4.4.2 Case 2: Silicone Valve with Moderate Stenosis

The second valve tested in vitro is a silicone valve representing a model of moderate AS. The pressure waveforms obtained in vitro are shown in Fig. 4.13. They are used as input to the numerical code. For this model the maximum GOA area was 1.4 cm^2 (at $t=0.26 \text{ s}$). A material property C_1 obtained for this case with moderate AS is 0.945 MPa (see Fig 4.14) (to find the value for C_1 an interpolation technique is used). In Fig. 4.15, the maximum opening of the valve leaflet is shown.

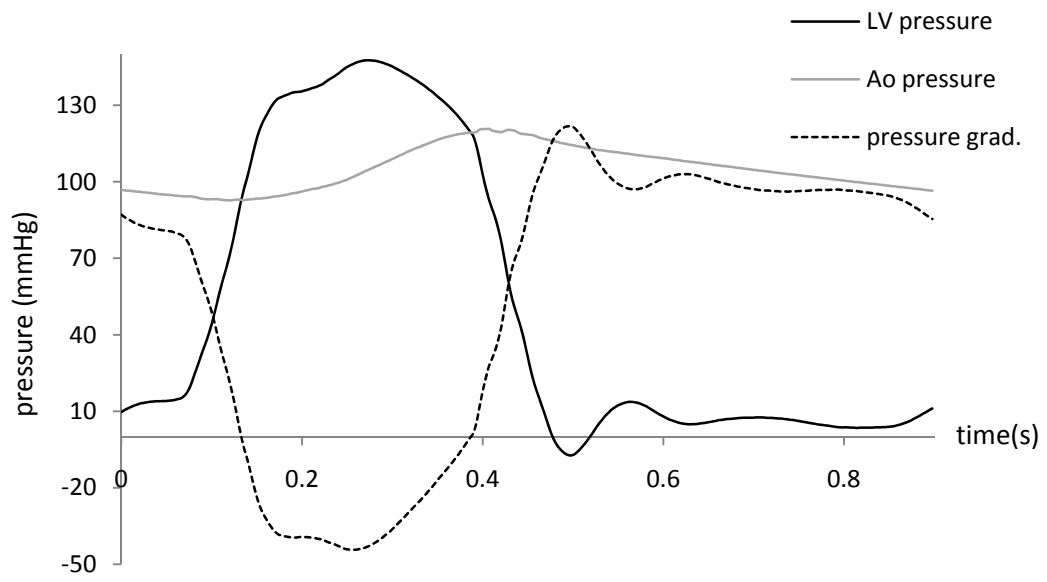


Figure 4.13 Time varying pressure wave forms for in vitro moderate AS.

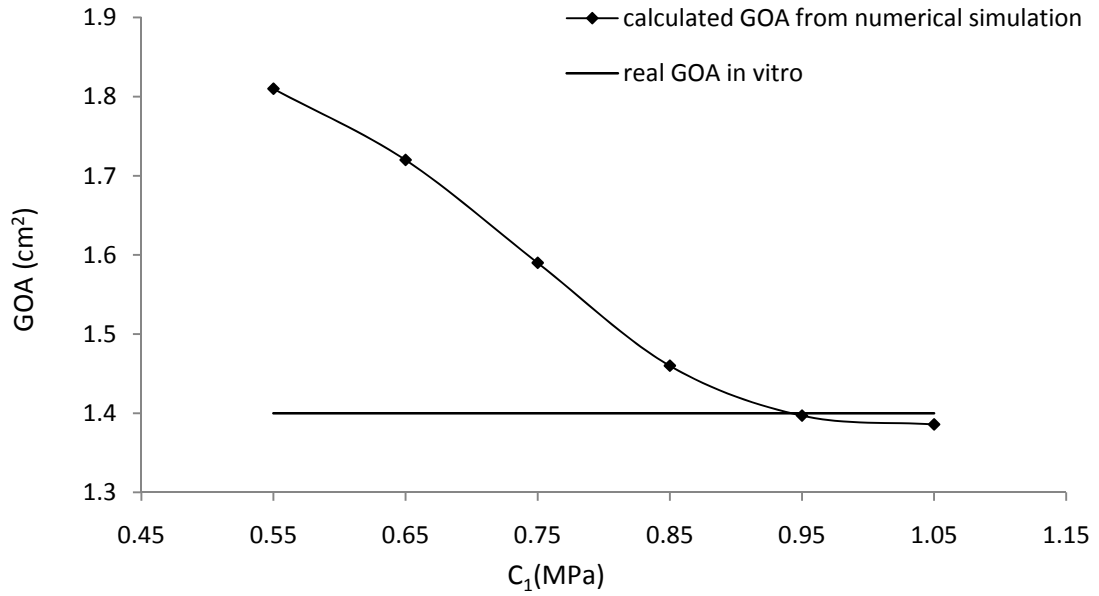


Figure 4.14 Variation of the GOA as a function of C₁ (in vitro), for moderate AS.

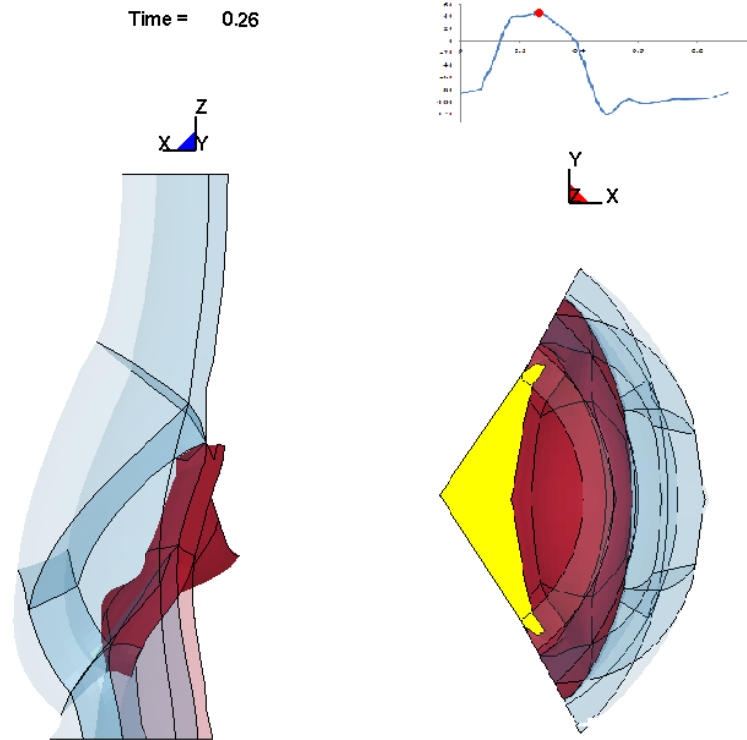
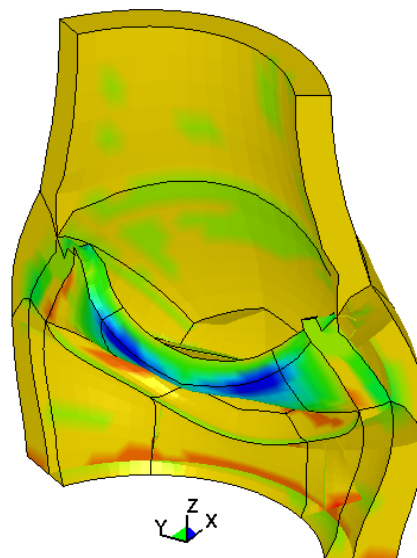
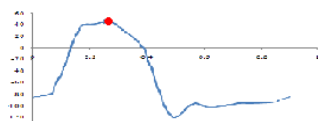
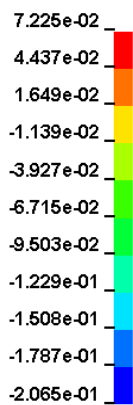


Figure 4.15 Maximum opening area of in the model of moderate AS. The yellow area represents the maximum GOA at $t=0.26$ s.

Also, the different results regarding stress analysis for this case at the instant of maximal opening are displayed on Figs. 4.16 and 4.17. The maximal values for the first, second and third principal stresses are 0.291 MPa, 0.179 MPa (at the location of leaflet attachment to the sinus, near to the sinutubular junction) and 0.072 MPa (at the middle of the belly leaflet), respectively. The simulations highlighted that the most critical points, in terms of stress level, are the points located at the junction between the valve leaflet and the sinus of valsalva.

Contours of Minimum Principal Stress
 max ipt. value
 min=-0.206549, at elem# 2824
 max=0.0722475, at elem# 4421

Fringe Levels



Contours of Maximum Principal Stress
 max ipt. value
 min=-0.0166752, at elem# 1310
 max=0.291268, at elem# 3562

Fringe Levels

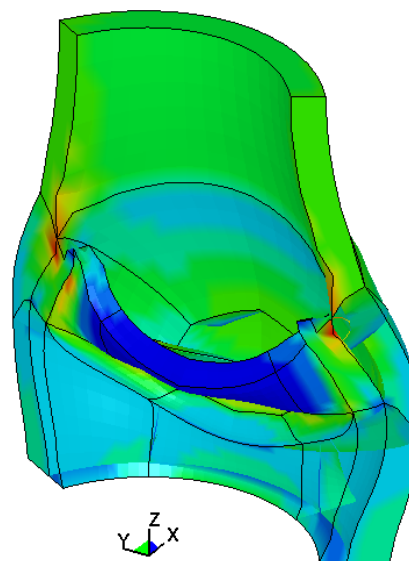
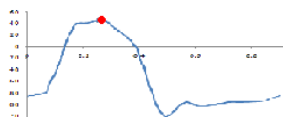
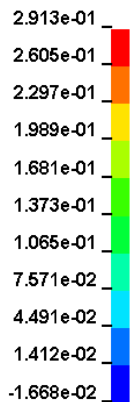
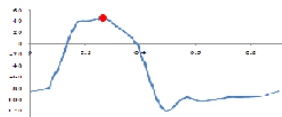
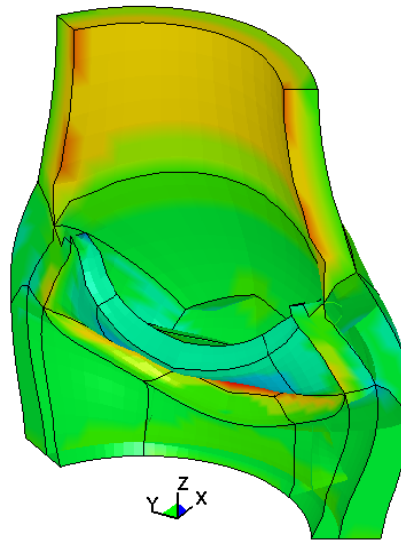
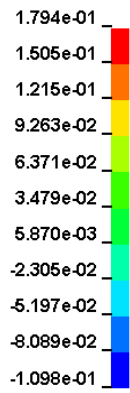


Figure 4.16 Contours of maximum and minimum principal stresses at the instant corresponding to the maximal opening of valve leaflets for the model of moderate AS.

Contours of 2nd Principal Stress
 max ipt. value
 min=-0.109805, at elem# 2752
 max=0.179384, at elem# 937

Fringe Levels



Contours of Effective Stress (v-m)
 max ipt. value
 min=0.0071165, at elem# 2977
 max=0.271698, at elem# 2743

Fringe Levels

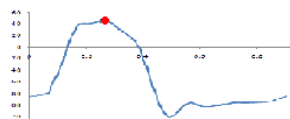
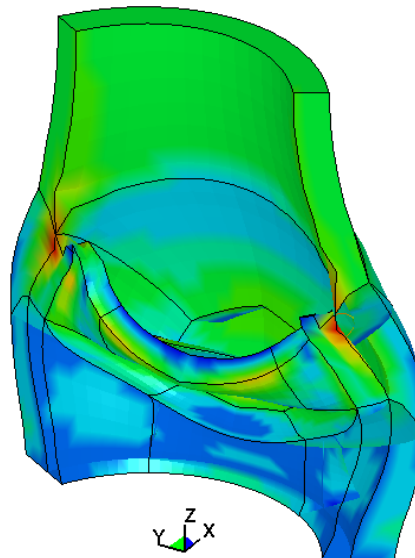
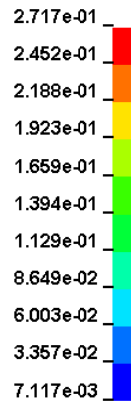


Figure 4.17 Contours of 2nd principal stress and Von- Mises stress at the instant of maximum opening of the valve leaflet for the model of moderate AS.

Figure 4.18 shows the aortic valve from two different views during the closure phase (diastolic phase). At this instant, it is expected to have a completely closed valve, like a healthy valve, (see Fig. 4.10). However, for a stenotic valve, this is not the case since a regurgitant area will persist (Wallerson, et al, (1986) and Zoghbi, (1988)). Interestingly, our simulations were capable of capturing the regurgitant orifice, approximately 9.1 mm^2 (yellow area in Fig. 4.18). Figures 4.19 and 4.20 show the stress distribution in the valve leaflet during the closure phase.

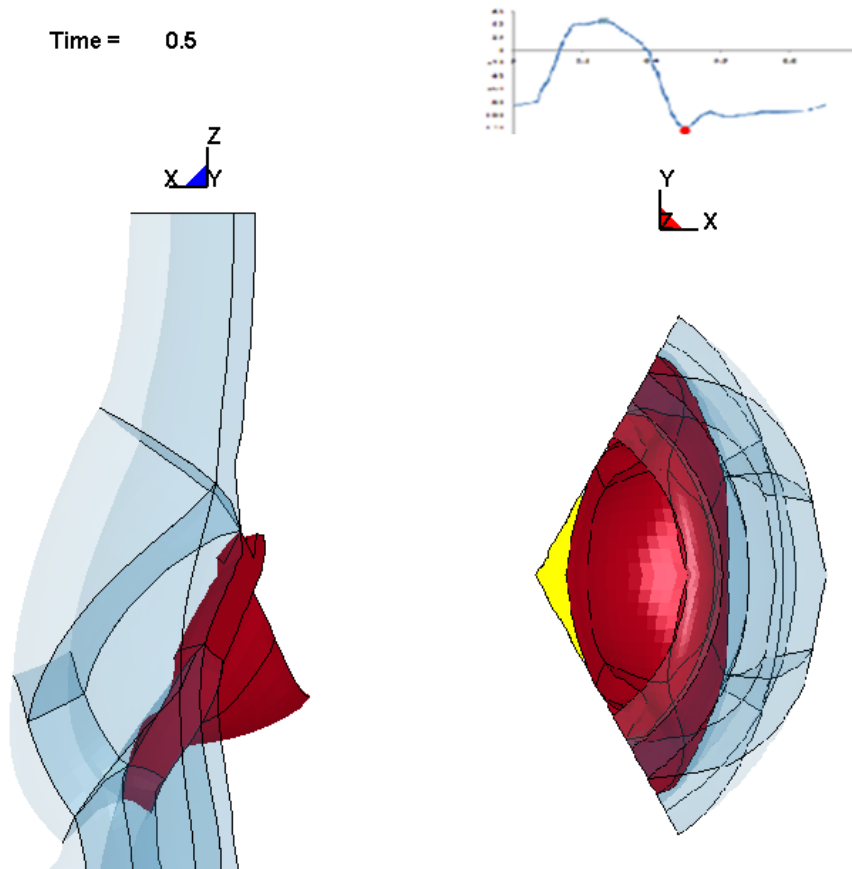
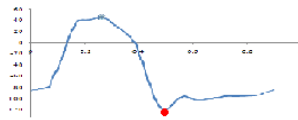
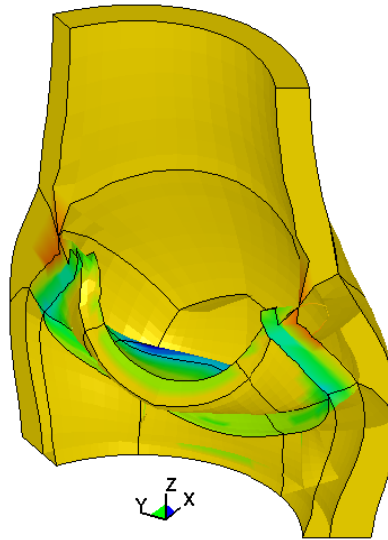


Figure 4.18 Minimum closure area in vitro moderate AS, yellow area is the simulated regurgitation area.

Contours of Minimum Principal Stress
 max ipt. value
 min=-0.518459, at elem# 2531
 max=0.172907, at elem# 1230

Fringe Levels



Contours of Maximum Principal Stress
 max ipt. value
 min=-0.112742, at elem# 2614
 max=0.923018, at elem# 2743

Fringe Levels

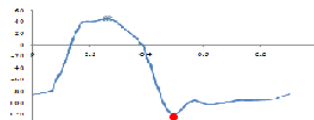
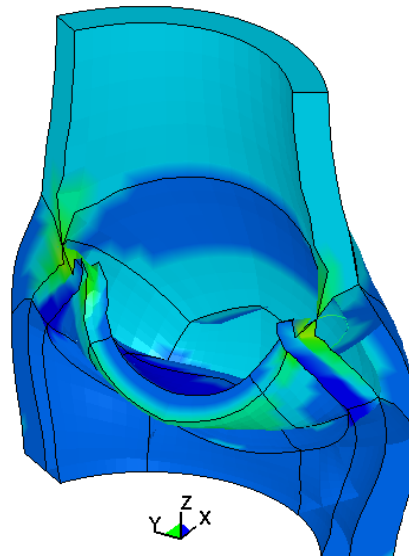
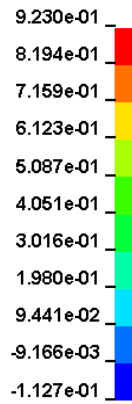
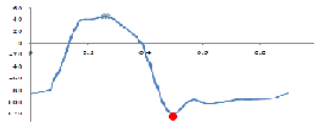
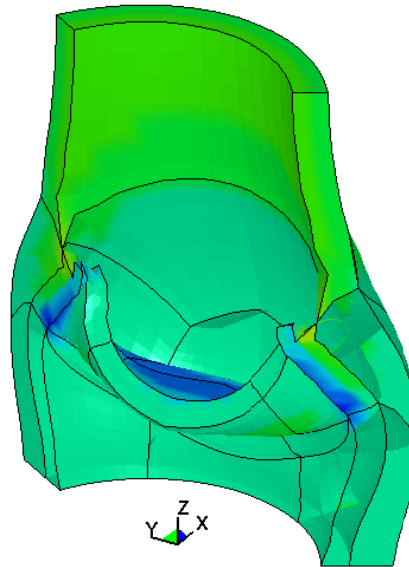
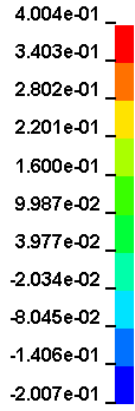


Figure 4.19 Contours of maximum and minimum principal stress during the closure phase, for the model of moderate AS.

Contours of 2nd Principal Stress
 max ipt. value
 min=-0.200663, at elem# 2612
 max=0.400409, at elem# 1228

Fringe Levels



Contours of Effective Stress (v-m)
 max ipt. value
 min=0.00547468, at elem# 1526
 max=0.914833, at elem# 2680

Fringe Levels

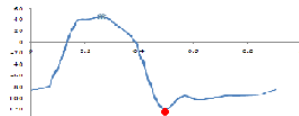
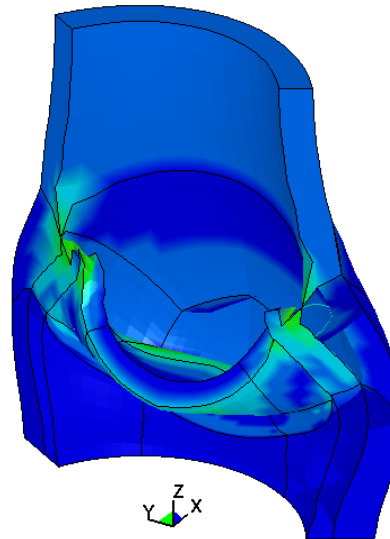


Figure 4.20 Contours of 2nd principal stress and Von- Mises stress during the closure phase, for the model of moderate AS.

It is also interesting to compare the ejection time, RVOT and RVCT obtained numerically with the experimental results (see table 4.4). The errors are in an acceptable range, except for the rapid valve opening time (38.9%).

Table 4.4 Opening and closing characteristics of the valve in vitro moderate AS.

	Numerical simulation	In vitro data	% error
ET (ejection time)	340 ms	295 ms	15.25 %
RVOT (rapid valve opening time)	100 ms	72 ms	38.9 %
RVCT (rapid valve closing time)	117 ms	108 ms	8.33 %

4.4.3 Case 3: Silicone Valve with Severe Stenosis

The third valve tested in vitro was mimicking a severe AS. This is achieved numerically by increasing the thickness of the valve leaflets up to 2.5 mm. Figure 4.21 shows the pressure waveforms obtained in vitro for this case. The maximum geometric orifice area obtained for this valve is 0.936 cm² (at a time of 0.26 s). Our simulations for this model of severe AS give a material property, C_1 , of 3.25 MPa (Fig. 4.22).

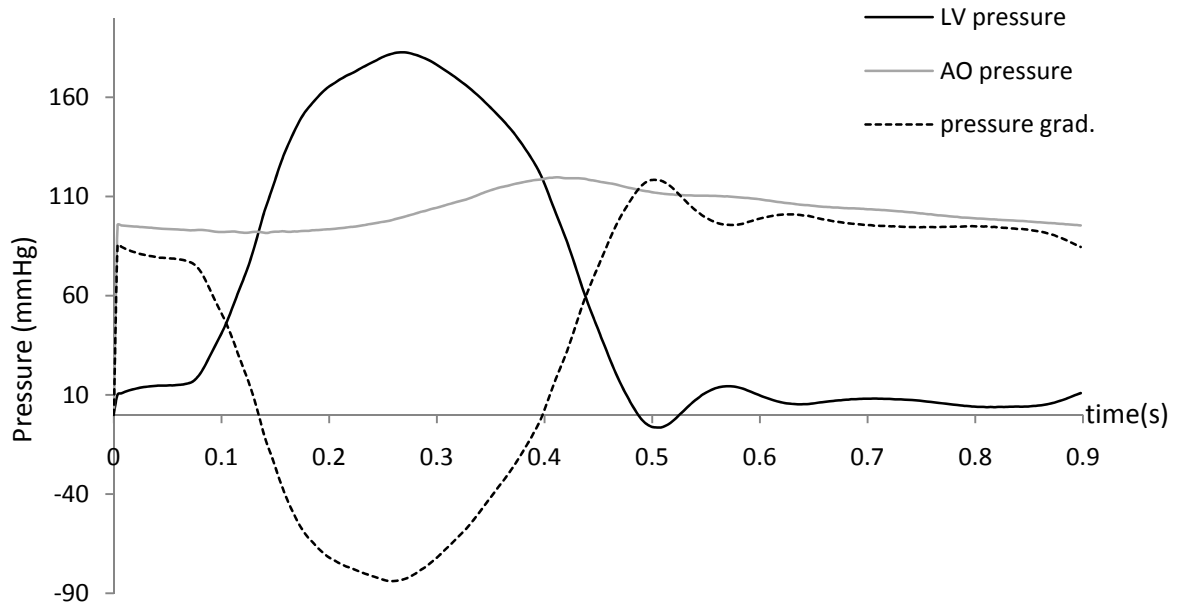


Figure 4.21 Time varying pressure wave forms for in vitro severe AS.

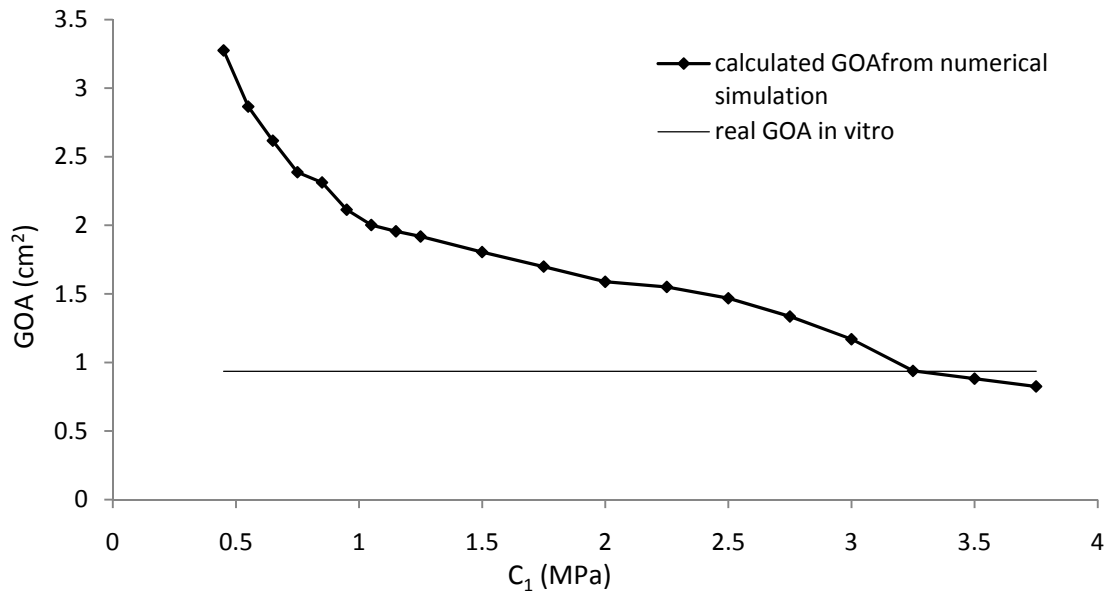


Figure 4.22 Variation of the GOA as a function of C_1 (in vitro), for severe AS.

In Fig. 4.23, the maximum opening of the valve leaflet is shown. Stress distribution contours of a valve with severe stenosis are shown in Figs. 4.24 and 4.25.

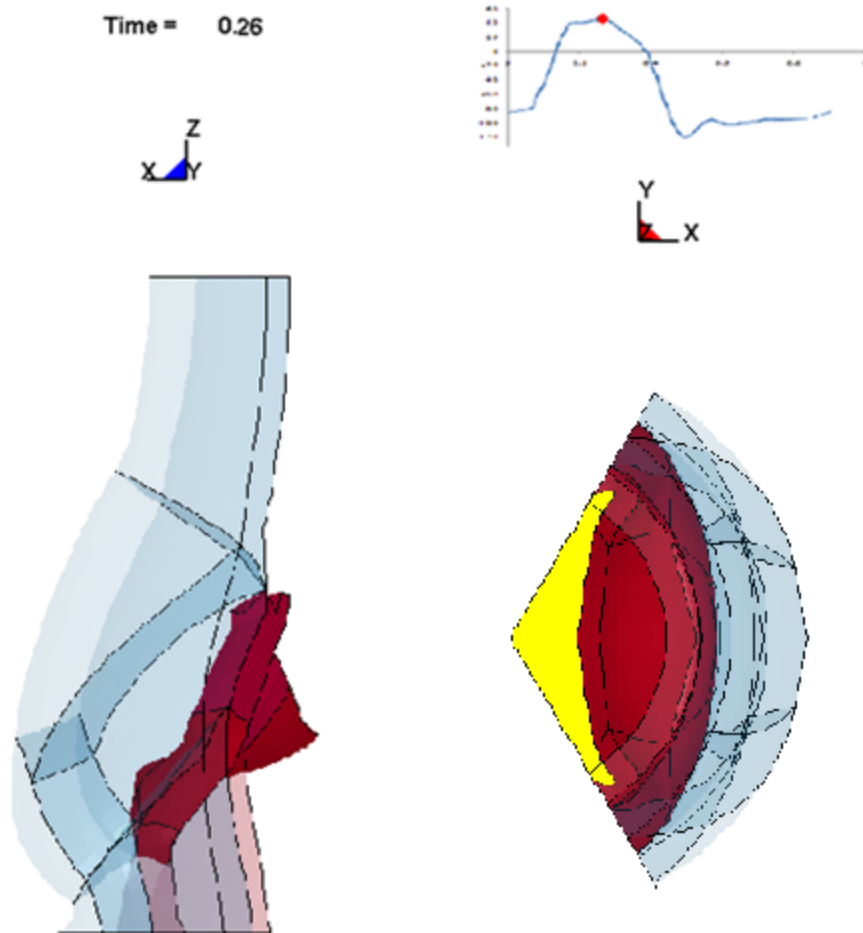
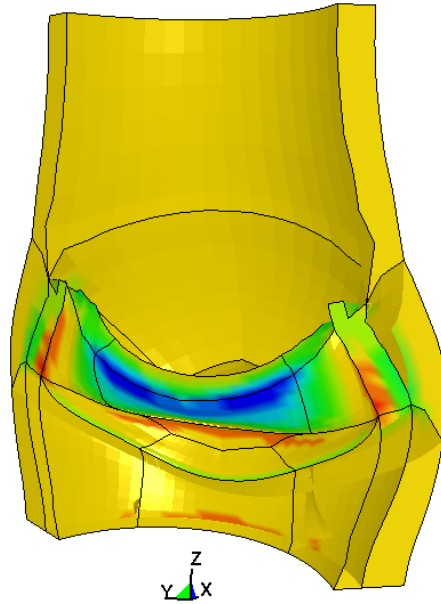
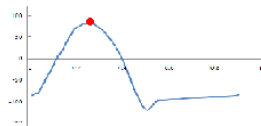


Figure 4.23 Maximum opening area of the model of severe AS, the yellow area is simulated GOA.

Contours of Minimum Principal Stress
 max ipt. value
 min=-0.522755, at elem# 1327
 max=0.189308, at elem# 1096

Fringe Levels



Contours of Maximum Principal Stress
 max ipt. value
 min=-0.0564989, at elem# 1239
 max=0.766934, at elem# 1092

Fringe Levels

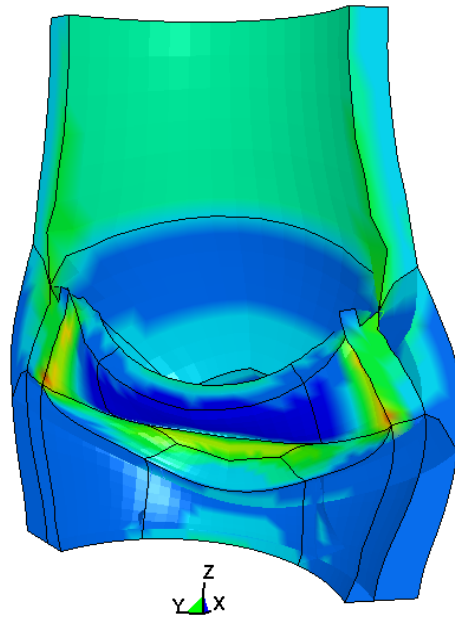
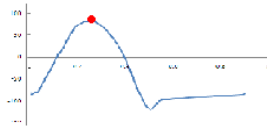
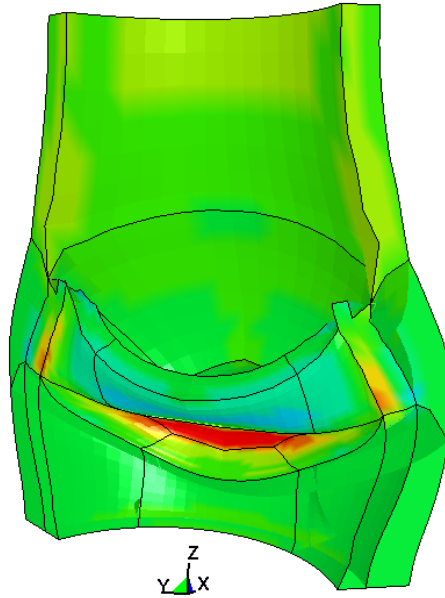
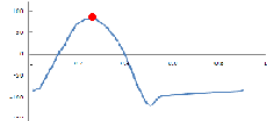
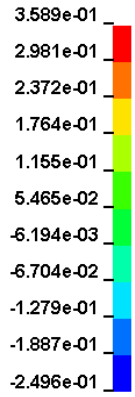


Figure 4.24 Contours of maximum and minimum principal stress at the instant of maximum opening for a model of severe aortic stenosis.

Contours of 2nd Principal Stress
 max ipt. value
 min=-0.249591, at elem# 2752
 max=0.3589, at elem# 2426

Fringe Levels



Contours of Effective Stress (v-m)
 max ipt. value
 min=0.00619665, at elem# 145
 max=0.644664, at elem# 1014

Fringe Levels

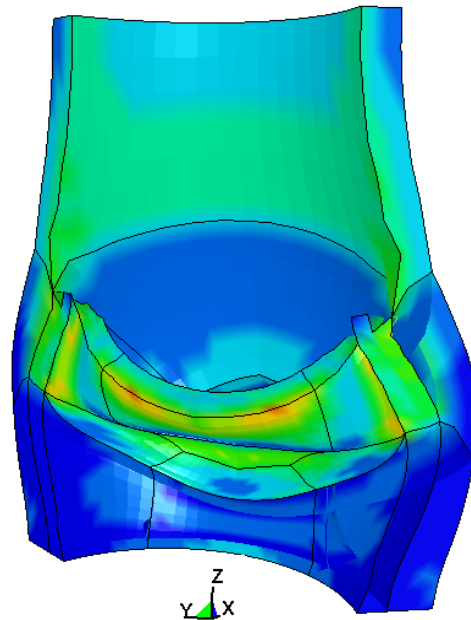
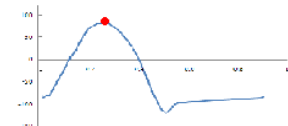


Figure 4.25 Contours of 2nd principal stress and Von- Mises stress at the instant of maximum opening for a model of severe aortic stenosis.

This model of valve with severe AS closes at $t=0.5$ s and the corresponding GOA (yellow area in Fig. 4.26), or regurgitant areas, is obtained 0.23 cm^2 . Figures 4.27 and 4.28 represent the stress distribution in the valve leaflet during the closure phase.

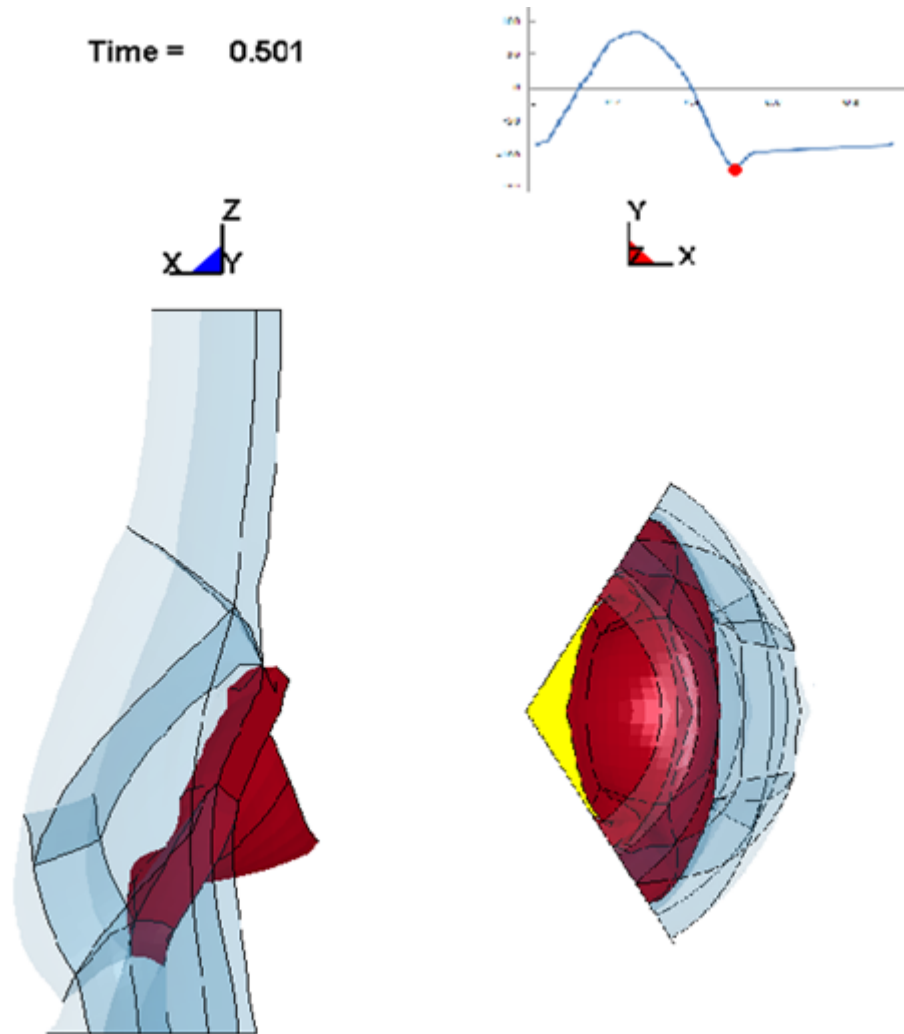
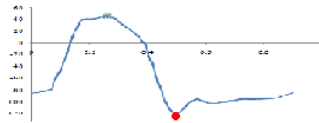
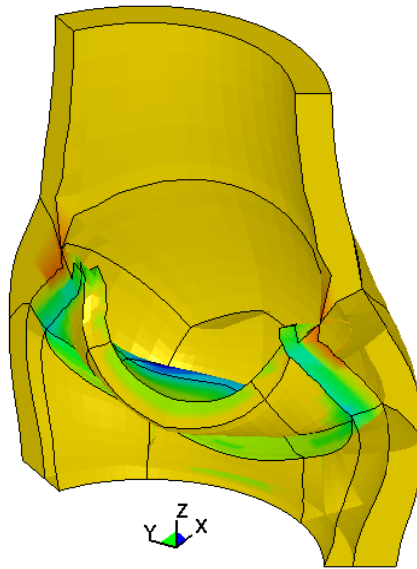


Figure 4.26 Minimum closure area in vitro severe AS, yellow area is the simulated regurgitation area.

Contours of Minimum Principal Stress
 max ipt. value
 min=-0.518459, at elem# 2531
 max=0.172807, at elem# 1230

Fringe Levels



Time = 0.0501
 Contours of Maximum Principal Stress
 max ipt. value
 min=-0.262273, at elem# 2607
 max=0.934394, at elem# 2743

Fringe Levels

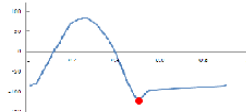
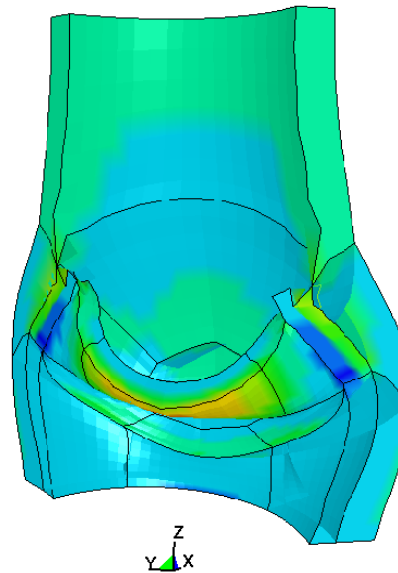
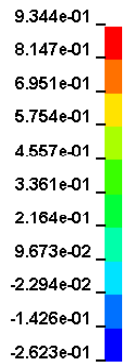


Figure 4.27 Contours of maximum and minimum principal stress at the minimum closing of valve leaflets for the model of severe AS.

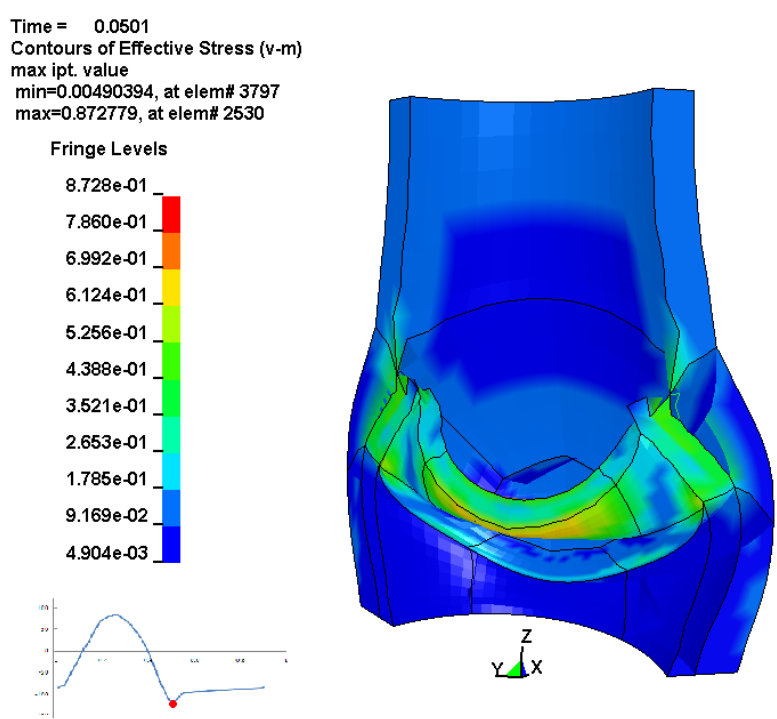
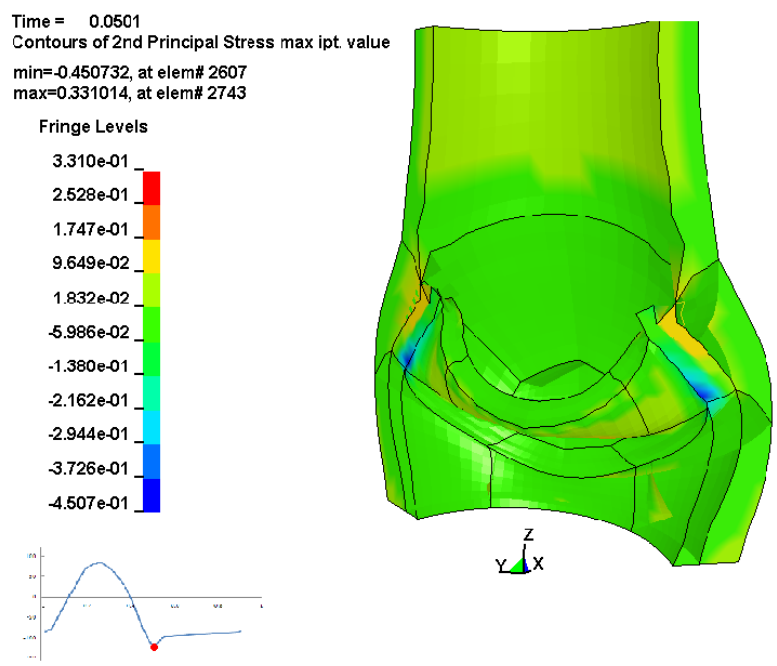


Figure 4.28 Contours of 2nd principal stress and Von- Mises stress at the minimum closing of valve leaflets for the model of severe AS.

Table 4.5 shows the comparisons of the ejection time, rapid valve opening time and rapid valve closing time between numerical predictions and experimental measurements. The errors are in a reasonable range.

Table 4.5 Opening and closing characteristics of the valve in vitro severe AS.

	Numerical simulation	In vitro data	% error
ET (ejection time)	355 ms	319 ms	11.28 %
RVOT (rapid valve opening time)	125 ms	144 ms	13.19 %
RVCT (rapid valve closing time)	135 ms	126 ms	7.41 %

4.5 In Vivo Application (Patients' Specific Aortic Stenosis)

Following the in vitro evaluation of the performance of the new proposed numerical procedure for the estimation of the material property (C_1) for an AS, in this section, the procedure is applied to in vivo cases to estimate in vivo material properties.

In vivo cases were obtained from the study of Garcia et al. (2005). In their study, left ventricular and aortic pressure waveforms were obtained for 6 patients with severe AS before and after valve replacement. However, in all patients, instead of measuring the GOA (point 2, on Fig. 4.29), the energy loss coefficient was determined. Three patients among this group are selected in this thesis to demonstrate the applicability of the proposed method in vivo. The energy loss coefficient characterizes the pressure loss in the presence of a severe contraction followed by an expansion. It is a function of the effective orifice area (EOA) (point 1, on Fig. 4.29), or the area of the vena contracta downstream of the stenotic valve, and the area of the ascending aorta at the sinotubular junction (A_A) (point 3, on Fig. 4.29). The energy loss coefficient represents a correction of the EOA with respect to A_A :

$$E_L C_o = \frac{EOA \cdot A_A}{A_A - EOA} = \frac{Q}{50 \cdot \sqrt{E_L}}$$

4-11

In this study, A_A is considered fixed with a value of 4.52 cm^2 and the EOA varies depending on the severity of the AS.

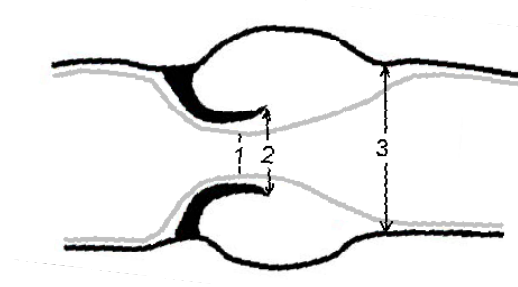


Figure 4.29 Definition of the different areas used in clinical studies, No. #1 represent effective orifice area (minimum cross-sectional area of the blood flow jet), No.#2 represent geometrical orifice area , No.#3 cross-sectional area of the ascending aorta at the sinotubular junction.

The ratio between EOA and GOA is called contraction coefficient, $C_c = \frac{EOA}{GOA}$, and it is in the range of 0.6 to 1 (Garcia et al. 2004). In this thesis, the value of 0.67 is considered for C_c .

Based on Eq. 4.12, one can calculate the EOA from the $E_L C_o$ reported by Garcia et al. (2005). Having the EOA for each patient and assuming a contraction coefficient of 0.67 allow estimating the GOA for each patient. The results for the three selected patients are listed in Table 4.6.

Table 4.6 Calculated GOA based on the energy loss coefficient (in vivo study).

Patient No.	$E_L C_O \text{ cm}^2$ (Garcia et al. 2004)	EOA cm^2 (Garcia et al. 2004)	GOA cm^2 (Current study)
1	0.52	0.50	0.74
2	0.85	0.72	1.07
3	0.45	0.41	0.61

4.5.1 In Vivo Case: Patient No. 1

Figure 4.30 represents the pressure waveforms for the patient #1. The corresponding GOA is then approximately computed as 0.74 cm^2 .

Figure 4.31 shows how to determine the patient-specific value for C_1 using numerical simulation. For this patient, C_1 is found equal to 1.35 MPa.

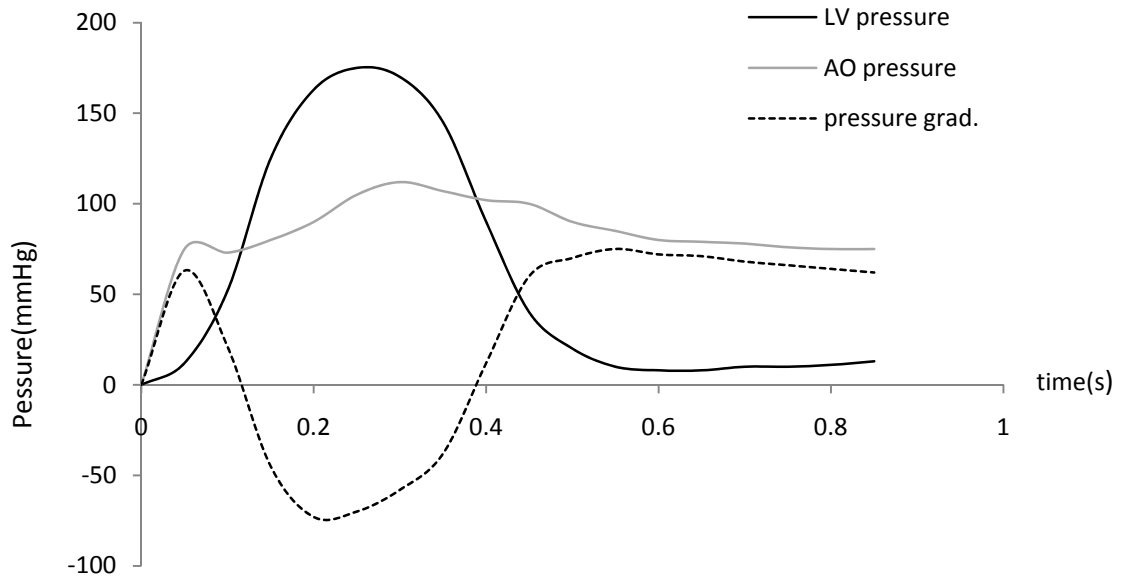


Figure 4.30 Time varying pressure waveforms (in vivo), for patient #1.

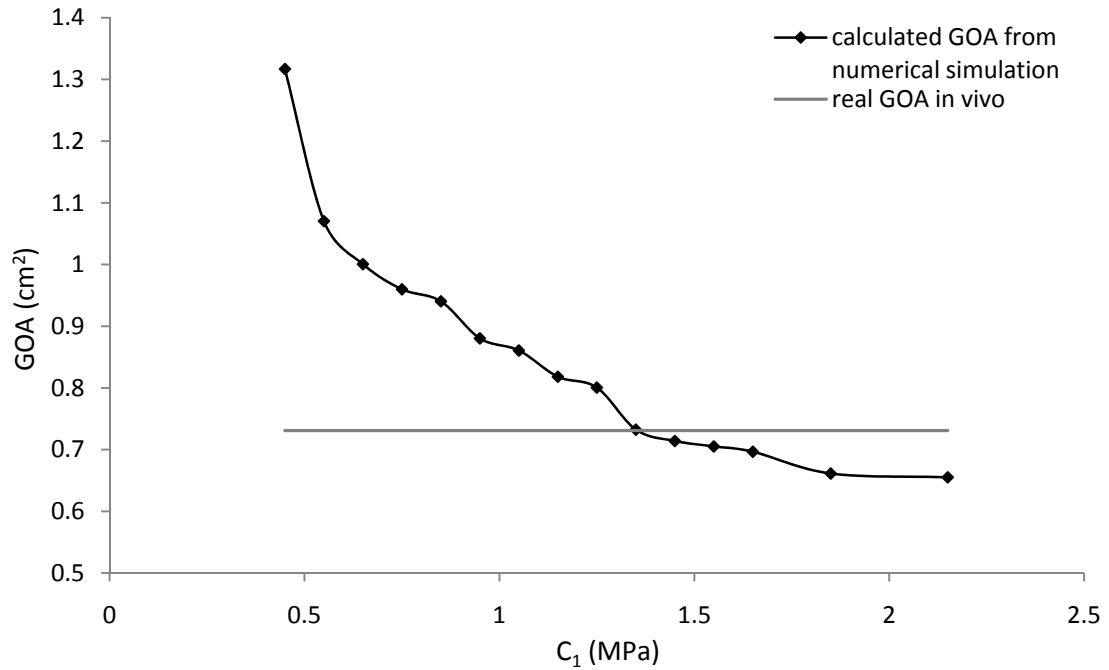


Figure 4.31 Variation of the GOA as a function of C_1 (in vivo), for patient #1.

Numerical simulations shows that maximum opening of the valve leaflets occurs at $t=0.23$ s and closure happens at $t=0.55$ s. At closure instant ($t=0.55$ s) the regurgitation area obtained numerically is 19 mm^2 .

Table 4.7 shows the numerically calculated time characteristics for this patient. Unfortunately, the corresponding in vivo results have not been reported and as a consequence it is not possible to validate these findings contrary to in vitro measurements.

Table 4.7 Opening and closing characteristics of the valve for patient #1.

Clinical property	Numerical simulation
ET (ejection time)	430 ms
RVOT (rapid valve opening time)	100 ms
RVCT (rapid valve closing time)	120 ms

Since different parameters can affect the computed value for C_1 , in this part a sensitivity analysis is performed for this specific patient.

As it described in the method section, because there is no access to the percentage of calcium on the patient's valve leaflets, the density of the leaflet was assumed to be 1250 kg/m^3 . It is the average between the normal density of leaflet tissue 1000 kg/m^3 and density of calcium (1500 kg/m^3). Sensitivity analysis shows if the density is chosen as $\rho=1500 \text{ kg/m}^3$ (the valve includes only calcium), the GOA would have been 0.79 cm^2 instead of 0.74 cm^2 , which represent an error of around 8%. For a density $\rho = 1000 \text{ kg/m}^3$ (there is no calcium on the leaflets) the GOA would reach to the 0.71 cm^2 which represents an error of 3%.

It is also interesting to evaluate how the value obtained for C_1 is sensitive to the errors in the measured GOA. Based on Fig. 4.32, which represents the GOA as a function of C_1 , a 10% error above of the reporting GOA (means $\text{GOA}=0.803 \text{ cm}^2$) will cause the 7.4% error on C_1 , ($C_1=1.25 \text{ MPa}$). However, for 10% error less than the real one (means $\text{GOA}=0.657 \text{ cm}^2$), the value of C_1 will be around 2.15 MPa (error is 59.25%). The error here is explained by the specific “J liked” shape of the curve GOA versus C_1 .

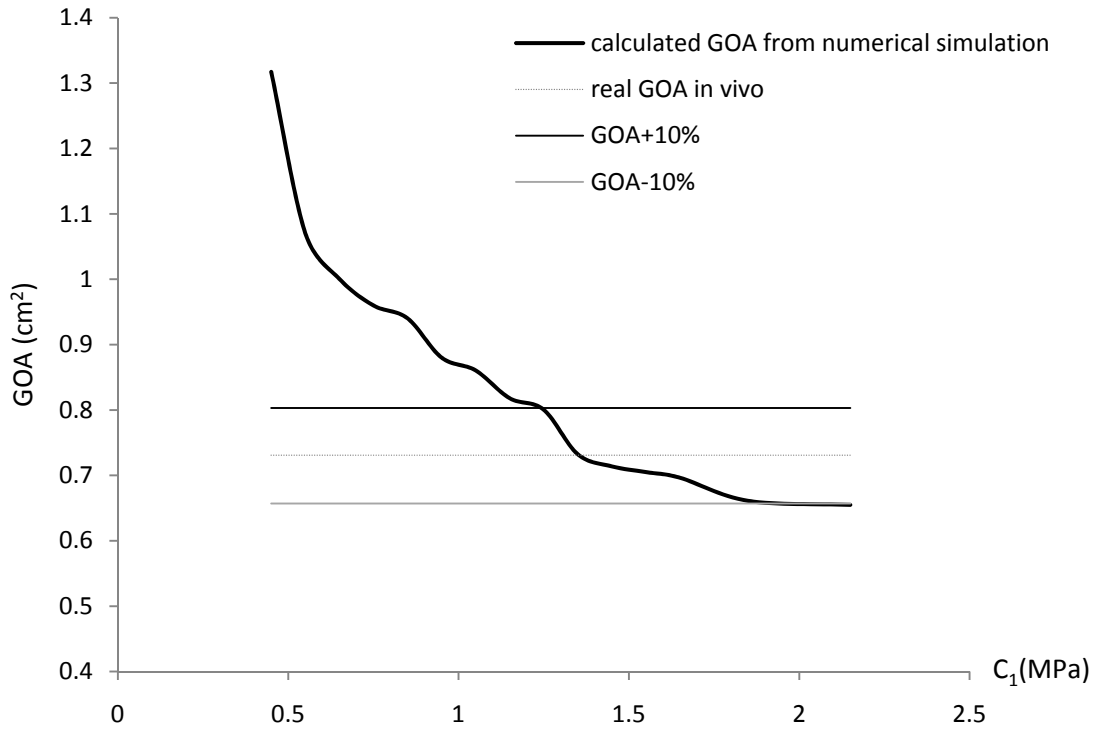


Figure 4.32 Sensitivity analysis with respect to variation in GOA for patient #1.

Another important parameter that could affect the results is the value for the thickness of the leaflets. In all cases, the thickness is set to 2 mm; however, in reality this may not be correct. Different values for thicknesses are assumed in the sensitivity test and the value of C_1 based on the different thicknesses are computed and shown in Fig. 4.33.

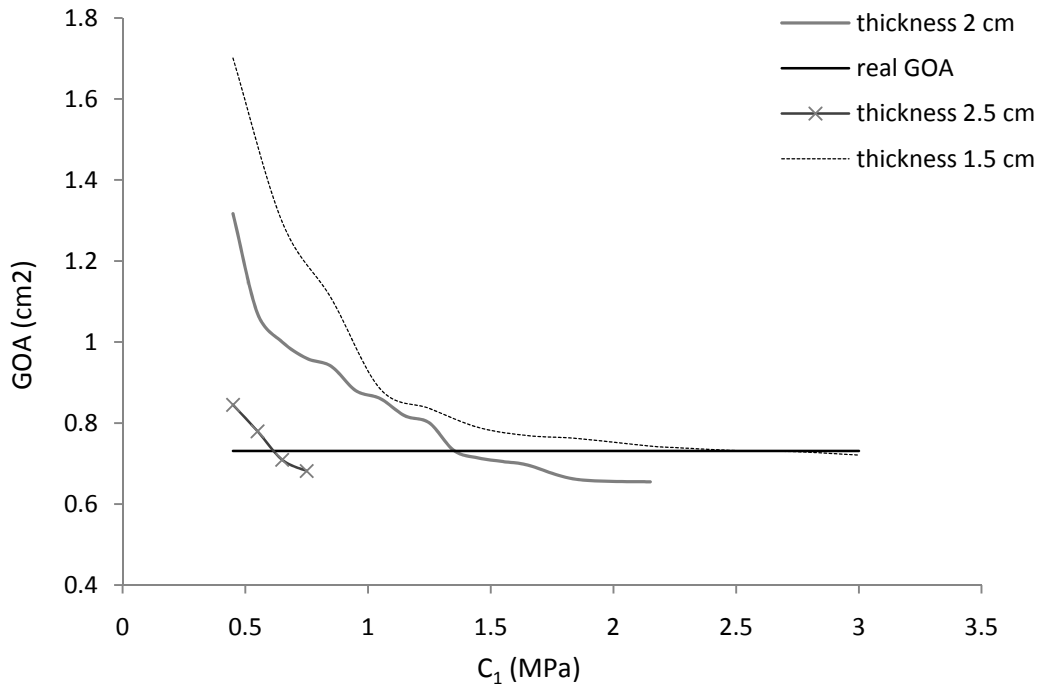


Figure 4.33 Sensitivity analysis with respect to variation in the leaflet thickness for patient #1.

The computed results for C_1 for each thickness are shown in a bar chart in Fig. 4.34. It is understood that with increasing the thickness, the value of C_1 decreases. Physically, it means that the stress distribution in thicker leaflets is lower (leaflets endure less stress) compared with thin or healthy leaflets. The computed values for C_1 for a thickness of 1.5 mm) and 2.5 mm, show relative differences around 93.4 % and 54.2 % respectively, when compared to C_1 when the thickness is 2 mm. This issue can be considered in future studies and is not the subject of the current study, as the access to the patient's specific value of thickness is difficult. Therefore, the value of 2 mm is taken for thickness of the severe stenotic leaflets.

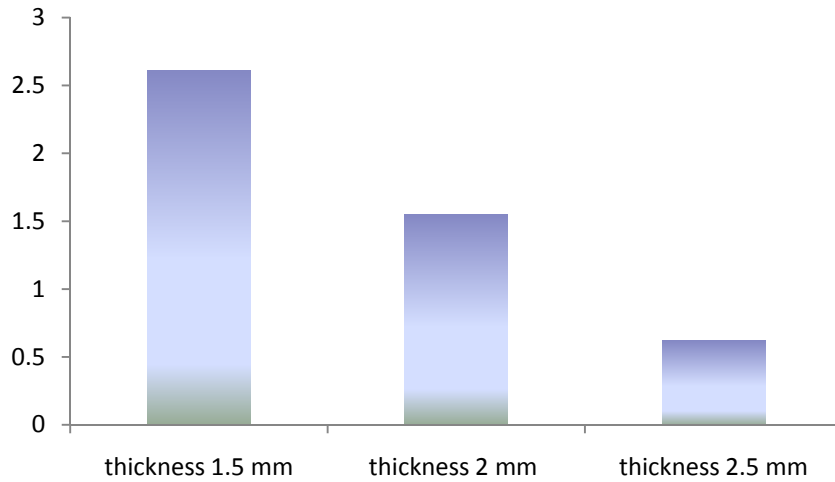


Figure 4.34 Material property for different value of valve leaflet thickness.

4.5.2 In Vivo Case: Patient No. 2

Figure 4.35 represents the pressure waveforms obtained in the patient No. 2, with a reported $E_L C_O$ of 0.85 cm^2 and corresponding GOA of 1.07 cm^2 .

For this patient, the numerical simulation results in a value of 1.0 MPa for C_1 as shown in Fig. 4.36. The maximum opening and minimum closing happen at 0.25 s and 0.50 s , respectively. At $t=0.50 \text{ s}$, the computed minimum closing area or regurgitation area (AR) is 0.16 cm^2 . Table 4.8 shows other calculated clinical properties for this patient.

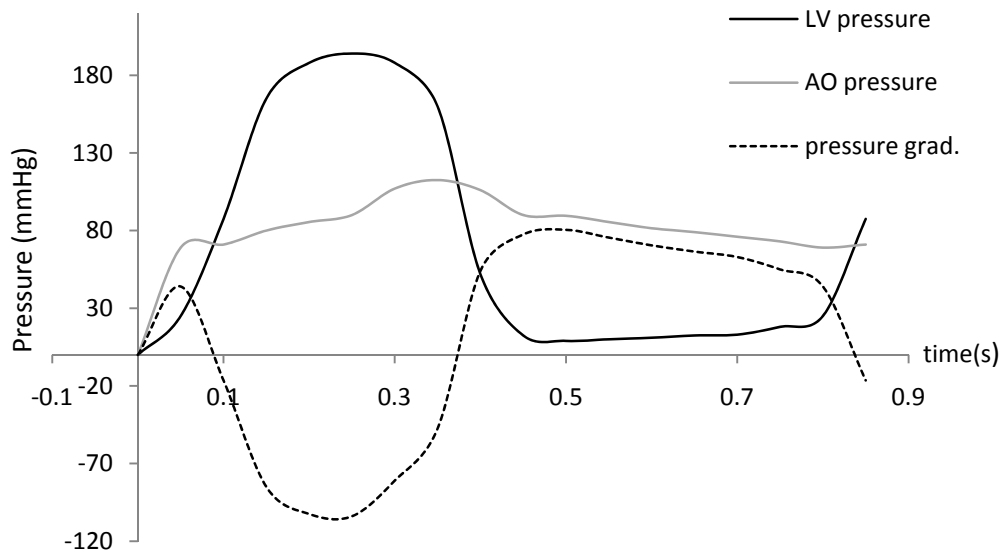


Figure 4.35 Time varying pressure waveforms (in vivo), for patient #2.

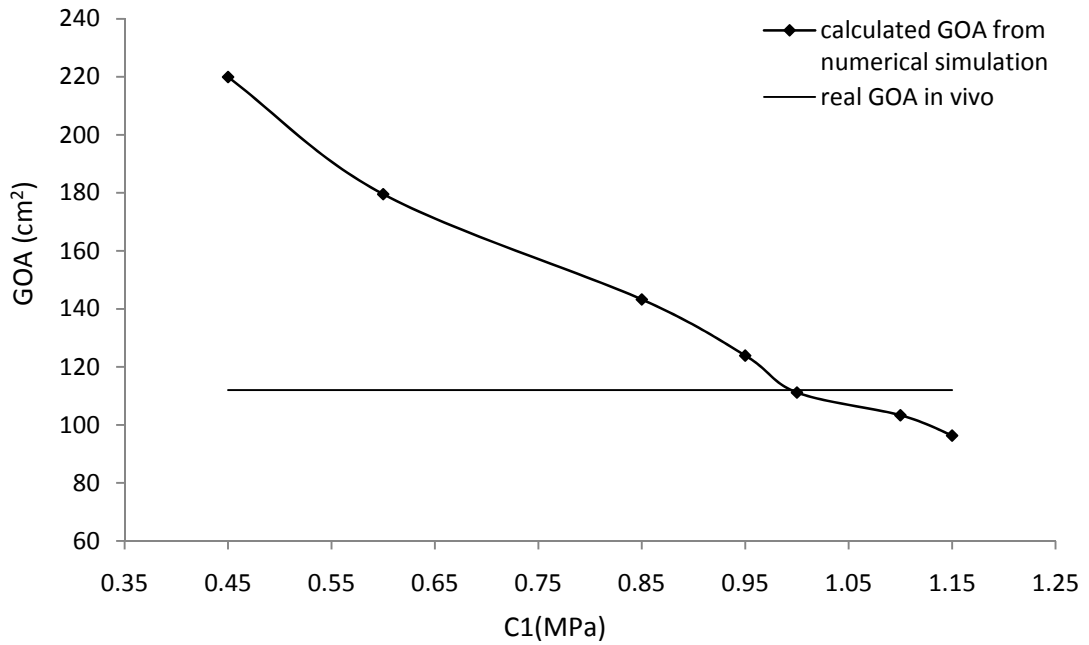


Figure 4.36 Variation of the GOA as a function of C_1 (in vivo), for patient #2.

Table 4.8 Opening and closing characteristics of the valve for patient #2.

	Numerical simulation
ET (ejection time)	340 ms
RVOT (rapid valve opening time)	90 ms
RVCT (rapid valve closing time)	90 ms

4.5.3 In Vivo Case: Patient No. 3

The last case analyzed in vivo represents a patient with an E_{LCO} of 0.45 cm^2 and a GOA of 0.61 cm^2 . Figure 4.37 represents left ventricular, aortic and pressure gradient waveforms recorded on this patient.

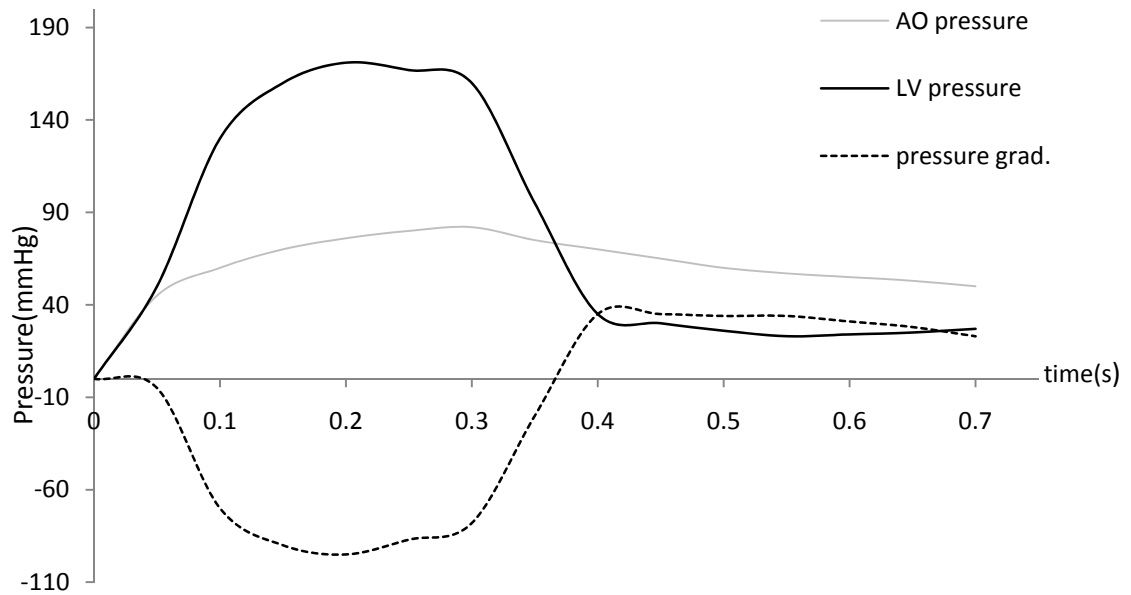


Figure 4.37 Time varying pressure waveforms (in vivo), for patient #3.

This patient had the most severe hemodynamic condition because of its small GOA. The value for C_1 obtained then significantly high: 7.38 MPa (see Fig. 4.38).

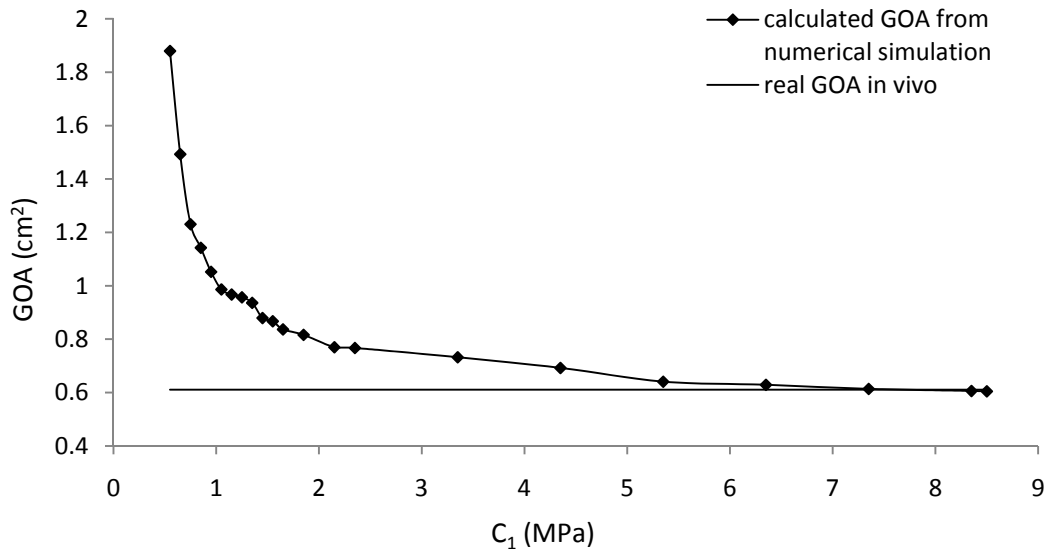


Figure 4.38 Variation of the GOA as a function of C_1 (in vivo), for patient #3.

The maximum opening and minimum closing happens at 0.22 s and 0.45 s, respectively. The computed AR is approximately 0.33 cm². Table 4.9 shows other calculated clinical properties for case No. 3 based on numerical model.

Table 4.9 Opening and closing characteristics of the valve for patient #3.

	Numerical simulation
ET (ejection time)	330 ms
RVOT (rapid valve opening time)	130 ms
RVCT (rapid valve closing time)	130 ms

4.6 Summary

A computational approach enabling the determination of an equivalent index for mechanical properties of stenotic aortic valves was developed and tested in vitro and in vivo. The results of this numerical modeling can be mainly used to have an idea on the material properties of valve leaflets prior to percutaneous valve replacement. This index was based on the value of the first constant for the formulation of the material properties (C_1). Sensitivity analysis demonstrated that uncertainty in C_1 is largely dependent on the value of the measured GOA and the thickness of the leaflets and less dependent on the density of leaflet material. Since, here the objective was to develop a reference model that can be applied for all patients, the thickness of the valve leaflets was kept constant 2 mm and then C_1 was mainly a function of the GOA. So, in this approach, a thicker valve will just produce a larger pressure gradient that will be translated as a higher C_1 .

To validate the code and present the methodology, three in vitro cases, a pericardial bioprosthetic valve, silicone valves with moderate and severe stenosis were tested and simulated numerically using structural modeling. Validation has been done by comparison with the instantaneous GOA experimentally and numerically. Also stress analysis was done to compare the results of this study with those published in the literature. The results showed a good agreement.

The results of the in vitro cases demonstrate that the value of C_1 should be greater than 1 MPa for stenotic valves. All values of C_1 for the six cases (3 in vitro cases and 3 in vivo cases) are presented in Fig. 4.39.

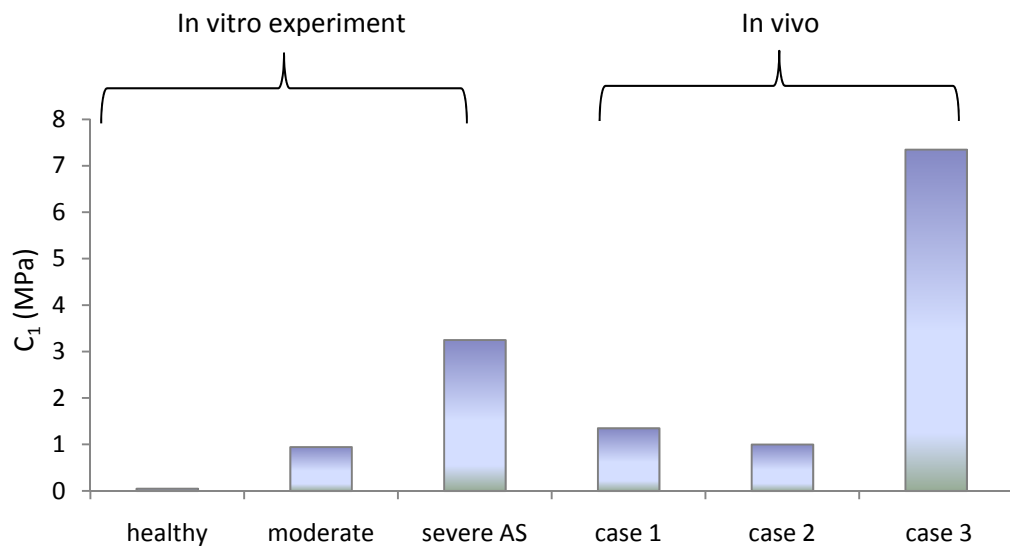


Figure 4.39 Obtained C_1 for all simulated cases.

Chapter 5: Fluid Structure Interaction Analysis of Healthy and Stenotic Aortic Valves

5.1 Introduction

The structural analysis (dry model) of aortic valve was investigated in the previous chapter. Although the dry model can directly be applied in vivo to estimate the mechanical properties of the valve leaflets prior to percutaneous valve replacement, it requires as boundary conditions, the in vivo recording of the pressure waveforms (aortic and ventricular) invasively. Moreover, the geometrical orifice of the valve must be determined with a reasonable accuracy (see sensitivity analysis in chapter 4). This requires high resolution imaging techniques. This chapter represents an attempt to extend our new algorithm to overcome these limitations of the dry model. This will be achieved by determining the effective orifice area of the aortic valve, instead of the geometrical orifice area, through fluid-structure interaction (FSI) simulations.

FSI applied to cardiovascular disease in general, and to aortic stenosis in particular, is still a recent research area and many improvement are still required. For example, in a recent study, Van Loon (2009) tried to investigate the flow through a model of aortic stenosis. However several drawbacks affected the results: the magnitude of the inlet velocity applied was not physiologically correct, the flow domain was discretized by less than 1000 elements and a material with linear properties was used. The same year, Weinberg et al. studied the dynamics of aged and calcified aortic valves by changing the thickness and material properties of the leaflets.

In this chapter, FSI is first briefly introduced and then more details on the implementation of FSI in LS-DYNA are provided. Second, FSI simulations are performed on two different cases: a healthy aortic valve and a stenotic aortic valve. Finally, the results obtained using FSI are analyzed and discussed.

5.2 Numerical Method in Fluid Structure Interaction Analysis

FSI is a coupling method to connect Eulerian/ALE (Arbitrary Lagrangian Eulerian) parts with Lagrangian parts in order to make them interact with each others. In this study, LS-DYNA is employed to perform FSI simulation on an aortic valve. This software employs an explicit time integration scheme because of its ability to solve the fully coupling between fluid and structure in the presence of large deformable and flexible structures. In addition, Lagrangian and Eulerian/ALE solution methods can be combined on the same model and the FSI can be handled by a coupling algorithm. Structural parts are modeled with Lagrangian elements whereas fluid parts can be modeled with Eulerian/ALE elements. To better understanding these concepts, here are some brief explanations:

Lagrangian approach: the mesh moves directly with the material and therefore elements and materials are able to translate, rotate, and deform together. Material does not cross element boundaries and it means that elemental masses remain constant and the conservation of mass is satisfied during the simulation. This approach is useful in structural analysis.

Eulerian approach: the mesh remains fixed while the material passes through it. This approach is suitable for large deformations, such as fluid flow. Herein, tracking surfaces and boundary conditions are difficult; however, because the mesh is stationary, mesh distortion cannot happen.

ALE approach: The ALE approach is based on the arbitrary movement of a reference domain. Fluid mesh/elements at the fluid-solid interface can move in a Lagrangian way and solid elements are following them as they are coupled together. Then an advection term is applied to remap the fluid mesh which is an adaptive technique. It is called operator split technique. A simple example to describe this approach is shown in Fig. 5.1. It represents the two cycles, Lagrangian cycle and advection cycle, within one time step. First cycle shown in the figure “a” represents the Lagrangian cycle and “b” represents the advection cycle.

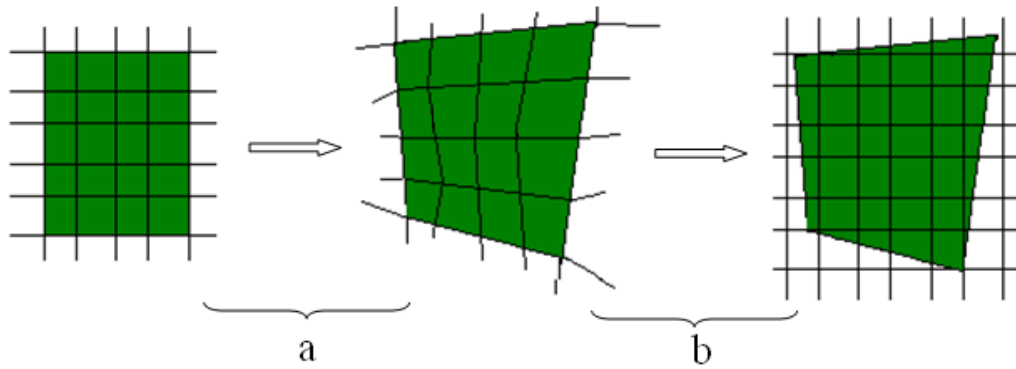


Figure 5.1 Movement of solid part in the fluid domain based on ALE approach during one time step, “a” is the Lagrangian cycle and “b” is the advection cycle (green represents solid domain and lines represent the fluid meshes).

Some limitations are associated with ALE modeling in LS-DYNA as mentioned by Day (2009). The ALE solver in LS-DYNA is mainly applicable to laminar flow, and also is not appropriate to model boundary layer flow effects. The solver is not well-matched to solve the problems with low pressure gradients which is not the case in the present study. The computational time is usually high due to the explicit time integration. The time step is limited based on the size of elements and material sound speed. ALE method is more time consuming when compared with Lagrangian one as a result of additional computation due to advection and interface reconstruction and coupling process.

In ALE algorithm, three coordinates are identified: arbitrary referential, Lagrangian and Eulerian coordinates. Based on the general ALE technique, the time derivative of a physical property, f , in a Lagrangian coordinate is (Askes et al., 2004)

$$\frac{\partial f(X_i, t)}{\partial t} = \frac{\partial f(x_i, t)}{\partial t} - w_i \frac{\partial f(x_i, t)}{\partial x_i} \quad 5-1$$

where t stands for time, X_i is the Lagrangian position, x_i the Eulerian position and w_i is the relative velocity between material and mesh nodes. If v_i shows the velocity of the material and u_i the velocity of the mesh; therefore, the relative velocity is $w_i = v_i - u_i$. The relative velocity is usually referred to as the convective or advective term.

Then governing equations for the ALE formulation can be presented as, (Souli et al. 1999)

a) The conservation of mass:

$$\frac{\partial \rho}{\partial t} = -\rho \frac{\partial v}{\partial x_i} - w_i \frac{\partial \rho}{\partial x_i} \quad 5-2$$

here ρ is density.

b) The conservation of momentum:

$$\rho \frac{\partial v}{\partial t} = -(\sigma_{ij} + \rho b_i) - \rho w_i \frac{\partial v_i}{\partial x_j} \quad 5-3$$

where σ is stress tensor and described as,

$$\sigma_{ij} = -p\delta_{ij} + \mu(v_{i,j} + v_{j,i}) \quad 5-4$$

where μ is flow viscosity, p is pressure and δ_{ij} is Kronecker's delta function.

c) Boundary and initial conditions:

If Γ stands for the whole boundary of the domain and Γ_1 and Γ_2 represent the partial boundaries of Γ as: $\Gamma_1 \cup \Gamma_2 = \Gamma$ and $\Gamma_1 \cap \Gamma_2 = 0$, the initial and boundary conditions on partial boundaries can be specified as $v_{i,j} = U_0$ on Γ_1 and $\sigma_{ij}n_i = 0$ on Γ_2 . The initial velocity is assumed to be zero in the entire domain. Herein n_i is the normal vector on the boundary.

5.3 Model Description

5.3.1 Geometry

A one-third model of aortic valve structure including meshes was generated using the pre-processor of the commercially available finite element software, ANSYS 11.0. Then, a Matlab code was written to translate the modeling information from ANSYS to LS-DYNA environment.

In FSI simulation, the same geometrical dimensions as for the dry model are used for the structure. To create the fluid domain, a one-third of cylinder is considered. The overall length of the flow domain is approximately 52 mm (equal to the structure height) and the radius is 21.2 mm. The complete model is shown in Fig. 5.2.

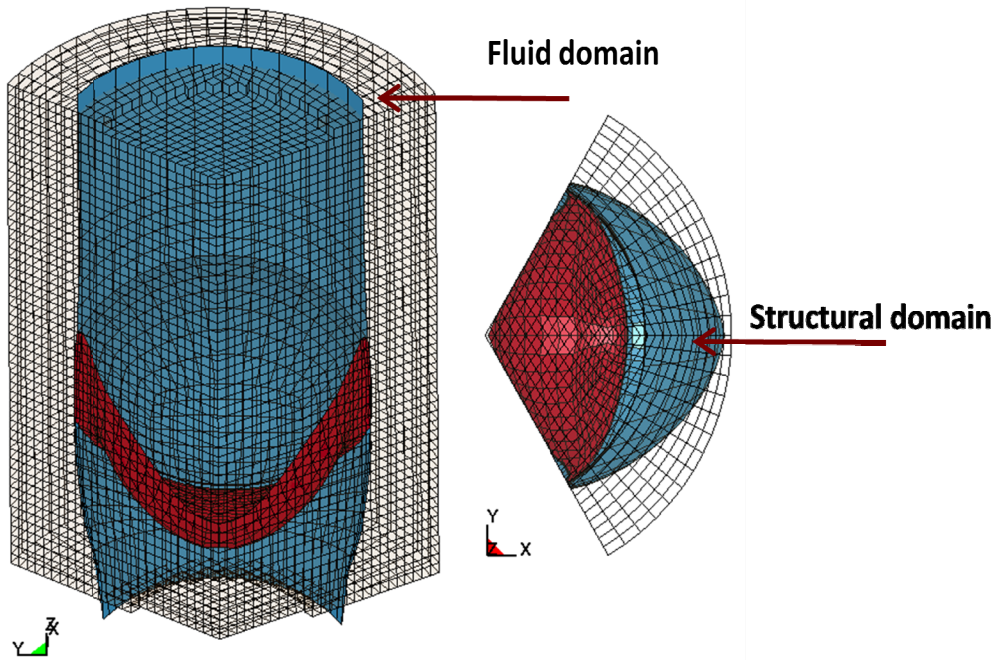


Figure 5.2 Aortic valve geometry and meshes merged in fluid domain.

5.3.2 Element Formulation

The structural model consists of the aortic root, sinuses and valve leaflet and is meshed with 1286 (4-noded Belytchko-Lin-Tsai) shell elements. Why shell elements are used to describe the structure instead of solid ones? The reason is related to the time step. Because the time step is set automatically in the software based on the time needed for a sound wave to pass through the smallest solid element in the model. But in shell elements, the time step is independent of the shell thickness and a shell element can have several integration points through its thickness. This means that shell element results in more efficient computation than solid brick elements in modeling thin-walled structures (Carmody et al., 2005).

The aortic root, sinuses and leaflets share nodes at their intersection. To define the shell element besides the four nodes, some additional parameters are required: a shear factor, four thicknesses at each four nodes and the number of integration points. Here, shear factor is taken as 1, the thicknesses are taken as 1 mm for stenotic and 0.5 mm for healthy valve. The number of integration points by default is considered to be 2.

All the structural parts of the model are surrounded by a fluid domain. Fluid domain is divided into three parts: inlet, middle reservoir and outlet sections. Fluid parts, which represent the blood flow domain, are described by eight-noded hexahedral brick elements with an Eulerian formation. The structure and fluid meshes are placed in the same spatial domain and forces exerted by one on the other are communicated in both directions. The fluid motion, first step, described by the Navier–Stokes equations is solved with Lagrangian approach and in the second step, the deformed meshes are returned to the unchanged location of Eulerian mesh.

Fluid domain has 25350 element numbers for the one third of a complete geometry. Compared to the previous works, the mesh used in this study is finer.

5.3.3 Material Properties

In current study, blood is modeled as a compressible (this is an assumption for modeling the fluid in ALE approach) Newtonian fluid. In LS-DYNA, fluid material is called “MAT_NULL” and the viscous deviatoric stresses is calculated by $\sigma_{ij} = 2\mu\varepsilon'_{ij}$, where μ is the dynamic viscosity and ε'_{ij} is deviatoric strain rate. Compressibility of fluid is governed by an equation of state as,

$$P = \rho_0 \cdot c^2 \eta + \gamma E \approx k\eta + \gamma E \quad 5-5$$

where P is the pressure, ρ_0 is the initial density, k is bulk modulus, and η is volumetric parameter equal to $(\frac{\rho}{\rho_0} - 1)$. Sound speed can be calculated as $c = \sqrt{\frac{k}{\rho}}$. The properties of blood were taken as the density of 1000 kg/m³ and dynamic viscosity of 0.004 Pa.s.

The solid domain is modeled as a hyperelastic and nonlinear, Mooney-Rivlin material. The material strain energy density function is defined as, (LS-DYNA user manual, 2007)

$$W = A(I - 3) + B(II - 3) + C(III^2 - 1) + D(III - 1)^2 \quad 5-6$$

where, A, B, C and, D are material constants and I, II, III = invariants of right Cauchy-Green Tensor. The value of A = 2 × 10⁴ (Pa is chosen as to fit the bending data test for the leaflet (Weinberg et al., 2007).

$$C = 0.5A + B \quad 5-7a$$

$$D = \frac{A(5\gamma-2)+B(11\gamma-5)}{2(1-2\gamma)} \quad 5-7b$$

where γ is Poisson's ratio (0.49). Density of material is considered as 1000 kg/m³.

To model a stenotic aortic valve, the value of A was considered two times larger than the healthy aortic valve.

5.3.4 Boundary Conditions

Boundary conditions should be defined for both fluid and solid domains. The inlet fluid boundary condition is time-varying pressure gradient and outlet boundary condition is zero pressure.

The true coaptation surfaces (the contact region of the leaflets' structures) are identified as master and slave scheme. If a slave node penetrates into a master surface, a penalty force is applied in order to bring back the slave node to the plane of the master surface. All other structural parts (except the leaflets) are considered fixed in the domain.

5.3.5 Coupling Implementation

The structural geometry of the aortic valve is represented as an immersed Lagrangian structure surrounded by the Eulerian fluid domain in LS-DYNA with a fully coupling between the fluid and the structure components. The coupling between the fluid and the structure is modeled by an exchange in the velocity and acceleration constrains between the Eulerian master (fluid domain) and the Lagrangian slave (the valve structure).

The following steps are used to couple the velocity and acceleration of the fluid and the structure: (Kunzelman et al., 2007)

- The fluid elements which contain structural nodes are determined. The mass of structural element nodes can be distributed to the fluid element nodes according to

$$m_i^{\text{fluid}} = m_i^{\text{fluid}} + h_i m^{\text{structure}} \quad 5-8$$

where i is the nodal index and h is a weighting coefficient between 0 and 1.

- The force of the structural nodes is distributed to the fluid nodes according to

$$F_i^{\text{fluid}} = F_i^{\text{fluid}} + h_i F^{\text{structure}} \quad 5-9$$

- The acceleration of the fluid nodes is calculated as,

$$a_i^{\text{fluid}} = \frac{F_i^{\text{fluid}}}{m_i^{\text{fluid}}} \quad 5-10$$

- Finally, the acceleration of the structural nodes can be calculated in constraint with the fluid nodes acceleration,

$$a_i^{\text{structure}} = \sum_{i=1}^8 h_i \cdot a_i^{\text{fluid}} \quad 5-11$$

For the velocity coupling, the structural nodal momentum is distributed to the fluid nodes by using a geometric weighting. The steps below represent the velocity coupling of the fluid and the structure (Kunzelman et al., 2007):

- In addition, the structural nodal momentums are distributed to the fluid element nodes according to

$$M_i^{\text{fluid}} = M_i^{\text{fluid}} + h_i M^{\text{structure}} \quad 5-12$$

- Then, the velocity of fluid nodes can be determined based on

$$u_i^{\text{fluid}} = \frac{M_i^{\text{fluid}}}{m_i^{\text{fluid}}} \quad 5-13$$

- Finally, the velocity of structural nodes are matched to the velocity of fluid nodes based on

$$u_i^{\text{structure}} = \sum_{i=1}^8 h_i \cdot u_i^{\text{fluid}} \quad 5-14$$

Small time steps are needed for the stability of the explicit time-integration scheme and to reduce numerical errors. For all modeling cases, the time step is selected 4.78×10^{-7} s. This shows the computational time cost that should be paid to model and couple the blood domain to the solid structure.

5.4 Results and Discussion

Velocity vector map at maximum opening of the valve is shown in Fig. 5.3 (for a healthy valve) and Fig. 5.4 (for a stenotic valve).

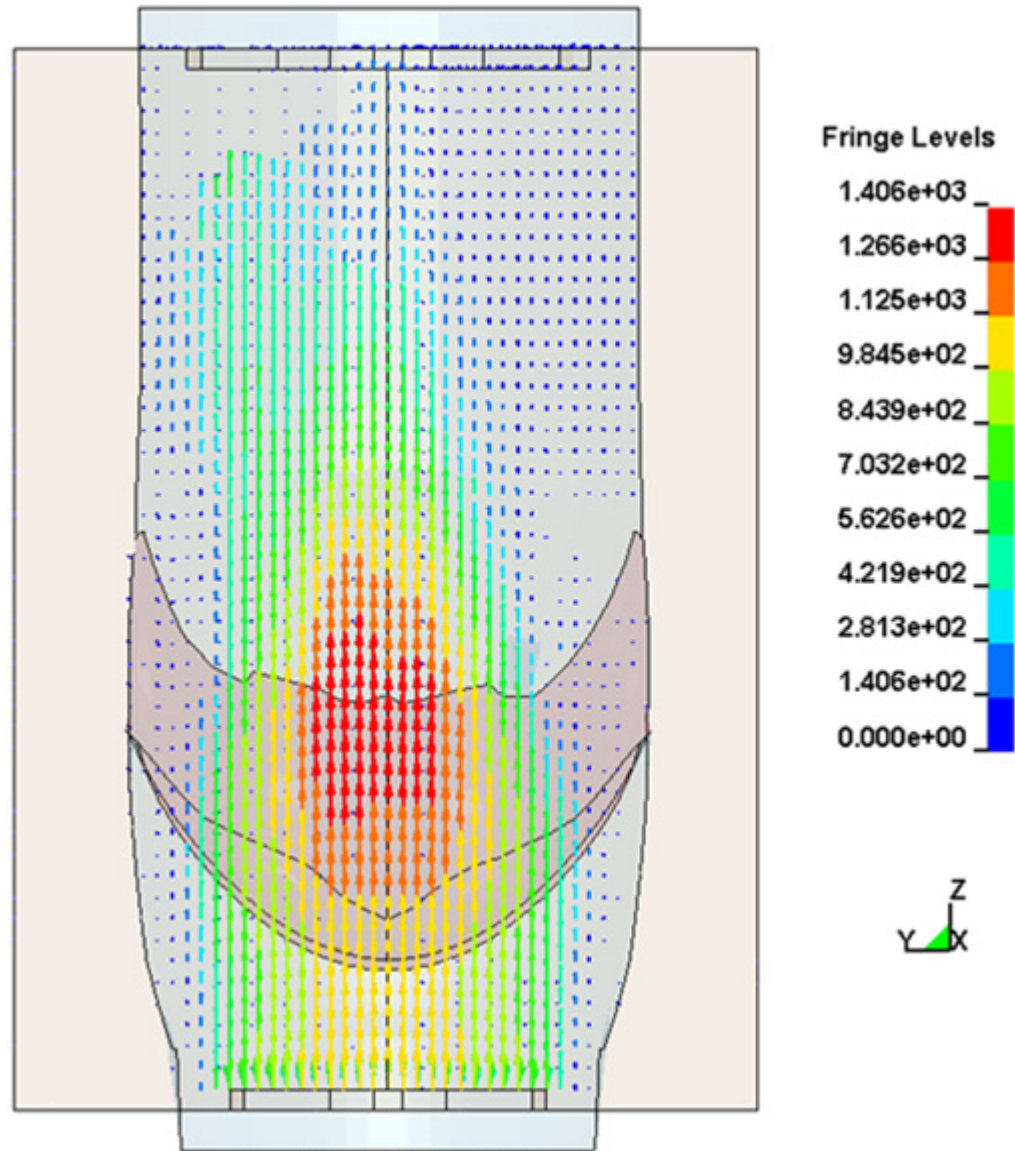


Figure 5.3 Velocity pattern at maximum opening for a healthy valve. Fringe level's unit is (mm/s).

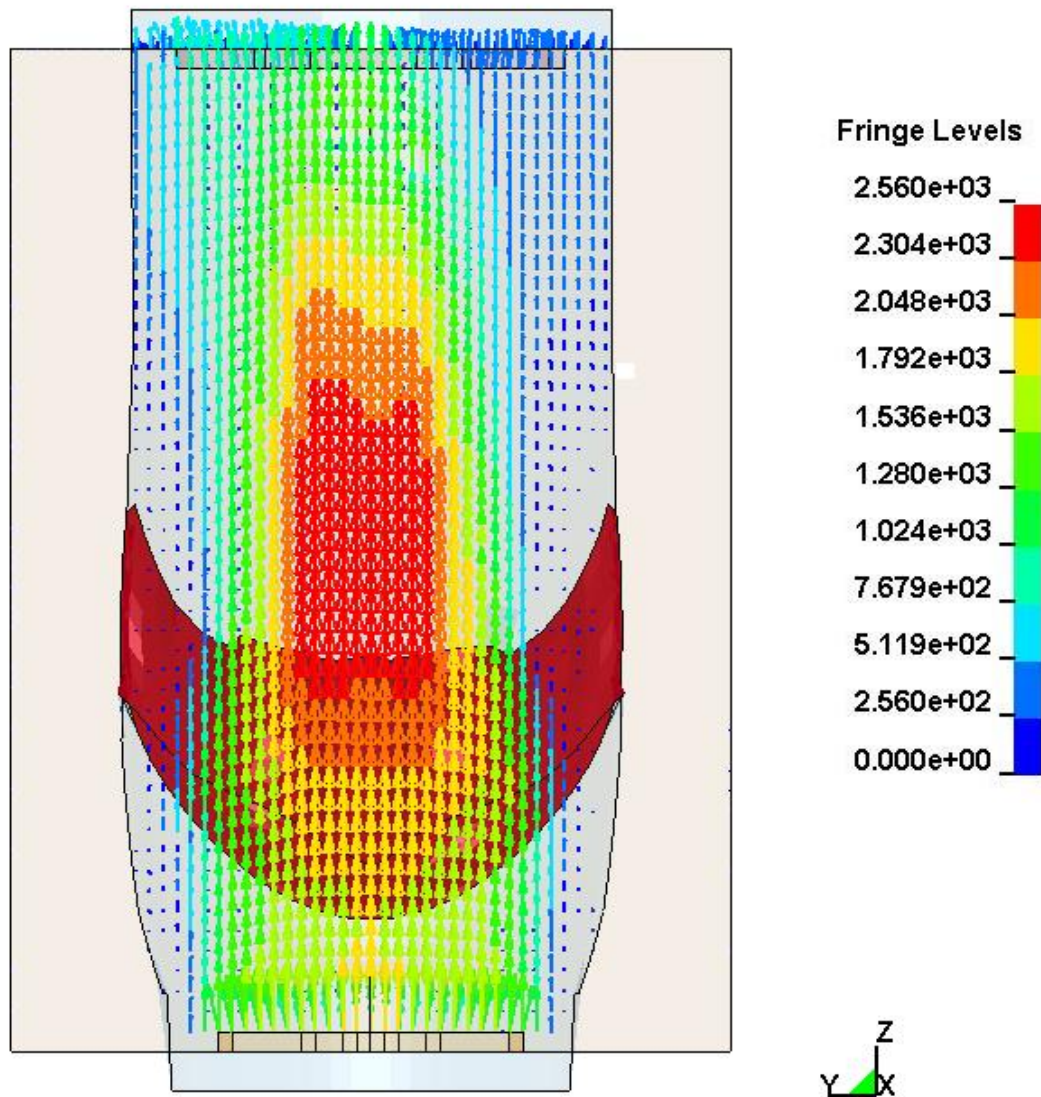


Figure 5.4 Velocity pattern at maximum opening for a stenotic valve. Fringe level's unit is (mm/s).

To validate these results, the maximum velocity is compared with the values obtained in the literature for a healthy valve. Carmody et al. (2004) found a maximum velocity of 0.75 m/s; Nicosia et al. (2003) reached a velocity of 1.32 m/s; Weinberg et al. (2007) reported a maximum velocity of 1 m/s; and Ranga et al. (2006) found the value around 1.1 m/s. In current work, the

maximum velocity for the healthy model is computed as 1.406 m/s. However, this value is found 2.56 m/s for a case of stenotic valve due to the narrowing of the flow path.

The two main parameters controlling this kind of flow are the Reynolds number ($Re = \frac{\rho u D}{\mu}$, where u is mean velocity and D is diameter of the aortic base upstream from the valve) and the Womersley number ($\alpha = \frac{D}{2} \sqrt{\frac{\omega \rho}{\mu}}$, in which ω is variational frequency). In this study, α is 14.41 and Reynolds number for healthy and stenotic valves are 1955 and 2875, respectively.

The obtained GOAs using FSI simulation are also compared with the GOAs obtained in vitro. The calculated GOA for healthy bioprosthetic valve (pericardial valve) using FSI analysis is 4.96 cm² while the measured GOA in vitro is 6.03 cm². This represents a difference of 17.75%. This difference can mainly be explained by the absence of dilatation of the aortic base (the aortic root was assumed without displacement) and can be due to use of different material properties in in vitro studies and in the numerical simulation.

For the stenotic valve, the simulated GOA is 3.34 cm². Although, this does not represent a severe aortic stenosis, but it shows the effect of increasing in thickness and changing the material properties on the behavior of an aortic valve. It should be mentioned that in order to investigate this effect, the same pressure boundary conditions as for the healthy case was used for the stenotic case.

The EOA can be calculated by considering the flow cross sectional plane of the maximum velocity. The area on this plane which includes the highest velocity magnitude is EOA. This region is shown by a closed pink line in Figs. 5.5 and 5.6 for the healthy and stenotic aortic valves respectively.

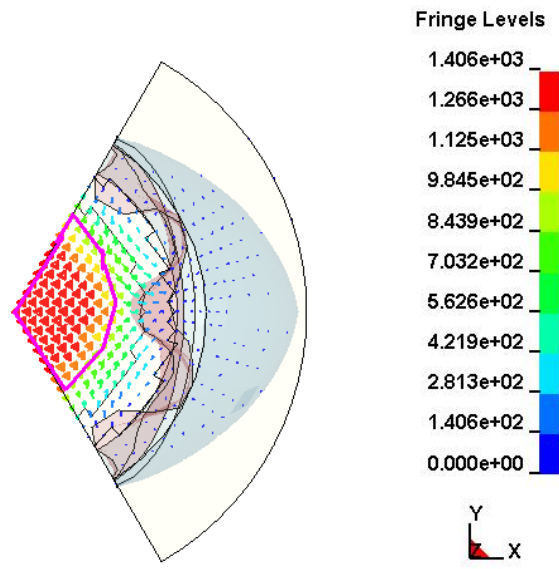


Figure 5.5 Transversal cross section of the aorta at the section corresponding to the maximum velocity for healthy valve (EOA: area inside pink line), Fringe level's unit is (mm/s).

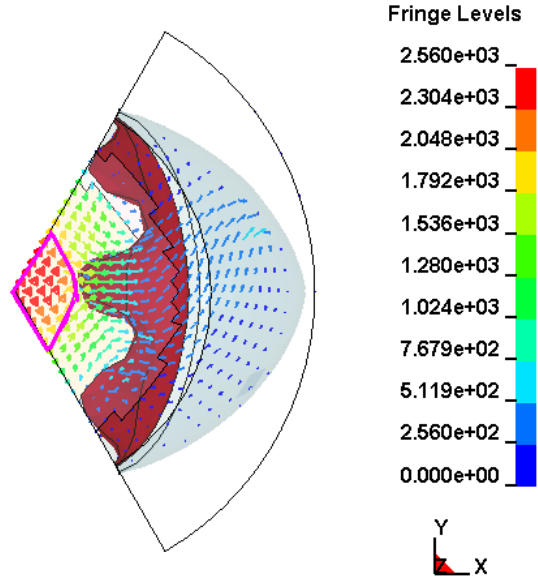


Figure 5.6 Transversal cross section of the aorta at the section corresponding to the maximum velocity for stenotic valve (EOA: area inside pink line), Fringe level's unit is (mm/s).

The velocity profiles at three different locations: upstream from the valve, at the vena contracta and downstream of the valve are plotted on Fig. 5.7 for the healthy valve.

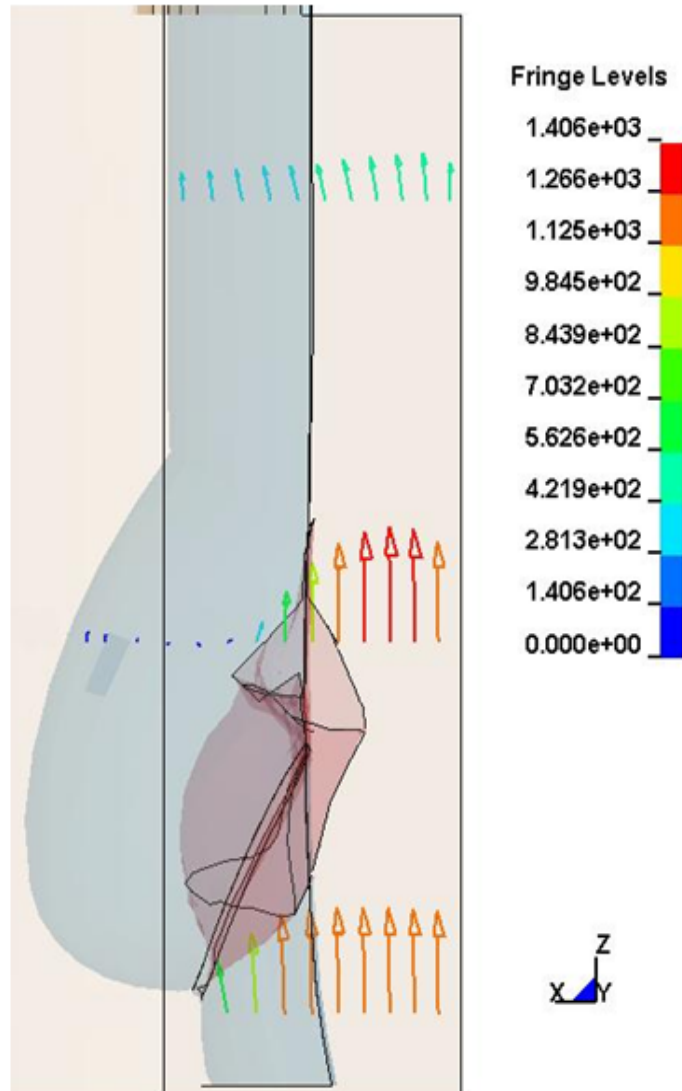


Figure 5.7 Velocity profiles for healthy valve (Max. opening), Fringe level's unit is (mm/s).

Figure 5.8 shows the velocity vectors at three different locations in a case of aortic stenosis. As the most interesting part in modeling the fluid domain is to analyze the velocity field, then the vectors in the sinuses are also shown on Fig. 5.8. Two vortices can be noticed: a strong

one and a weak one. These vortices play a crucial role in optimal valve closure (Bellhouse and Talbot, 1969).

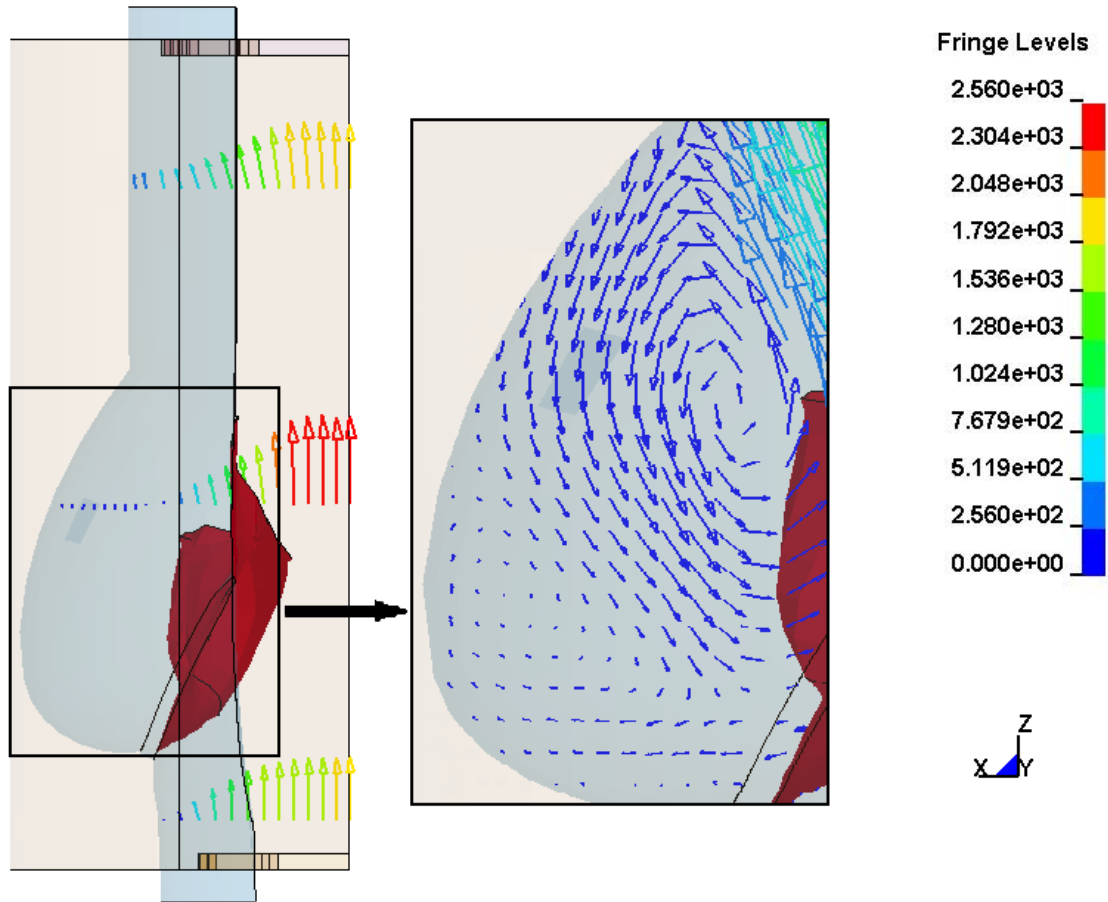


Figure 5.8 Velocity profiles for a stenotic valve (Max. opening), Fringe level's unit is (mm/s).

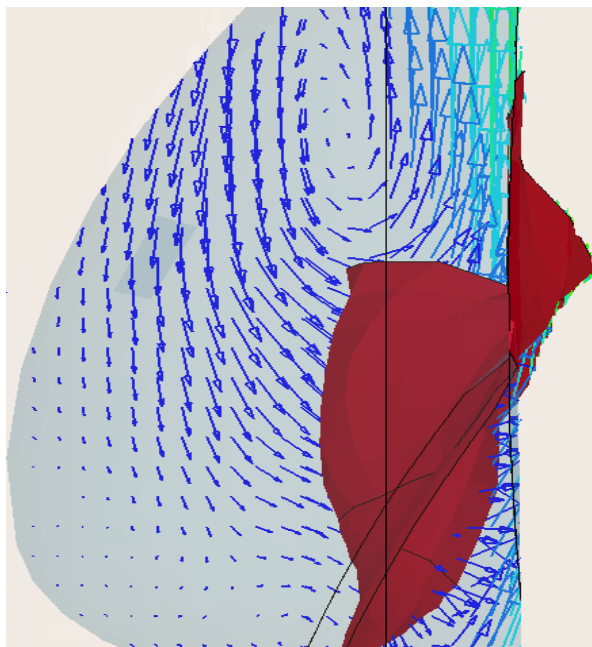


Figure 5.9 Velocity profile at mid-valve closure.

In the deceleration phase, these vortices grow and move towards the center of the aorta which causes valve closure. Figure 5.8 shows the vortex at the maximum opening and Fig. 5.9 shows the same vortex when valve is at mid-closure.

Fig. 5.10 summarizes the values for the maximal velocity at each location on the centerline along Z direction for both healthy and stenotic valves.

Velocity (m/s) at Max. Opening

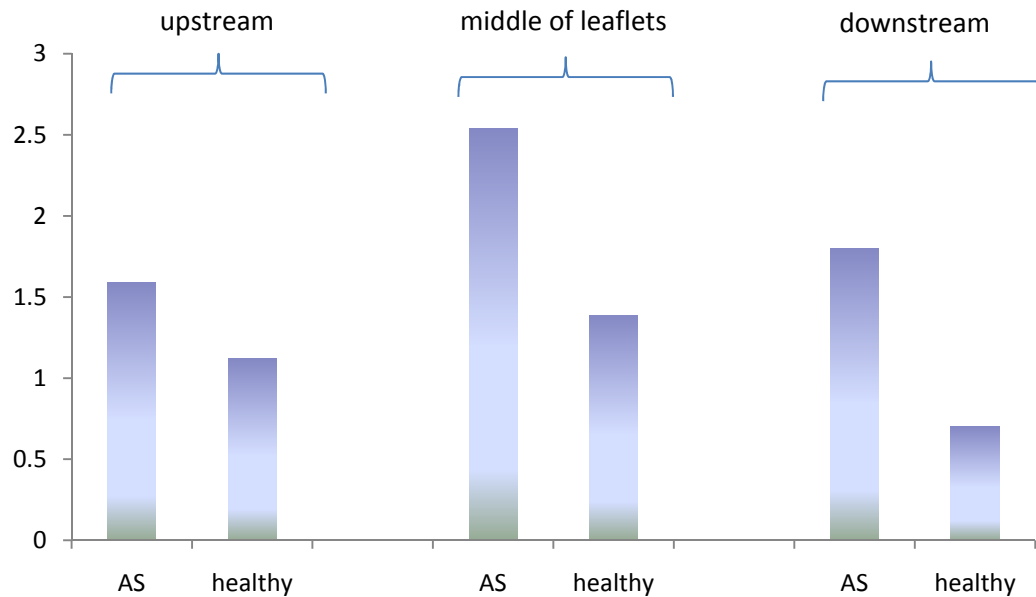


Figure 5.10 Comparison of maximal velocity upstream from the aortic valve, the vena contracta and downstream of the valve for healthy and stenotic valve at Max. opening.

The ratio of upstream flow velocity in a stenotic valve and a healthy valve is 1.4; this difference shows the effect of AS on upstream velocity. This ratio in the plane of maximum velocity (this plane is located between the three leaflets when they are completely open) is 1.83, representing an increase in velocity due to the narrowing of the flow path. Finally, the ratio of downstream the flow velocity in a stenotic valve and a healthy valve is 2.57; indicating the effect of aortic stenosis on the flow velocity in aorta. Such information cannot be obtained using the dry model.

In Chapter 4, the comparison between the in vitro experiment and the numerical simulation for ET, RVOT and RVCT were performed. It is good to have a comparison between the dry model, FSI model and the experiments (see Fig. 5.11).

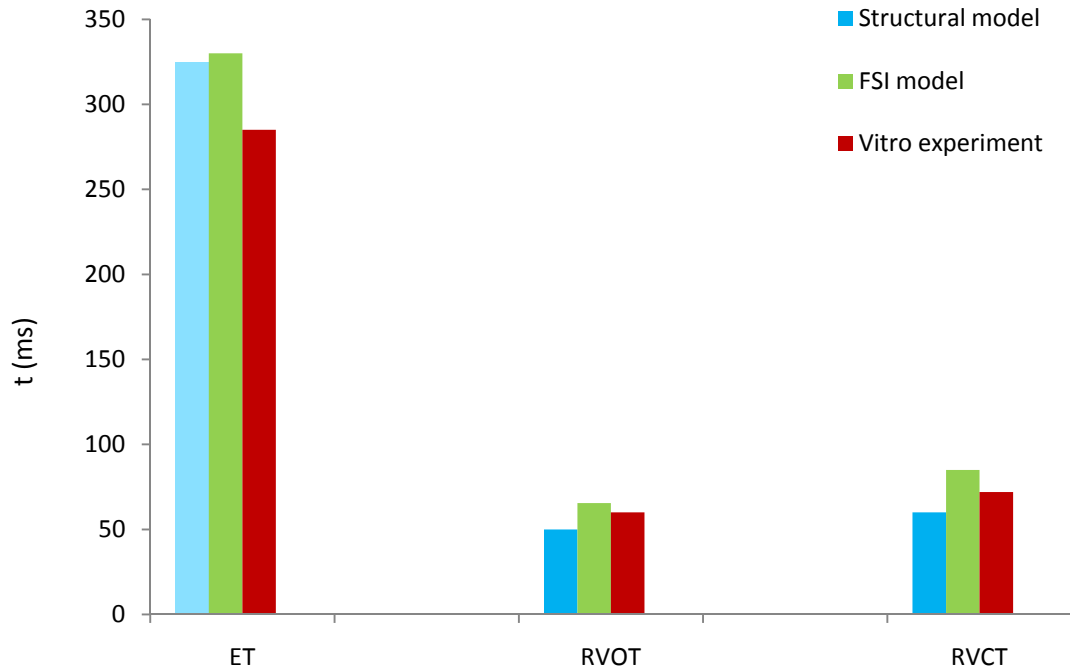


Figure 5.11 Comparison of ET, RVOP and RVCT using the dry model; FSI model and comparison with experimental model (for healthy valve).

The results show mainly that FSI modeling lead to more accurate results when compared to experiments.

Figure 5.12 shows the opening and closure of the healthy pericardial valve leaflet during one cardiac cycle. A, B, C, D and E represents the points which were selected in Fig. 4.8.

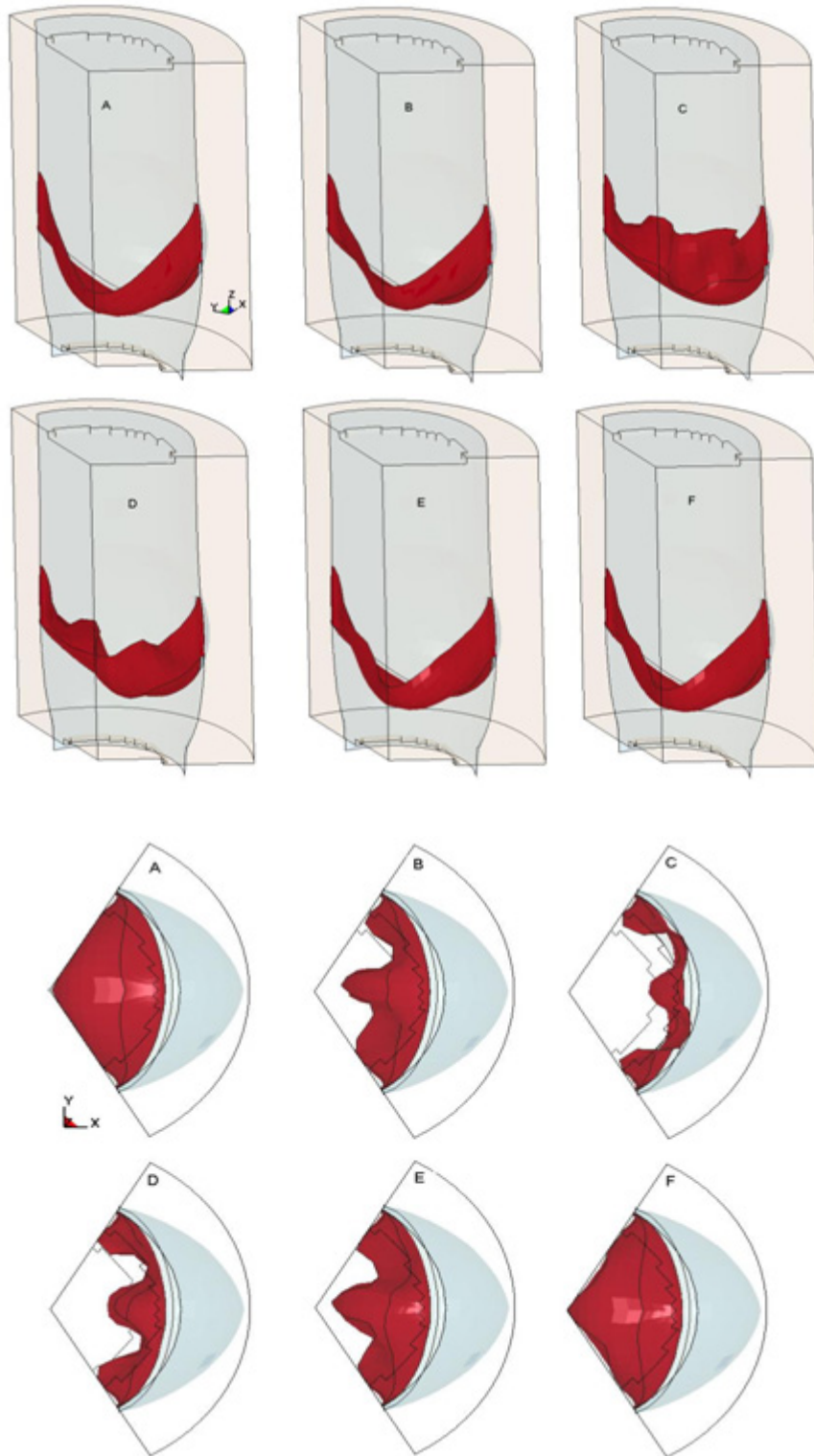


Figure 5.12 Opening and closure of a healthy pericardial aortic valve at different points selected in Fig. 4.8.

5.5 Limitations of the Current FSI Model

This preliminary investigation of the flow through a stenotic aortic valve using FSI modeling has certain limitations that are listed below:

- Turbulent flow is not considered due to software limitation.
- Except for the leaflet all the parts are considered as rigid body (without dilatation).
- Material properties are not optimized like for the dry model. This needs to be further investigated.

5.6 Summary

A numerical FSI modeling for a stenotic aortic valve and healthy valve was developed based on the pressure curves obtained in vitro for a bioprosthetic valve. A one-third model of the aortic valve structure is represented as an immersed Lagrangian structure surrounded by the Eulerian fluid domain with a fully coupling between the fluid and the structure components. The coupling between the fluid and the structure is modeled by exchange in the velocity and acceleration constrains between the Eulerian master (fluid domain) and the Lagrangian slave (the valve structure).

The comparison between the results of stenotic valve and healthy valve is done in terms of velocity magnitude and patterns. The velocity magnitude in a stenotic valve is increased while the GOA and EOA are decreased. The trend of opening and closure for the valve shows better agreements with in vitro tests, in terms of the deformation shape of the leaflets (compare Fig. 5.12 and 3.10) and the clinical parameters: ET, RVCT and RVOT.

Material properties to model these valves were obtained from previous works, but more work has to be done to optimize them.

Chapter 6: Conclusion and Future Work

The main objective of this thesis was to investigate and study the mechanical behavior of the aortic valve with an emphasis on aortic stenosis (AS). Moreover, this thesis aimed to characterize the severity of AS in term of material property.

In chapter one the importance of implanting percutaneous aortic valves was explained. The development of percutaneous valves allowed valve replacement without open chest surgery and that is the most desirable option in patients where the surgical risks are elevated. To avoid the risk of failure in percutaneous valve implantation, determination of material properties of the diseased leaflets before surgery is necessary. Detailed investigation of AS in vivo needs insertion of instruments into the body and in vitro experiment can be expensive and unrealistic. Therefore, in this study a series of numerical simulations and experimental validation were performed to address the objectives of this research.

The numerical simulations were done using structural and fluid structure interaction (FSI) modeling (wet model). The dimensions used to establish the geometry of the aortic root were obtained from a published data by Labrosse et al. in 2010. To validate the numerical methodology and algorithm, the results of numerical and experimental studies were first compared in a case of a pericardial prosthetic heart valve. The validation was done by comparing the instantaneous GOA from both studies. Also, the stress distribution in leaflet structure was compared with the results found in the literature.

The numerical simulation of the AS was developed based on data obtained from in vivo and in vitro studies. A left heart simulator capable of reproducing the flow and pressure conditions existing in the human heart was used in order to perform the experimental tests.

Numerical simulation shows that the proposed stiffness characteristic of material of the valve increases with increasing the severity of AS. Changing the thickness of the leaflets causes a significant effect on both GOA and material properties. With a same GOA, increase in leaflet thickness leads to decrease in the material property C_1 .

A series of sensitivity tests have been done in terms of density and geometric orifice area: The sensitivity test on first in vivo case revealed that changing density in a range of 1250 ± 250 kg/m^3 has 2.9 – 7.6 % effect on the C_1 . An error in reported (obtained clinically) GOA in a range of ± 10 %, results a difference of 7.4 -59.25 % in estimated material properties. This range shows that the results are strongly depend on the reported GOA.

In stress analysis of AS, there is not available reported data for comparison. However, the thesis found some interesting points that do match qualitatively well with literature:

- 1) The maximum principal stress happens at diastolic phase in the attachment area of the leaflets to the sinuses near sinotubular junction. This is consistent with the work of Li et al. (2001).

- 2) The other critical region is in the middle of the belly leaflets in systolic phase, which might explain why this is the common place of tissue as rupture reported by Carpentier et al. (1976).

- 3) In addition, it is found that increasing the leaflet thickness lead to reduction in principal stress. This behavior was reported by Thoronton et al. (1997).

The future plans for this research are as follows: In collaboration with clinicians, one can establish different in vivo tests to have access noninvasively to the patients' specific pressure

curves and EOA. This information as input to the numerical code will lead to determination of the material property of the valve for each specific patient.

Some plans can be targeted more specifically towards the numerical code itself. Instead of modeling one-third of the aortic valve, it would be interesting to model a complete valve. Moreover, the effect of left and right coronary arteries can be considered in the model by interaction between aortic stenosis and coronary blood flow.

Calculated GOA against C_1 in this study (Fig. 6.1) shows a curvilinear trend when considering all six aortic valve cases. Interestingly, these results could be compared to the results of Messika-Zeitoun et al. (2004) who found the relationship between the aortic valve area and EBCT score. This score represents the intensity of pixels that construct the calcified regions of the leaflets. In addition, they showed that there is a direct relationship between EBCT score and calcium weight. It means that the calcium weight and aortic valve area have a curvilinear trend as shown in Fig. 6.2. Their study showed an increase in EBCT score with decrease in aortic valve area. As a consequent, our numerical simulations can be considered as an additional noninvasive tool or even replaces the EBCT score, as the patients will not need exposure to X-rays. This requires however a larger number of cases to make a more proper judgment on the correlation between EOA and material property.

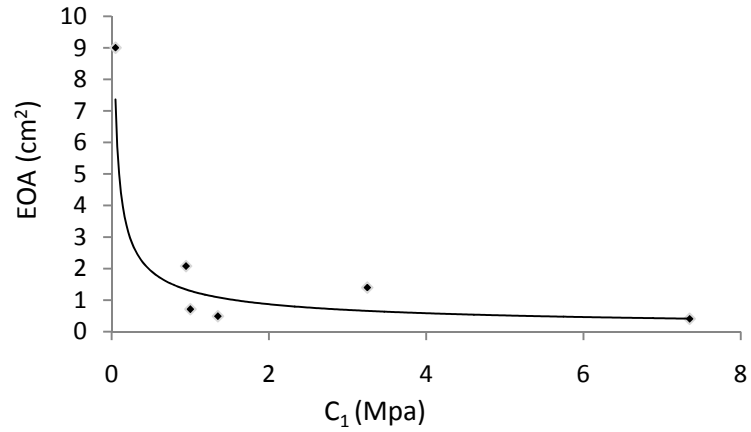


Figure 6.1 Curvilinear relationship between the EOA and material properties, each point represents one case study (this thesis).

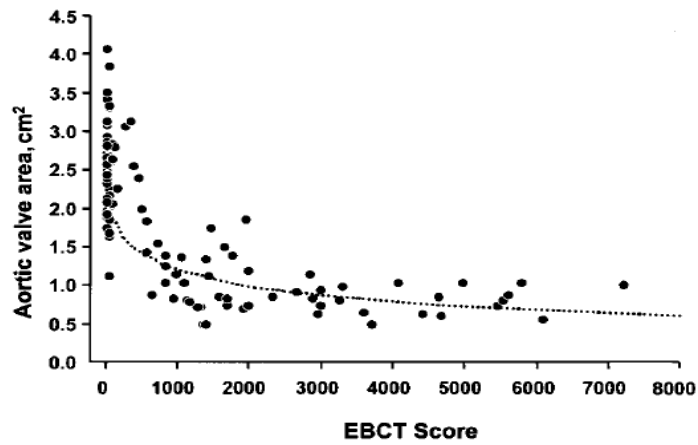


Figure 6.2 Curvilinear relationships between the EOA and EBCT score (Messika-Zeitoun et al., 2004).

In this study, the stenotic aortic valve was mimicked geometrically by thickening the leaflets. Another approach to investigate the mechanical behavior of the stenotic leaflets is to add different layers of calcium at different locations on the leaflets (some preliminary results of this idea are described in Appendix 1 employing a FSI analysis). The specific locations on the leaflets can be easily found by taking images from patients' calcified leaflets.

To simulate more realistic dynamic behavior of the aortic valve, employing a FSI analysis was necessary. Although, structural modeling is able to show the mechanical behavior of aortic valve, it is important to understand also the valve hemodynamic. Chapter 5 discussed about FSI modeling of the healthy and stenotic valves. The flow velocity profiles were determined in addition to the dynamic behavior of the valve structure. The opening of the valve leaflets including the velocity vector map and stress analysis of the leaflets were extracted.

It is difficult to verify the FSI simulation results quantitatively as it has a complex physics and it is difficult to find the same case in the literature to compare with. However, the results are qualitatively in a good acceptable range. The maximum velocities at the maximum opening of the valve are 1.406 m/s and 2.56 m/s for healthy and stenotic valves respectively, which are consistent with the reported values for healthy valves and AS at the same level of severity.

Using FSI analysis can improve the determination of parameters describing time duration of the dynamic behavior of the leaflets. The calculated ET, RVOT and RVCT using FSI modeling are more close to the in vitro experiment compared with the results of structural modeling. Moreover, FSI analysis simulates more realistic dynamic behavior of the aortic valve.

In future, some modifications can be proposed to improve the performance and accuracy of the FSI analysis. It can be interesting to increase the number of fluid elements to investigate the sensitivity of the results, although in this thesis, the numbers of fluid elements were in the same or higher range compared with the ones used in the FSI literature. The proposed flowchart for estimating the material property of a stenotic aortic valve (Figure 4.3) using the structural modeling can be extended by using noninvasive clinical data and FSI simulation. More accurate validation of FSI results is still required. This will be performed through experimental measurements using particle image velocimetry (PIV).

References

Articles & Books:

- Agatston, A.S., Janowitz, W.R., Hildner, F.J., Zusmer, N.R., Viamonte, M., Jr, 1990. Quantification of coronary artery calcium using ultrafast computed tomography. *Journal American College Cardiology* 15, 827-832.
- Arcidiacono, G., Corvi, A., Severi, T., 2005. Functional analysis of bioprosthetic heart valve. *Journal of Biomechanics* 33 (5), 521-530.
- Askes, H., Kuhl, E., Steinmann, P., 2004. An ALE formulation based on spatial and material settings of continuum mechanics. part 2: classification and applications. *Computer Methods in Applied Mechanics and Engineering* 193, 4223-4245.
- Bellhouse, B. J. , Talbot, L., 1969. The fluid mechanics of the aortic valve. *Journal of Fluid Mechanics* 35, 721-735.
- Billiar, K., Sacks, M., 2000. Biaxial mechanical properties of the natural and glutaraldehyde treated aortic valve cusp-part I: experimental results. *Journal of Biomechanical Engineering* 122 (1), 23-30.
- Billiar, K., Sacks, M., 2000. Biaxial mechanical properties of the natural and glutaraldehyde treated aortic valve cusp-part II: experimental results. *Journal of Biomechanical Engineering* 122 (4), 327-335.
- Black, M.M., Howard, I.C., Huang, X., Patterson, E.A., 1991. A three-dimensional analysis of a bioprosthetic heart valve. *Journal of Biomechanics* 24 (9), 793-801.
- Blais, C., Burwash, I.G., Mundigler, G., Dumesnil, J.G., Loho, N., Rader, F., Baumgartner, H., Beanlands, R.S., Chayer, B., Kadem, L., Garcia, D., Durand, L.G., Pibarot, P., 2006. The projected valve area at normal flow rate improves the assessment of stenosis severity in patients with low flow, low gradient aortic stenosis. *Circulation* 113, 711-721.
- Bloomfield, P., 2002. Choice of heart valve prosthesis. *Heart* 87 (6), 583-589.
- Bonow, R.O., Carabello, B.A., Chatterjee, K., de Leon, A.C., Jr, Faxon, D.P., Freed, M.D., Gaasch, W.H., Lytle, B.W., Nishimura, R.A., O’Gara, P.T., O’Rourke, R.A., Otto, C.M., Shah, P.M., Shanewise, J.S., 2006. ACC/AHA guidelines for the management of patients with valvular heart disease. *Circulation* 114, e84-e231.
- Burriesci, G., Howard, I., Patterson, E., 1999. Influence of anisotropy on the mechanical behaviour of bioprosthetic heart valves. *Journal of Medical Engineering & Technology* 23 (6), 203-215.
- Cacciola, G.R., 1998. Design, simulation and manufacturing of fiber reinforced polymer heart valves. Ph.D. Thesis, Eindhoven University of Technology, Eindhoven, Netherland.
- Cacciola, G.R., Peters, G.W.M., Schreurs, P.J.G., 2000. A three-dimensional mechanical analysis of a stentless fibre-reinforced aortic valve prosthesis. *Journal of Biomechanics* 33 (5), 521- 530.

- Carmody, C., Burriesci, G., Howard, I., Patterson, E., 2006. An approach to the simulation of fluid-structure interaction in the aortic valve. *Journal of Biomechanics* 39 (1), 158-169.
- Carpentier, A., Deloche, A., Relland, J. and Dubost, C., 1976. Valvular xenograft and valvular bioprosthesis: 1965–1975. In: Kalmanson, D. (Ed.), *The Mitral Valves: A Pluridisciplinary Approach*, Edward Arnold, London, 505–518.
- Chew, G., Howard, I., Paterson, E., 1999. Simulation of damage in a porcine prosthetic heart valve. *Journal of Medical Engineering & Technology* 23 (5), 178-189.
- Ching P.C., Wu S.Q., 1998. On approximated sampling theorem and wavelet denoising for arbitrary waveform restoration. *IEEE Transactions on Circuits and Systems-II: Analog and Digital Signal Processing* 45 (8). 1102-1106.
- Conti, C.A., Votta, E., Della Corte, A., Del Viscovo, L., Bancone, C., Cotrufo, M., Redaelli, A., 2010. Dynamic finite element analysis of the aortic root from MRI-derived parameters. *Journal of Mechanical Engineering & Physics* 32, 212-221.
- Cribier, A., Eltchaninoff, H., Bash, A., Borenstein, N., Tron, C., Bauer, F., Derumeaux, G., Anselme, F., Laborde, F., Leon, M.B., 2002. Percutaneous transcatheter implantation of an aortic valve prosthesis for calcific aortic stenosis first human case description. *Circulation* 106, 3006-3008.
- Croft, L.R., Kaazempur Mofrad, M.R., 2010. Computational modeling of aortic heart valves (Chapter 7). In: De, S., Guilak, F., Kaazempur Mofrad, M.R. (Eds.), *Computational Modeling in Biomechanics*. Springer, New York, 221-252.
- De Hart, J., Peters, G.W.M., Schreurs, P., Baaijens, F., 2000. A two-dimensional fluid structure interaction model of the aortic valve. *Journal of Biomechanics* 33 (9), 1079-1088.
- De Hart J., 2002. Fluid-structure interaction in the aortic heart valve. Ph.D. Thesis, Eindhoven University of Technology, Eindhoven, Netherland.
- De Hart, J., Peters, G.W.M., Schreurs, P., Baaijens, F., 2003. A computational fluid structure interaction analysis of a fiber-reinforced stentless aortic valve. *Journal of Biomechanics* 36, 699-712.
- De Hart, J., Peters, G.W.M., Schreurs, P., Baaijens, F., 2003. A three-dimensional computational analysis of fluid-structure interaction in the aortic valve. *Journal of Biomechanics* 36, 103-112.
- Dumesnil, J.G., Pibarot, P., Akins, C., 2008. New approaches to quantifying aortic stenosis severity. *Current Cardiology Reports* 10(2), 91-97.
- Feldman T., 2006. Percutaneous valve repair and replacement challenges encountered, challenges met, challenges ahead. *Circulation* 113, 771-773.
- Fung, Y.C., 1984. *Biodynamics: Circulation*, Springer-Verlag, Berlin-Heidelberg-New York.
- Fuster, V., Alexander, R.W., O'Rourke, R.A., Roberts, R., King III, S. B., Nash, I.S., Prystowsky, E.N., 2004, 11th Edition. *Hurst's the Heart*, McGraw-Hill Professional, USA.

- Garcia, D., Barenbrug, P.J.C., Pibarot, P., Dekker, A.L.A.J., van der Veen, A.H., Maessen, J.G., Dumesnil, J.G., Durand, L.G., 2005. A ventricular-vascular coupling model in presence of aortic stenosis. *AJP - Heart and Circulatory Physiology* 288, H1874–H1884.
- Garcia, D., Kadem, L., 2006. What do you mean by Aortic Valve Area: Geometric Orifice Area, Effective Orifice Area, or Gorlin Area?. *Journal of Heart Valve Disease* 15, 601-608.
- Garcia D., Pibarot P., Landry C., Allard A., Chayer B., Dumesnil J.G., Durand L.G., 2004. Estimation of aortic valve effective orifice area by Doppler echocardiography: effects of valve inflow shape and flow rate. *Journal of the American Society of Echocardiography* 17 (7), 756-765.
- Gott, V.L., Alejo, D.E., Cameron, D.E., 2003. Mechanical heart valves: 50 years of evolution. *The Annals of Thoracic Surgery* 76, S2230-S2239.
- Grande, K., Cochran, R., Reinhall, P., Kunzelman, K., 1998. Stress variations in the human aortic root and valve: the role of anatomic asymmetry. *Annals of Biomedical Engineering* 26, 534-545.
- Grande K.J., Cochran R.P., Reinhall P.G., Kunzelman K.S. 1999. Mechanisms of aortic valve incompetence in aging: a finite element model. *The Journal of Heart Valve Disease* 8, 149-156.
- Grande, K., Cochran, R., Reinhall, P., Kunzelman, K., 2000. Mechanisms of aortic valve incompetence finite element modeling of aortic root dilation. *Annals of Biomedical Engineering* 69 (6), 1851-1857.
- Grande, K.J., Cochran, R.P., Reinhall, P.G., Kunzelman, K.S., 2001. Mechanisms of aortic valve incompetence: Finite-element modeling of Marfan syndrome. *Journal of Thoracic and Cardiovascular Surgery* 122, 946-954.
- Grixti, K., 2004. Prosthetic heart valves (Chapter 22). In: Mackay, J.H., Arrowsmith, J.E. (Eds.), *Core Topics in Cardiac Anesthesia*, Cambridge University Press, UK.
- Guccione, J.M., Costat, K.D., McCulloh, A.D., 1995. Finite element stress analysis of left ventricular mechanics in the beating dog heart. *Journal of Biomechanics* 28 (10), 1167-1177.
- Guccione, J.M., McCulloh, A.D., Waldman L.K., 1991. Passive material properties of intact ventricular myocardium determined from a cylindrical model. *Journal of Biomechanical Engineering* 113 (1), 42-55.
- Haj-Ali, R., Dasib, L.P., Kima, H., Choia, J., Leoa, H.W., Yoganathan, A.P., 2008. Structural simulations of prosthetic tri-leaflet aortic heart valves, *Journal of Biomechanics* 41, 1510-1519.
- Hanzel, G.S., O'Neill W.W., 2006. Complications of percutaneous aortic valve replacement: experience with the Cribier-Edwards™ percutaneous heart valve. *EuroIntervention Supplements* 1 (Supplement A), A3-A8.
- Huang, X., Black, M.M., Howard, I.C., Patterson, E.A., 1990. A two-dimensional finite element analysis of a bioprosthetic heart valve. *Journal of Biomechanics* 23 (8), 753-762.

- Hufnagel, C.A., Harvey, W.P., Rabil, P.J., McDermott, T.F., 1954. Surgical correction of aortic insufficiency. *Surgery* 35, 673-683.
- Jing, L., Stephansson, O., 2007. *Fundamentals of Discrete Element Methods for Rock Engineering: Theory and Applications*, Elsevier, Oxford, UK.
- Katayama, S., Umetani, N., Sugiura, S., Hisada, T., 2008. The sinus of Valsalva relieves abnormal stress on aortic valve leaflets by facilitating smooth closure. *The Journal of Thoracic and Cardiovascular Surgery* 136, 1528-1535.
- Kisslo, J., Firek, B., Ota, T., Hyun Kang, D., Fleishman, C.E., Stetten, G., Li, J., Ohazama, C.J., Adams, D., Landolfo, C., Ryan, T., von Ramm, O., 2000. Real-time volumetric echocardiography: the technology and the possibilities. *Echocardiography* 17(8),773-779.
- Koch, T.M., Reddy, B.D., Zilla, P., Franz, T., 2009. Aortic valve leaflet mechanical properties facilitate diastolic valve function. *Computer Methods in Biomechanics and Biomedical Engineering* 13 (2), 225-234.
- Labrosse, M.R., Beller, C.J., Mesana, T., Veinot, J.P., 2009. Mechanical behavior of human aortas: experiments, material constants and 3D finite element modeling including residual stress. *Journal of Biomechanics* 42 (8), 996-1004.
- Labrosse, M.R., Beller, C., Robicsek, F., Thubrikar M., 2006. Geometric modeling of functional trileaflet aortic valves: development and clinical applications. *Journal of Biomechanics* 39, 2665-2672.
- Labrosse, M.R., Lobo, K., Beller, C., 2010. Structural analysis of the natural aortic valve in dynamics: From unpressurized to physiologically loaded. *Journal of biomechanics* 43 (10), 1916-1922.
- Li, J., Luo X.Y., Kuang, Z.B., 2001. A nonlinear anisotropic model for porcine aortic heart valves. *Journal of Biomechanics* 34, 1279-1289.
- Lobo, K., 2009. Finite element modeling of the natural aortic valve. Master Thesis, University of Ottawa, Ottawa, Canada.
- Mackerle, J., 2005. Finite element modeling and simulations in cardiovascular mechanics and cardiology: a bibliography 1993-2004. *Computer Methods in Biomechanics and Biomedical Engineering* 8(2), 59-81.
- May-Newman, K., McCulloch, A.D., 1998. Homogenization modeling for the mechanics of perfused myocardium. *Progress of Biophysics and Molecular Biology* 69, 463-481.
- Messika-Zeitoun, D., Aubry, M.C., Detaint, D., Bielak, L.F., Peyser, P.A., Sheedy, P.F., Turner, S.T., Breen, J.F., Scott, C., Tajik, J., Enriquez- Sarano, M., 2004. Evaluation and clinical implications of aortic valve calcification measured by electron-beam computed tomography. *Circulation* 110, 356-362.
- Morse, D., Steiner, R.M., Fernandez, J., 1985. *Guide to Prosthetic Cardiac Valves*. Springer-Verlag, New York.

- Nair, K., Muraleedharan, C.V., Bhuvaneshwar, G.S., 2003. Developments in mechanical heart valve prosthesis. *Sadhana: Academy Proceedings in Engineering Sciences*, 28(3,4),575-587.
- Narracott, A.J., Zervides, C., Diaz, V., Rafiroiu, D., Lawford, P.V., Hose, D.R., 2010. Analysis of a mechanical heart valve prosthesis and a native venous valve: two distinct applications of FSI to biomedical applications. *International Journal for Numerical Methods in Biomedical Engineering* 26, 421-434.
- Nicosia, M., Cochran, R., Einstein D., Rutland, C., Kunzelman, K., 2003. A coupled fluid structure finite element model of the aortic valve and root. *Journal of Heart Valve Disease* 12, 781-789.
- Nishimura, R.A., 2002. Aortic Valve Disease. *Circulation* 106, 770-772.
- Omens, J.H., Usyk, T.P., Li, Z., Mcculloch, D.A., 2002. Muscle LIM protein deficiency leads to alterations in passive ventricular mechanics. *American Journal Physiology Heart and circulatory Physiology* 282, H680–H687.
- Otto, C.M., Lind, B.K., Kitzman, D.W., Gersh, B.J., Siscovick, D.S., 1999. Association of aortic-valve sclerosis with cardiovascular mortality and morbidity in the elderly. *The New England Journal of Medicine* 341 (3), 142-147.
- Oury, J.H., Hiro, S.P., Maxwell, J.M., Lamberti, J.J., Duran, C.M., 1998. The Ross Procedure: current registry results. *Annual Thoracic Surgery* 66, S162-S165.
- Patel, D.J., Fry, D.L., 1966. Longitudinal tethering of arteries in dogs. *Circulation Research* 19 (6), 1011-1021.
- Pick, A., 2006. *The Patient's Guide to Heart Valve Surgery*. Heart Valve Interactive Corp., California, USA.
- Quek, S.S., Liu G.R., 2003. *The Finite Element Method: A Practical Course*. Butterworth-Heinemann. Oxford, UK.
- Rajamannan, N.M., Bonow, R.O., Rahimtoola, S.H., 2007. Calcific aortic stenosis: an update. *Nature Clinical Practice Cardiovascular Medicine* 4, 254-262.
- Ranga, A., Mongrain, R., Mendes Galaz, R., Biadillah, Y., Cartier, R., 2004. Large displacement 3D structural analysis of an aortic valve model with nonlinear material properties. *Journal of Medical Engineering & Technology* 28 (3), 95-103.
- Ranga, A., Bouchot, O., Mongrain, R., Ugolini, P., 2006. Cartier, R., Computational simulations of the aortic valve validated by imaging data: evaluation of valve-sparing techniques, *Interaction Cardiovascular. Thoracic. Surgery*. 5, 373–378.
- Rao, S.S., 2005. *The Finite Element Method in Engineering*. 4th Edition, Elsevier Butterworth-Heinemann, Massachusetts, USA.
- Sauren, A.A.H.J., 1981. *The Mechanical Behaviour of the Aortic Valve*. Ph.D. Thesis, Eindhoven University of Technology, Eindhoven, Netherland.

- Schoen, F.J., Levy, R.J., 1999. Tissue heart valves: current challenges and future research perspectives, *Journal of Biomedical Materials Research* 47(4), 439-465.
- Souli, M., Ouahsine A., Lewin L., 2000. ALE formulation for fluid-structure interaction problems. *Computational Methods in Applied Mechanical Engineering* 190, 659-675.
- Southard, J.A., Low, R.I., 2006. Percutaneous valve therapies (Chapter 10). In: Tremmel, J. (Ed.), *SIS Yearbook*, Seattle, 115-128.
- Stelzer, P., Weinrauch, S., Tranbaugh, R.F., 1998. Ten years of experience with the modified Ross procedure. *The Journal of Thoracic and Cardiovascular Surgery* 115 (5), 1091-1100.
- Stijnen, J.M.A., 2004. Interaction between the Mitral and Aortic Heart Valve. Ph.D. Thesis, Eindhoven University of Technology, Eindhoven, Netherland.
- Sun, W., Abad, A., Sacks, M.S., 2005. Simulated bioprosthetic heart valve deformation under quasi-static loading. *Journal of Biomedical Engineering* 127 (6), 905-914.
- Takamizawa, K., Hayashi, K., 1987. Strain energy density function and uniform strain hypothesis for arterial mechanics. *Journal of Biomechanics* 20 (1), 7-17.
- Thornton, M.A., Howard, I.C., Patterson, E.A., 1997. Three dimensional stress analysis of polypropylene leaflets for prosthetic heart valves. *Medical Engineering and Physics* 19 (6), 588-597.
- Thubrikar, M.J., 1990. *The Aortic Valve*. CRC Press Inc., Boca Raton, Florida, USA.
- Van Loon, R., 2010. Towards computational modeling of aortic stenosis. *International Journal for Numerical Methods in Biomedical Engineering* 26, 405-420.
- Vesely, I., Noseworthy, R., 1990. Micromechanics of the Fibrosa and the Ventricularis in Aortic Valve Leaflets. *Journal of Biomechanics* 25(1), 101-113.
- Waggoner, A.D., Barzilai, B., Perez, J.E., 1991. Two-dimensional Doppler echocardiographic derived aortic valve area in aortic stenosis. *Journal of Diagnostic Medical Sonography* 7, 64-72.
- Wallerson, C.D., Dubin, J., Devereux, R.B., 1987. Assessment of cardiac hemodynamics and valvular function by Doppler echocardiography. *Bulletin of the New York Academy of Medicine* 63 (8), 762-796.
- Weinberg, E.J., Kaazempur Mofrad, M.R., 2007. Transient, three-dimensional, multiscale simulations of the human aortic valve. *Cardiovascular Engineering* 7, 140-155.
- Weinberg, E.J., Kaazempur Mofrad, M.R., 2008. A multiscale computational comparison of the bicuspid and tricuspid aortic valves in relation to calcific aortic stenosis. *Journal of Biomechanics* 41 (16), 3482-3487.
- Weinberg, E.J., Schoen, F.J., Kaazempur Mofrad, M.R., 2009. A computational model of aging and calcification in the aortic heart valve. *PLoS ONE*. 4 (6), e5960 (1-10).

Xiong, F.L., Goetz, W.A., Chong, C.K., Chua, Y.L., Pfeifer, S., Wintermantel, E., Yeo, J.H., 2010. Finite element investigation of stentless pericardial aortic valves: relevance of leaflet geometry. *Annals of Biomedical Engineering* 38 (5), 1908-1918.

Zoghbi, W.A., 1988. Echocardiography and Doppler ultrasonic evaluation of valvular aortic stenosis, *Journal of Echocardiography* 5(1), 23-38.

Technical Manuals:

LS-DYNA Keyword User's Manual. Livermore Software Technology Corporation, 2007, California, USA.

LS-DYNA Theoretical Manual. Livermore Software Technology Corporation, 2007, California, USA.

ViVitro Operating Manual. ViVitro Systems Inc., 2006, Victoria, Canada.

Web Sites:

Aortic Valve Stenosis, Medicin Net: http://www.medicinenet.com/aortic_stenosis/article.htm.

Arthur's Free Clipart: www.arthursclipart.org/.

Heart and Vascular Health, Cleveland Clinic: www.clevelandclinic.org/heart/.

The Circulatory System: www.teachnet.ie/farmnet/Circulatory.htm.

Appendix

Appendix 1

As the first tried to develop an FSI analysis, a two dimensional geometry of an aortic valve was considered. The simulation results were accepted and presented at the European Society of Biomechanics (ESB) conference in 2010. The complete geometry and its meshes were created with LS-DYNA. The dimensions used to create the model are shown in Table A1.1. The geometry consisted of the fixed sinuses and aortic root with two flexible leaflets. The fluid was considered Newtonian with the density of 1000 kg/m^3 and viscosity of $3.8 \times 10^{-3} \text{ Pa.s}$. The number of elements for the fluid and the structure parts were 3687 and 164 respectively. The leaflets were modeled by 4-noded Belytchko-Lin-Tsai shell elements with Mooney-Revlin material which has anisotropic, nonlinear material property (see Fig. A1.1). The material properties of leaflets were selected as: $\rho = 1000 \text{ kg/m}^3$, $A = 0.5 \text{ MPa}$, $B = 0.14 \text{ MPa}$ and $\nu = 0.49$.

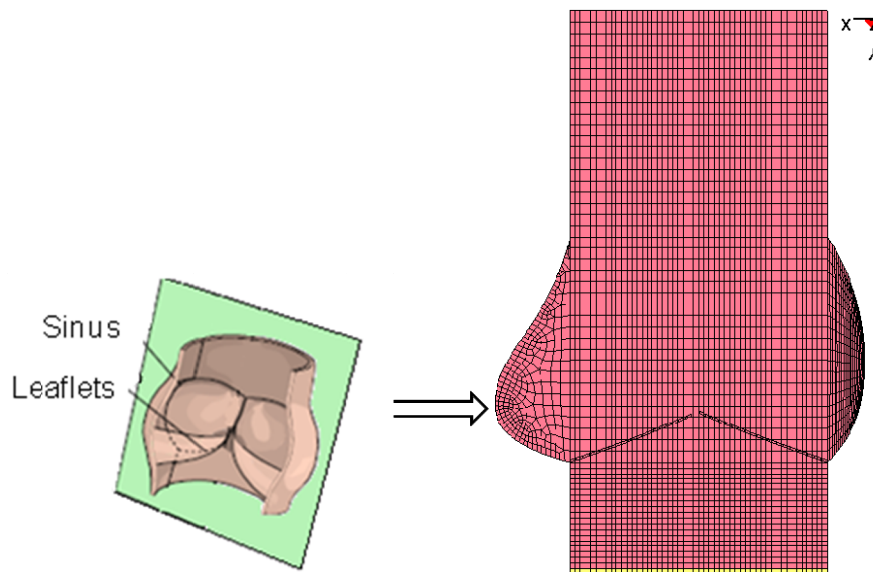


Figure A1.1 A 2D Geometry of aortic valve.

Table A1.1 Dimensions for human aortic valve.

Base diameter	Commissural diameter	Sinus height	Leaflet height	Leaflet free edge
24.0 mm	23.6 mm	20.5 mm	13.3 mm	30.9 mm

In this thesis, one of the proposed strategies for modeling the AS was to place a layer of calcium on the aortic side of the leaflets which is shown in Fig. A1.2 with green color. This approach can be used as an alternative to the already employed strategy through out of this thesis which was increasing the thickness of the leaflets, the density and young's module of the material to model AS. In order to have a comparison between the dynamical behavior and hemodynamics of healthy and diseased valves, two simulations were done with and without adding the calcium layer.

The time-varying pressure curves applied at the inlet and outlet of the domain are shown in Fig. A1.2. Also, the no slip boundary condition was employed in order to model the fixed sinuses and aortic root.

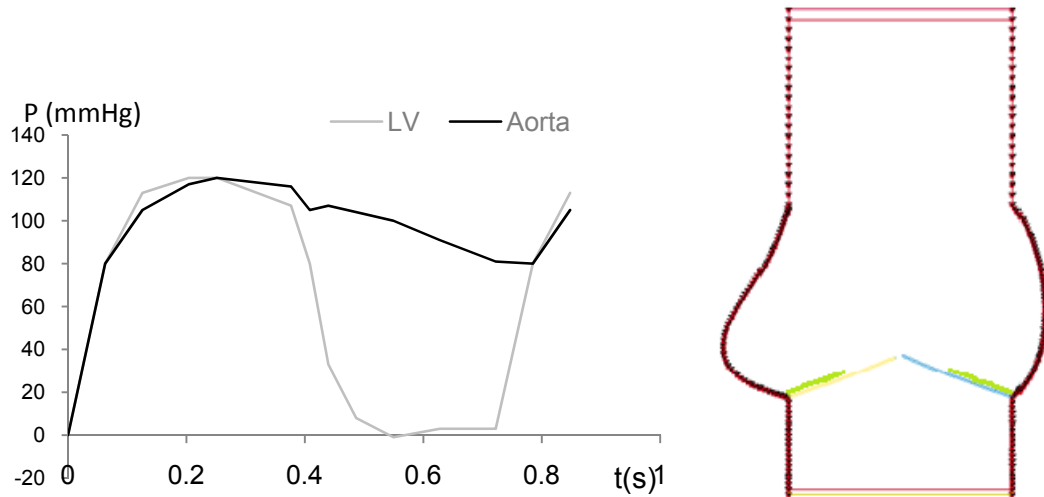


Figure A1.2 (Left) aortic and left ventricular pressure wave forms applied as the boundary condition; (right) the boundary of the domain.

The velocity vectors at three different planes are shown in Fig. A1.3 for both healthy and stenotic valves. The maximum velocity at the maximum opening of the valve in healthy case is 0.84 m/s which is in agreement with the results of De Hart et al. (2003). The maximum velocity in the case of stenotic valve is computed 2.2 m/s.

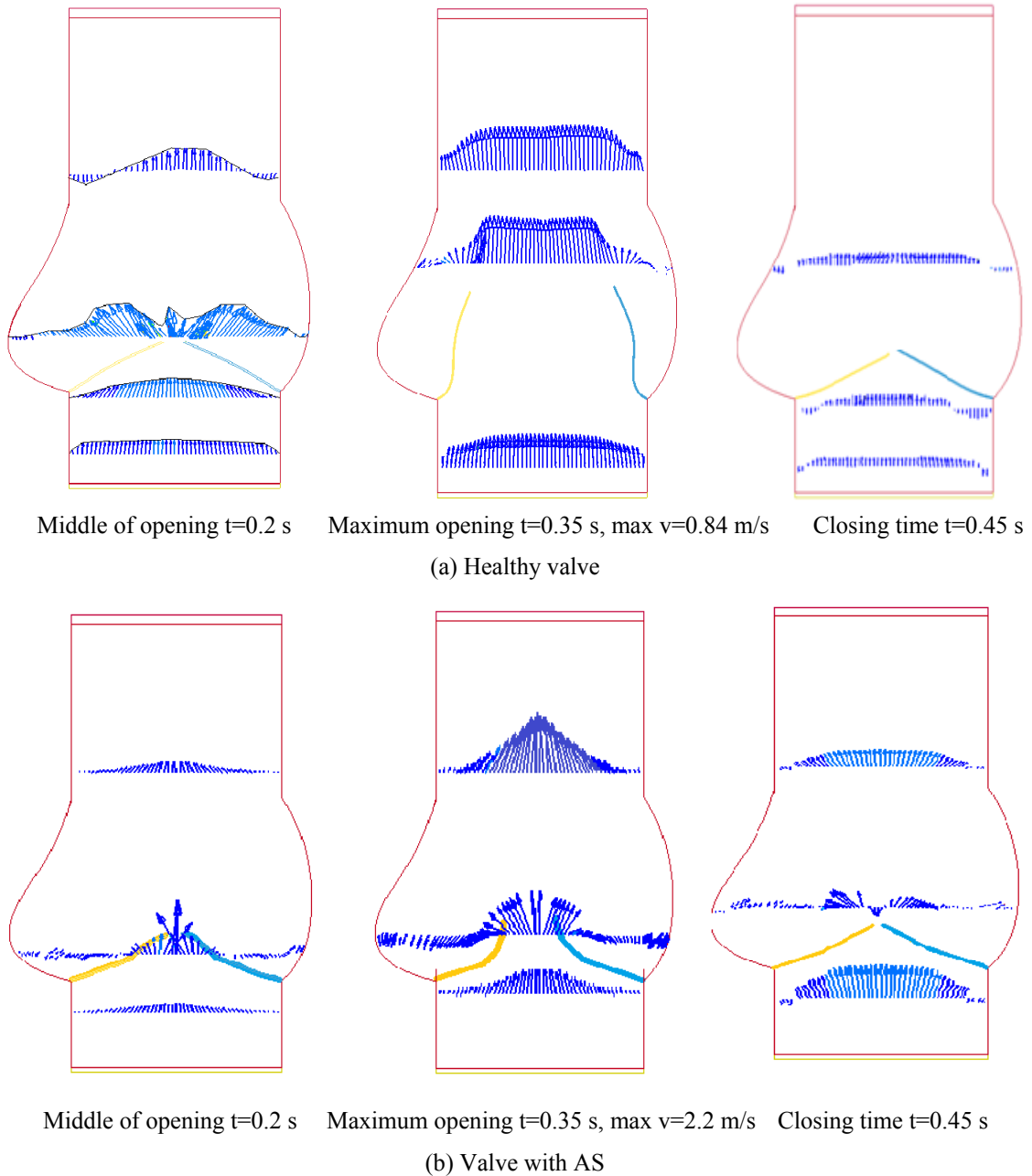


Figure A1.3 Velocity vector map at different instants and planes: (a) Healthy valve; (b) valve with AS.

Appendix 2

The goal of this thesis necessitates employing a computational algorithm capable to handle the analysis of fluid and structure dynamics together. A list of available professional software is shown in Table A2.1. Among them, LS-DYNA, ABAQUS and MSC-DYTRAN software use explicit finite element (FE) method to obtain numerical solutions for time-dependent governing physical equations of the fluid and structure (a comprehensive discussion on explicit methods in FE is included in Chapter 4). In this thesis a commercially available combined computational fluid and solid dynamics (CFD and CSD) software package, LS-DYNA 971 (LSTC, Livermore, CA, USA) is used to simulate fluid and structure parts.

Table A2.1 Commercially available software and methods used. (Lio and Quek, 2003)

Software	Method used	Application
ABAQUS	FEM (implicit, explicit)	Structural analysis, acoustics, thermal analysis
I-deas	FEM (implicit)	Structural analysis, acoustics, thermal analysis
LS-DYNA	FEM (explicit)	Structural computational fluid dynamics, FSI
ANSYS	FEM (implicit)	Structural analysis, acoustics, thermal analysis, ...
ADINA-DYNA	FEM (implicit)	Structural analysis computational fluid dynamics, FSI
MSC-DYTRAN	FEM + FVM (explicit)	Structural dynamics, computational fluid dynamics, FSI

LS-DYNA is a general purpose finite element package for analyzing the large deformation dynamic of structures separately or coupled with fluids. Mainly, the large dynamic motion of the aortic valve leaflets in a short period of time (a cardiac cycle) and existence of a highly coupled fluid and structure physics make this software an appropriate candidate to be used in this study.